Sea Water in Coastal Aquifers

GEOLOGICAL SURVEY WATER-SUPPLY PAPER 1613-C

Sea Water in Coastal Aquifers

By HILTON H. COOPER, JR., FRANCIS A. KOHOUT, HAROLD R. HENRY, *and* ROBERT E. GLOVER

RELATION OF SALT WATER TO FRESH GROUND WATER

GEOLOGICAL SURVEY WATER-SUPPLY PAPER 1613-C

A group of short papers, by the individual authors, on the circulation of sea water and the position of the salt-water front

UNITED STATES GOVERNMENT PRINTING OFFICE, WASHINGTON : 1964

UNITED STATES DEPARTMENT OF THE INTERIOR

STEWART L. UDALL, *Secretary*

GEOLOGICAL SURVEY

Thomas B. Nolan, *Director*

For sale by the Superintendent of Documents, U.S. Government Printing Office
Washington, D.C. 20402

PREFACE

By Hilton H. Cooper, Jr.

Over a period of about 35 years the sea water in the Biscayne aquifer of southeastern Florida advanced progressively inland, owing to a lowering of the fresh-water head. The drainage of the Everglades, which began shortly after the turn of the century (Parker and others, 1955, p. 584–591), was the principal cause of this lowering. Applying the Ghyben-Herzberg relation, Parker (Parker and others, 1944, p. 18) predicted that the salt water at the base of the aquifer would continue to advance "* * * until ultimately it [would] come to rest in equilibrium with the fresh water where the average annual two and one-half foot contour on the water table [occurred]."

If it had advanced as predicted, the wedge of salt water would eventually have enveloped numerous water-supply wells, including those of the Miami municipal supply in the Miami Springs well field. Early in the 1950's, however, the advancement of the salt water appeared to cease, although the front of the wedge was still as much as 8 miles seaward of the predicted ultimate position. Whether the front had stabilized or whether its advance had merely slowed was not only a question of economic importance but also a matter of scientific interest because the seemingly premature stabilization could not be explained by any known theory. The question therefore became the topic of several discussions among the writer and his colleagues, including R. R. Bennett, G. G. Parker, N. D. Hoy, and F. A. Kohout. From these discussions evolved the idea that whereas the salt water was continuing to flow inland as expected, the wedge front was continually being "eroded" by a seaward flow of mixed water in the zone of diffusion. This idea led to the concept that perpetual circulation of sea water in coastal aquifers was a necessary consequence of the dispersion of salts in the zone of diffusion (Cooper, 1959).

At the time, this concept seemed to be novel, but Todd (1960) and Bear and Todd (1960) have found mentions of inland flow of salt water by several investigators. For example, Nomitsu and others (1927, p. 288) state:

> Near the contact surface, agitated by the moving fresh water, the salt water will tend to be transported seawards, although it may be very very slowly. By way of compensation, sea water in the lower part will continue to infiltrate landwards.

Todd (1960), believing that Nomitsu and his associates were the first to postulate the concept, proposed that the dispersion-induced circulation be recognized as the Nomitsu circulation. However, Nomitsu and his associates may not have recognized dispersion as the motivating factor. Their statement that salt water along the interface is "agitated" by the moving fresh water implies that they visualized a circulation maintained through forces of viscosity at the interface. In an open body of water, such as an estuary, such a circulation could be appreciable, but the extent to which such forces could operate to maintain a macroscopic circulation through the pores of an aquifer is not clear. Moreover, a circulation was postulated much earlier by Drabbe and Badon Ghyben (1889) in their report describing what was later to become known as the Ghyben-Herzberg principle. This report contains the passage:

> Perhaps one is therefore not far from the truth in assuming that, in the deeper layers also, two currents exist and have existed for many centuries. The one, by far the more powerful, consisting of sweet water going from the dunes to the Zuiderzee; under this at the Zuiderzee coast, a weak, brackish water current directed inland that mingles there with the lowest part of the first mentioned stream.

The theoretical considerations or field information that led to this conclusion are not clear from this report. There can be no doubt, however, that both Senio (1951, p. 175) and Carrier (1958, p. 484) properly related a circulation to dispersion. Senio, on the basis of an analysis of field data, postulated a landward flow which he explains as follows:

> This may be due to the diffusion across boundary of the brine water, the diffusion being more intense in moving water than in still water, * * *. But the diffusion is not the only cause, as the upper region above the Herzberg's boundary is occupied with fresh water. It may be related to the fluctuation of water level and to the water of Lake Nakanoumi.

Carrier reasoned that the seaward discharge of salty water from the zone of diffusion must be balanced by an inflow of sea water.

Aside from purely scientific aspects, the circulation of sea water in a coastal aquifer has several practical implications. First, the landward part of this circulation, being accompanied by head losses, causes the toe of the salt-water wedge to be displaced seaward of the position of the interface that would exist in the absence of dispersion. Second, the landward flow, persisting over a long period of time, could alter the lithology of some aquifer materials through ion exchange. Third, the circulation would warrant consideration in connection with proposals to inject radioactive wastes into the salt water in coastal aquifers under the supposition that such water is essentially static.

The Geological Survey, therefore, began to investigate the phenomenon in 1957. The investigation consisted of a field study of the patterns of flow, head, and salt concentration in the Biscayne aquifer near Miami, Fla., and a mathematical program to obtain solutions for the patterns of flow and concentration when considering the effects of dispersion. Also, to provide a basis for comparing the position of the diffused salt-water front with that of the interface that would occur in the absence of diffusion, solutions for the interfaces under a variety of conditions were derived.

The idea of a circulation due to the dispersion constitutes the first section of the report (p. C1–C12). The second section (p. C12–C32) gives the results of the field investigation of this phenomenon. The third (p. C32–C35) and fourth (p. C35–C70) sections present mathematical solutions for the position of the sharp interface that would occur in the absence of diffusion, and the fifth treats the effects of dispersion (p. C70–C82). The ideas and findings have been published in part and in preliminary form in the Journal of Geophysical Research and in Publication 52 of the International Association of Scientific Hydrology. (See papers by Cooper, Kohout, Henry, and Glover in "References.")

CONTENTS

ILLUSTRATIONS

TABLES

RELATION OF SALT WATER TO FRESH GROUND WATER

SEA WATER IN COASTAL AQUIFERS

A HYPOTHESIS CONCERNING THE DYNAMIC BALANCE OF FRESH WATER AND SALT WATER IN A COASTAL AQUIFER

By HILTON H. COOPER, JR.

ABSTRACT

The dispersion of salts produced by reciprocative motion of the salt-water front in a coastal aquifer induces a flow of salt water from the floor of sea into the zone of diffusion and back to the sea. The head losses that accompany the landward flow tend to lessen the extent to which the salt water occupies the acquifer.

INTRODUCTION

Published explanations of the steady-state balance between salt water and fresh water in a coastal aquifer begin with Badon Ghyben (1889) and Herzberg (1901) and commonly assume that the salt water is static. Under this assumption the balance would be as shown in figure 1. The depth below sea level to a point on the interface would be (Hubbert, 1940, p. 872)

$$z=\frac{\rho_f}{\rho_s-\rho_f}h,$$

where ρ_f is the density of the fresh water, ρ_s is the density of the sea water, and h is the head of fresh water above sea level at the point on the interface. An equation for determining the shape and position of the interface with a known rate of discharge of fresh water under one set of boundary conditions has been devised by Glover (see p. C32–C35, this report) through an adaptation of a solution by Kozeny (1953) for an analogous problem of free-surface gravity flow. Equations for the interface under several sets of boundary conditions have been derived by Henry. (See p. C35–C70.)

It is the thesis of this paper that where a zone of diffusion exists, the salt water is not static but flows perpetually in a cycle from the floor of the sea into the zone of diffusion and back to the sea. This flow tends to lessen the extent to which the salt water occupies the aquifer.

This cycle must exist to some degree if salty water continuously discharges from the zone of diffusion into the sea (fig. 2). If such a discharge exists, the sea itself must be the source of the salts that are carried back to the sea, and the salts must be transported from the floor of the sea through the aquifer into the zone of diffusion. Any

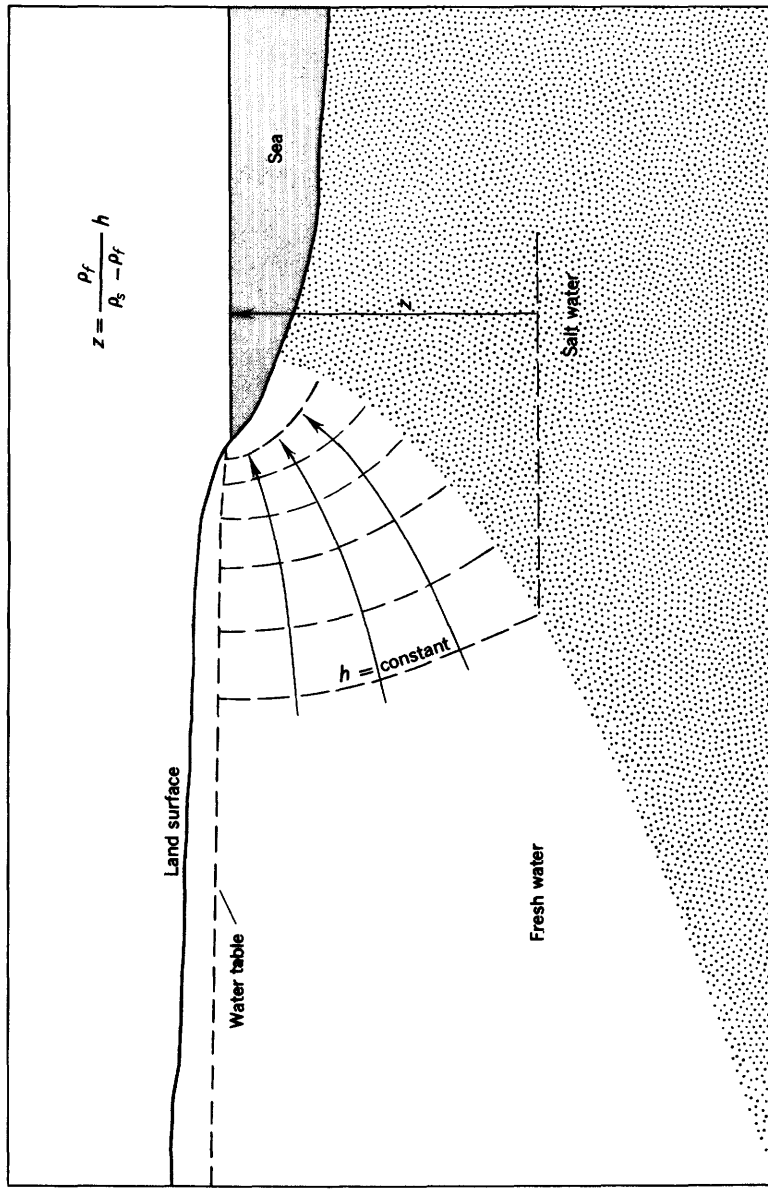

FIGURE 1.—Balance between fresh water and salt water in a coastal aquifer in which the salt water is static.

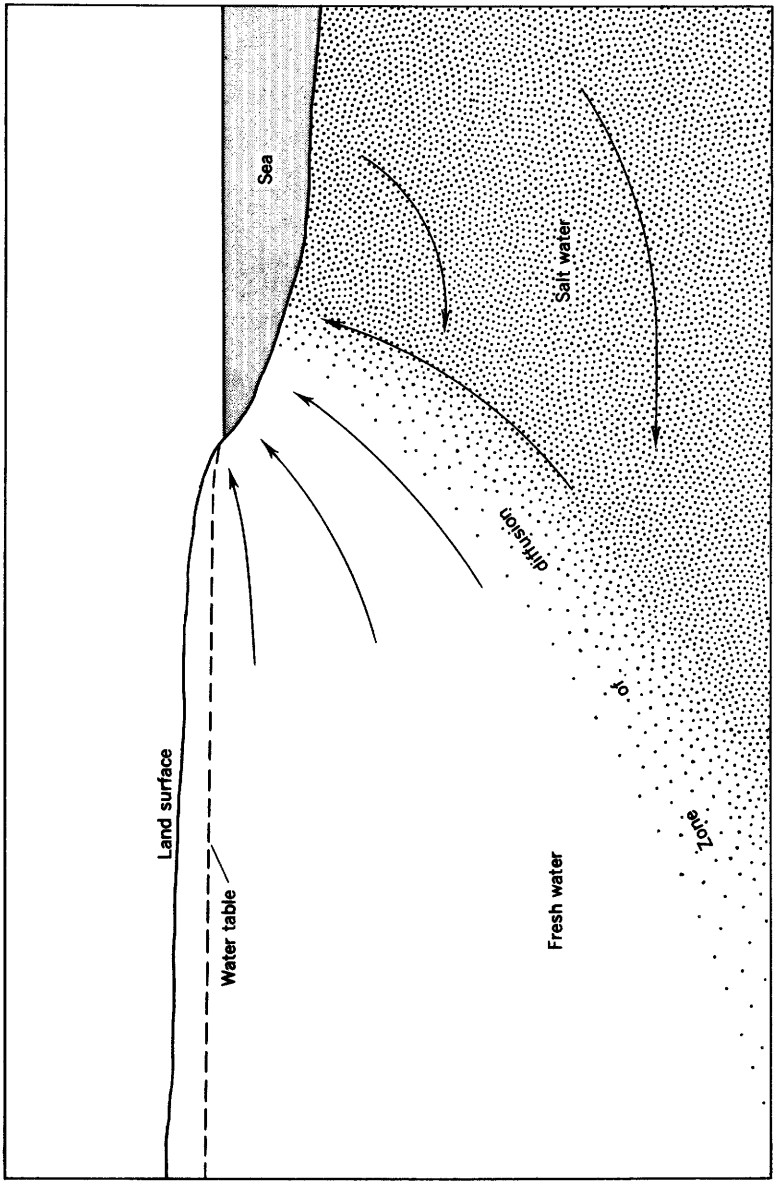

FIGURE 2.—Circulation of salt water from the sea to the zone of diffusion and back to the sea.

form of dispersion or diffusion as the principal mode of transportation of the salts from the sea to the zone of diffusion may be eliminated because these processes occur only in the presence of a concentration gradient, and the concentration gradient that exists across the zone of diffusion will not generally extend in sufficient magnitude all the way back to the sea floor. Therefore, the salts are transported largely by a flow of the salt water, as indicated in figure 2, with a consequent loss of head in the salt-water environment.

One example of a discharge of salty water from the zone of diffusion is the flow of springs around Pearl Harbor, Hawaii. Ordinarily, most of the seaward discharge of water from a coastal aquifer occurs at the floor of the sea, but around Pearl Harbor the discharge issues from terrestrial springs as the result of the presence of the caprock, a nearly impervious blanket of weathered volcanic debris that underlies and rims the harbor and forces some of the ground water from the basaltic aquifer to discharge in springs along its inland perimeter. Typical of these is Waimano Springs (fig. 3), consisting of several orifices that yield water of different salinities. The total flow from the several orifices of Waimano Springs ranges from 15 to 20 million gpd (gallons

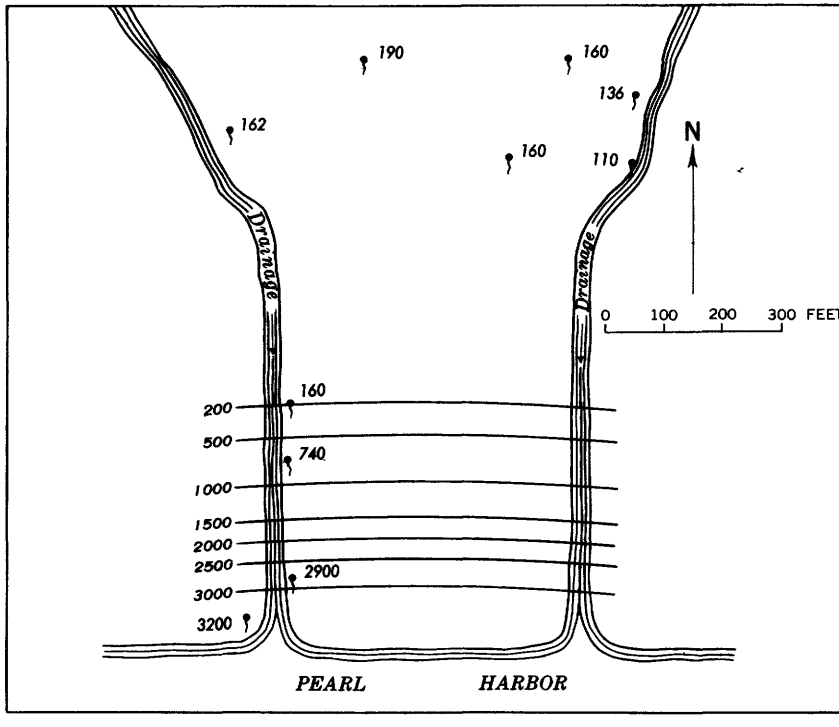

FIGURE 3.—Map of Waimano Springs, Oahu, Hawaii, showing the chloride content of water from orifices, 1957; lines and figures represent the chloride content, in parts per million.

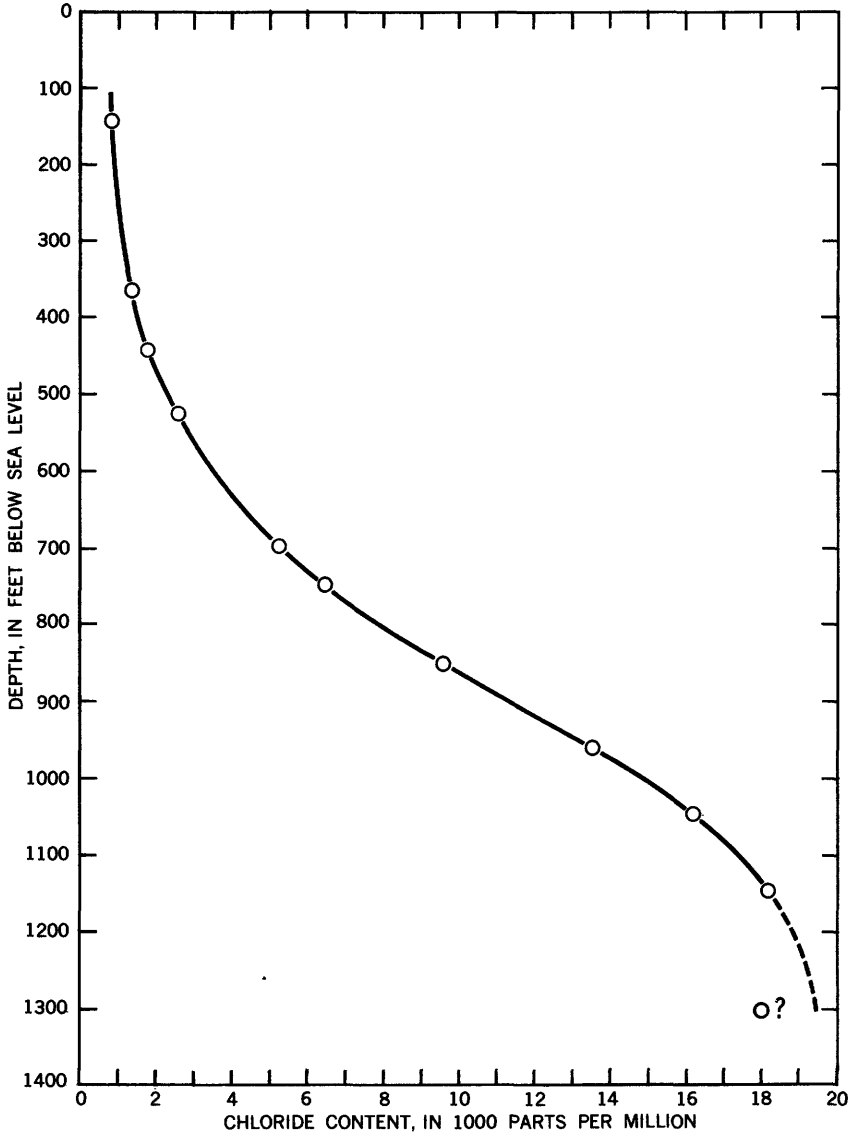

FIGURE 4.—Chloride content of water in a test well at Pearl Harbor, 1958.

per day). The water from these orifices increases in salinity toward the sea, and the chloride content ranges from less than 200 ppm (parts per million) at the orifices farthest inland to as much as 3,000 ppm at the one nearest the shore. The chloride content of sea water at most places is about 19,000 ppm.

The great thickness of the zone of diffusion beneath the Pearl Harbor area is indicated by figure 4, which shows the choride content

of water at various depths as determined from the drilling of a deep test well. The zone beings at a depth of about 200 feet and ends at perhaps 1,200 feet; thus it has a thickness of 1,000 feet or more.

Another place at which there is evidence of discharge from the zone of diffusion is the Cutler area near Miami, Fla. The zone of diffusion in the Biscayne aquifer of this area—an aquifer that consists predominantly of cavernous limestone—is represented by the isochlors in figure 5. The control points for the isochlors are shown by the black dots which represent the bottoms of fully cased wells. These wells were drilled to extract water samples and to measure presssure heads at isolated depths, as a part of an investigation by the U.S. Geological Survey of the various factors relating to the hypothesis described in this paper. The thickness of the zone of diffusion is limited by the thickness of the aquifer, but its horizontal breadth at the base of the aquifer, as reckoned from the isochlors, is probably about 2,000 feet. The zone extends several hundred feet beyond the shoreline. The distributon of salts is doubtless influenced by the presence of beds of low permeability in the aquifer.

As most of the seaward discharge from the Biscayne aquifer occurs at the floor of the sea, there is no opportunity to obtain representative samples to determine the salinity of the water being discharged. Nevertheless, that salty water is being discharged can be inferred from the fact that the shallow wells which end in the zone of diffusion beneath the floor of the sea tap salty water under sufficient head to rise above sea level.

ACKNOWLEDGMENTS

The author is grateful to D. A. Davis and F. N. Visher of the U.S. Geological Survey at Honolulu for their generous permission to publish figures 3 and 4 prior to their own publication of their findings. He is indebted to F. A. Kohout of the U.S. Geological Survey at Miami for the collection and compilation of the data shown in figure 5, and to R. E. Glover of the U.S. Geological Survey at Denver for suggesting the equation for the tide-produced displacement of water in a coastal aquifer. Richard Skalak, of Columbia University, reviewed the manuscript and made helpful suggestions.

MECHANICS OF THE CYCLIC FLOW OF SEA WATER

What causes the sea water to move in its cycle through the aquifer? Since the water has the same fluid potential when it reenters the sea as when it leaves, one might reason that there can be no hydraulic gradient and hence no flow. To understand how a flow may exist under these circumstances, consider the processes that operate in the zone of diffusion. Sea water and fresh water become intimately mixed in the zone of diffusion by the mechanism that creates this zone.

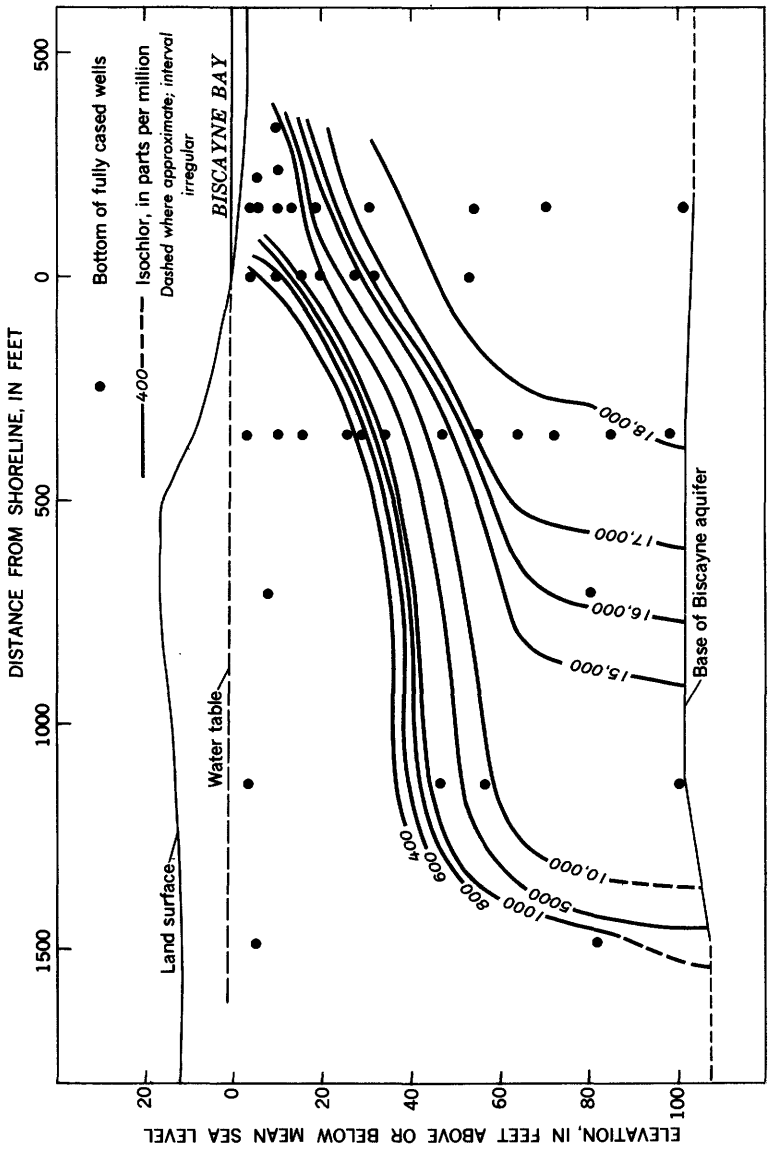

FIGURE 5.—Section through the Cutler area, near Miami, Fla., showing the zone of diffusion, September 8, 1958.

The effect of this is the same as if some of the salt ions were extracted from the sea water and injected into the flowing fresh water. The diluted sea water, becomes less dense than native sea water and rises along a seaward path. The resulting circulation is analogous to the circulation in thermal convection, differing only in that changes in density are produced by changes in concentration rather than by changes in temperature. Meanwhile, the salts that are introduced into the fresh-water environment are carried back to the sea by the flow of the fresh-water system.

The circulation, therefore, is induced by the transfer of salts out of the salt-water environment. The forces that effect this transfer must be powerful enough to recreate the zone of diffusion continuously as it is dissipated by the flow of mixed water to the sea. Molecular diffusion is much too feeble for this.

DISPERSION

A mechanism that appears powerful enough to cause sufficient mixing is the reciprocative motion of the salt-water front resulting from ocean tides and from the rise and fall of the water table due to variations in recharge and other forces, including pumping. Palmer (1927, p. 51–52) and Wentworth (1948) theorized that this to-and-fro motion creates the zone of diffusion. The process by which two miscible liquids interfuse about their boundary when hydraulic flow causes the boundary to move is known as dispersion. In laminar flow through permeable porous media, dispersion results from the combined effects of convection (transfer of a fluid into the region of another due to variations in velocities within the interstices) and molecular diffusion (Taylor, 1953, p. 187). During a movement of the salt-water front in either direction, the convection component of dispersion causes elements of each fluid to be transferred into the opposite environment, wherein to a large extent they become inseparably blended with the other fluid by mixing and molecular diffusion. If the displaced elements were not blended, but if, instead, they were to remain discrete during and after the transfer, the potential gradients acting upon them in the foreign environments would drive each back to its original environment. Furthermore, the dispersion would be mostly negated at each reversal of motion if the elements were to retain their identity in continuous filaments and retrace their path. Thus, both convection and molecular diffusion are important parts of the dispersion process—convection in producing large transfers, and molecular diffusion in completing the blending.

From the results of their experiments with Ottawa and Monterey sands, Rifai, Kaufman, and Todd (1956) concluded that the coefficients of longitudinal dispersion (dispersion in the direction of flow)

with unidirectional flow in granular permeable media is practically proportional to the mean velocity of flow, so that $D=Mv^n$, where D is the coefficient of dispersion, M is a constant whose magnitude depends on the properties of the medium, v is the mean interstitial velocity, and the exponent n is approximate unity. They found the values of M to be 0.063 cm (centimeter) for Ottawa sand and 0.13 cm (computed from their table 5; the value of 0.013 cm given in their fig. 18 appears to be incorrect) for Monterey sand. Experiments by Orlob and Radhakrishna (1958) indicate that the medium dispersion constant M increases with the uniformity coefficient of the medium and becomes as high as 2.79 cm for a sand having a uniformity coefficient of 3.88.

If the coefficient of longitudinal dispersion is proportional to the first power of the mean interstitial velocity, it may, in the case of dispersion due to ocean tides, be expressed as

$$D=4MA/t_0, \tag{1}$$

where A is the amplitude, and t_0 is the period of the displacement of water in the aquifer caused by ocean tides.

The amplitude of the tide-produced displacement of water may be related approximately to the amplitude of the tide and the distance from the shoreline as follows. The tide-produced change in the artesian head with reference to its mean in a semi-infinite artesian aquifer is (Jacob, 1950, p. 365; Ferris, 1951, p. 149)

$$h=h_0 \exp\left(-x\sqrt{\pi S/t_0 T}\right)\cdot\sin\left(2\pi t/t_0-x\sqrt{\pi S/t_0 T}\right),$$

where

h_0=amplitude of the tide,
x=distance from the shoreline,
t_0=period of the tidal cycle,
t=time referred to the beginning of a tidal cycle,
S=coefficient of storage, and
T=coefficient of transmissibility.

The gradient producing the displacement will therefore be

$$\frac{\partial h}{\partial x}=-h_0\sqrt{\pi S/t_0 T}\exp\left(-x\sqrt{\pi S/t_0 T}\right)\cdot\left[\sin\left(2\pi t/t_0-x\sqrt{\pi S/t_0 T}\right)+\cos\left(2\pi t/t_0-x\sqrt{\pi S/t_0 T}\right)\right].$$

The displacement will be zero at a time t_1 when $\partial h/\partial x$ is a maximum or when the quantity in parentheses is $\pi/4+n\pi$. It will be extreme at a time t_2 when $\partial h/\partial x=0$ or when the quantity in parentheses is $3\pi/4+n\pi$. Thus, with the substitutions

$$u=2\pi t/t_0-x\sqrt{\pi S/t_0 T}$$
$$du=2\pi dt/t_0,$$

the amplitude of the displacement will be

$$A = K/\theta \int_{t_1}^{t_2} (\partial h/\partial x)\, dt$$

$$= (Kh_0/\theta)\sqrt{t_0 S/4\pi T}\, \exp\, (-x\sqrt{\pi S/t_0 T}) \cdot \int_{\pi/4}^{3\pi/4} (\sin u + \cos u)\, du$$

$$= (Kh_0/\theta)\sqrt{t_0 S/2\pi T}\, \exp\, (-x\sqrt{\pi S/t_0 T}), \qquad (2)$$

where K is the permeability and θ is the effective porosity of the aquifer.

The coefficients of tide-produced dispersion at given distances from the shoreline in a typical coastal aquifer may be estimated by using equations 1 and 2 and assuming that the medium dispersion constants obtained from experiments with unidirectional flow are applicable and that the displacements of the interface will be the same as the displacements that would occur if the water in the aquifer were all of one density. The latter assumption seems reasonable because, in most aquifers, the interface will move very slowly in response to changes in head and its maximum displacement will be only a fraction of that which would be required for it to adjust completely to the extremes of the tide. Equation 2 was derived for artesian aquifers but probably will give a fair approximation of the amplitude of the displacement in a nonartesian aquifer if an appropriate value for the coefficient of storage is used.

The amplitude of the oscillation of water at various distances from the shoreline in a hypothetical nonartesian aquifer of sand is illustrated in figure 6. If the medium dispersion constant of the sand were 1.0 cm, the coefficient of dispersion would be 100 cm^2 per day at about 300 feet from the shoreline and 10 cm^2 per day at about 900 feet from the shoreline. Beyond 1,400 feet it would not be significantly larger than 1 cm^2 per day, which is approximately the coefficient of molecular diffusion of sodium chloride (Hodgeman, 1945, p. 1695).

It is likely, however, that in aquifers that consist of alternate beds of high and low permeabilities, as practically all aquifers do, there is a mixing mechanism that will produce rates of dispersion much larger than those indicated by laboratory experiments on unidirectional flow through homogeneous sand. Suppose, for example, that an aquifer is made up of alternate beds having permeabilities in the ratio of 10 to 1 and that initially a sharp interface lies diagonally across the beds. If, with a rise of the tide, the interface were to move landward a distance of x units in a bed of high permeability, it would move only about $0.1x$ units in an adjacent bed of low permeability. Consider, now, what would happen if the fresh water were then to begin flowing in a direction diagonally across the beds in an upward path toward the sea. Apparently, the water in the various beds would become

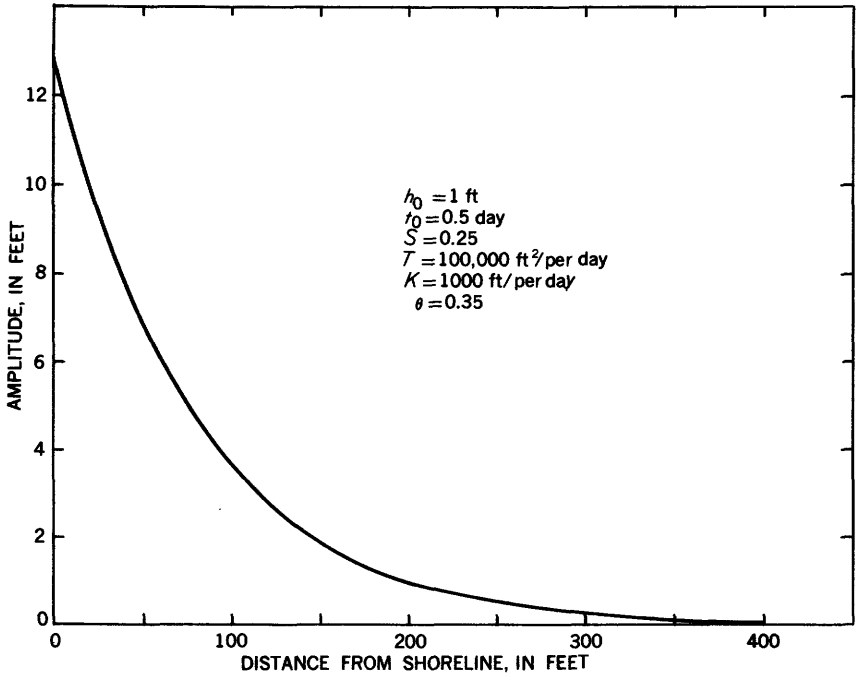

FIGURE 6.—Amplitude of tide-produced motion of water in a coastal aquifer.

fairly well mixed, so that there would result a zone nearly x units wide in which the concentration of salts would be some fraction of that of sea water. This fraction would be dependent on the relative thicknesses and porosities of the beds. With each additional tidal cycle the zone would widen further until ultimately the distribution of salts would come to a steady state wherein the average rate at which the salts were carried into an element of the aquifer by dispersion would be in balance with the rate at which they were carried out of it by hydraulic flow. The rate of dispersion produced by this process would doubtless be greater in an aquifer of cavernous limestone or basalt than in one of laminated sand.

The reader will understand that the hydraulics are more complicated than postulated here. The example given is merely a device to illustrate the idea of dispersion by differential displacement and cross-bed mixing. The displacements and mixings will not, of course, occur as separate alternate events but will operate simultaneously much of the time, each playing a more prominent part in one phase of the tidal cycle than in another.

SUMMARY

Wherever a zone of diffusion exists in a coastal aquifer, sea water will flow from the floor of the sea into a zone of diffusion. The flow

may be interrupted or reversed during low stages of the tide or high stages of the water table, but on the average it will persist in a landward direction. Apparently, the only question in a given case is one of magnitude. The magnitude of the flow evidently will be governed chiefly by that of the dispersing mechanism that induces it, and it may be large enough in some places to produce head losses in the salt-water environment that would lessen appreciably the extent to which the salt water occupies the aquifer.

THE FLOW OF FRESH WATER AND SALT WATER IN THE BISCAYNE AQUIFER OF THE MIAMI AREA, FLORIDA

By FRANCIS A. KOHOUT

ABSTRACT

Investigations in the coastal part of the Biscayne aquifer, a highly productive aquifer of limestone and sand in the Miami area, Florida, show that the salt-water front is dynamically stable as much as 8 miles seaward of the position computed according to the Ghyben-Herzberg principle. This discrepancy results, at least in part, from the fact that the salt water in the Biscayne aquifer is not static, as explanations of the dynamic balance commonly assume. Cross sections showing lines of equal fresh-water potential indicate that during periods of heavy recharge, the fresh-water head is high enough to cause the fresh water, the salt water, and the zone of diffusion between them to move seaward. When the fresh-water head is low, salt water in the lower part of the aquifer intrudes inland, but some of the diluted sea water in the zone of diffusion continues to flow seaward. Thus, salt water circulates inland from the floor of the sea through the lower part of the aquifer becoming progressively diluted with fresh water to a line along which there is no horizontal component of flow, after which it moves upward and returns to the sea.

This cyclic flow is demonstrated by a flow net which is constructed by the use of horizontal gradients determined from the low-head equipotential diagram. The flow net shows that about seven-eighths of the total discharge at the shoreline originates as fresh water in inland parts of the aquifer. The remaining one-eighth represents a return of sea water entering the aquifer through the floor of the sea.

INTRODUCTION

Investigations during the past 20 years confirm that the salt-water front in the Biscayne aquifer is dynamically stable as much as 8 miles seaward of the position computed by either the Ghyben-Herzberg principle or the theory of dynamic equilibrium (fig. 7). The concept of dynamic balance between flowing fresh water and static sea water in a coastal aquifer is shown in figure 1.

Recent studies indicate that the lack of agreement results from the fact that two assumptions inherent in the Ghyben-Herzberg and dynamic-equilibrium concepts are not fulfilled in the Biscayne aquifer. These assumptions are (1) that a sharp interface exists between fresh water and salt water in a coastal aquifer and (2) that the salt water in a coastal aquifer is static. As hypothesized by Cooper

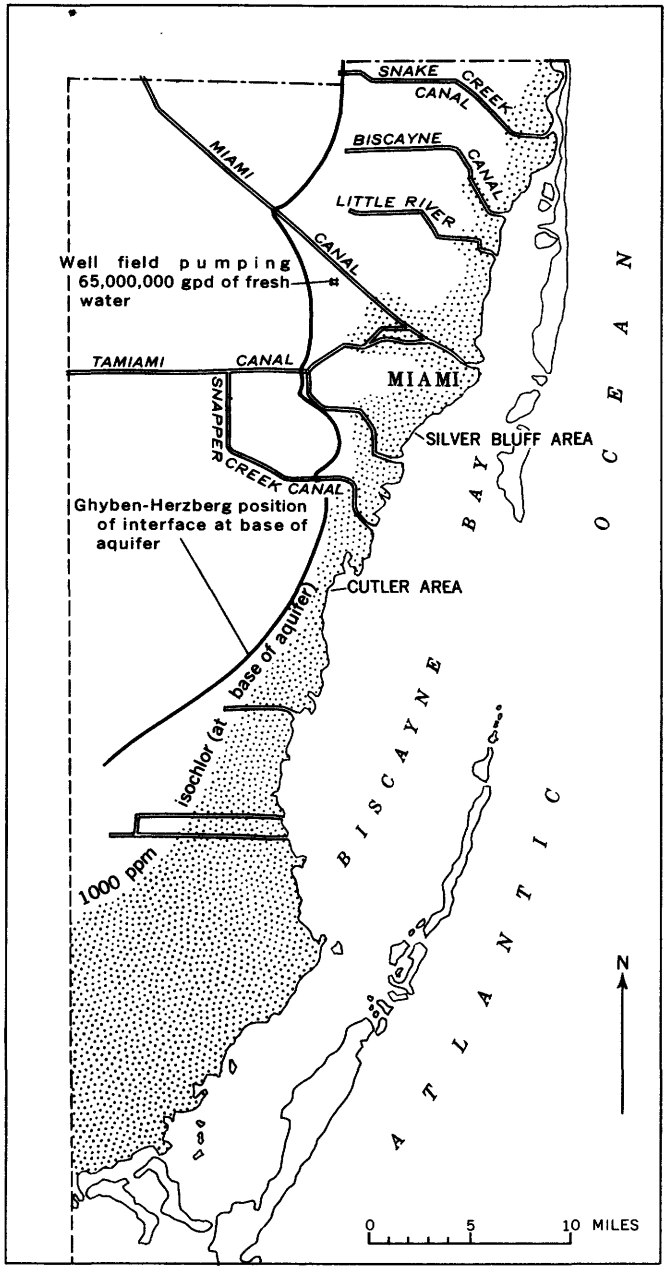

FIGURE 7.—Map of the eastern part of Dade County, Fla., showing the theoretical Ghyben-Herzberg position and the actual position of salt water at the base of the Biscayne aquifer.

(see p. C1–C12, this report), a circulation of salt water is induced by the dispersion of salts produced by the reciprocative motion of the salt-water front due to tidal action. Henry (see p. C70–C84) has confirmed this circulation analytically.

This section of the report describes the characteristics of flow in the Biscayne aquifer of the Miami area and, by a flow net constructed from field data, shows the pattern of fresh and salt water flow for a low-head condition.

ACKNOWLEDGMENTS

The writer is grateful to H. H. Cooper, Jr., N. D. Hoy, and Howard Klein of the U.S. Geological Survey for advice and review of the paper. He is indebted to Richard Skalak of Columbia University for suggesting the method of constructing the flow net.

GEOLOGIC AND HYDROLOGIC CHARACTERISTICS OF THE BISCAYNE AQUIFER

The Biscayne aquifer consists of solution-riddled limestone and calcareous sandstone. It is a water-table aquifer and extends from land surface to an average depth of 100 feet below mean sea level. In general, the coefficient of permeability ranges from 50,000 to 70,000 gpd per sq ft (Parker, 1951, p. 824).

THE ZONE OF DIFFUSION

In the Biscayne aquifer the zone of diffusion is a thick zone in which there is a gradation of salt content from that of fresh water, which contains 16 ppm chloride, to that of sea water, which contains about 19,000 ppm chloride. Figures 8 and 9 are cross sections through the zone of diffusion in the Silver Bluff and Cutler areas; the location of these areas is indicated in figure 7.

The distance from the bay to the inland tow of the saltwater wedge is more than 12,000 feet in the Silver Bluff area but only about 1,600 feet in the Cutler area. The toe of the wedge has a blunted shape in both areas. As pointed out by Henry (see p. C70–C84) this configuration results partly from the boundary requirement that no dispersion or diffusion may occur across the impermeable base of the aquifer, so that isochlors must approach the base of the aquifer perpendicularly.

SEAWARD FLOW OF SALTY WATER

The fluctuation of chloride content in well G 519A, which is 400 feet from Biscayne Bay in the Silver Bluff area, is shown in figure 10 (see fig. 8 for the position of the open-hole part of well G 519A). The rapid decrease in chloride content at the three sampling depths during October 1953 resulted from a large increase in fresh-water head following heavy rainfall in early October. After the rain,

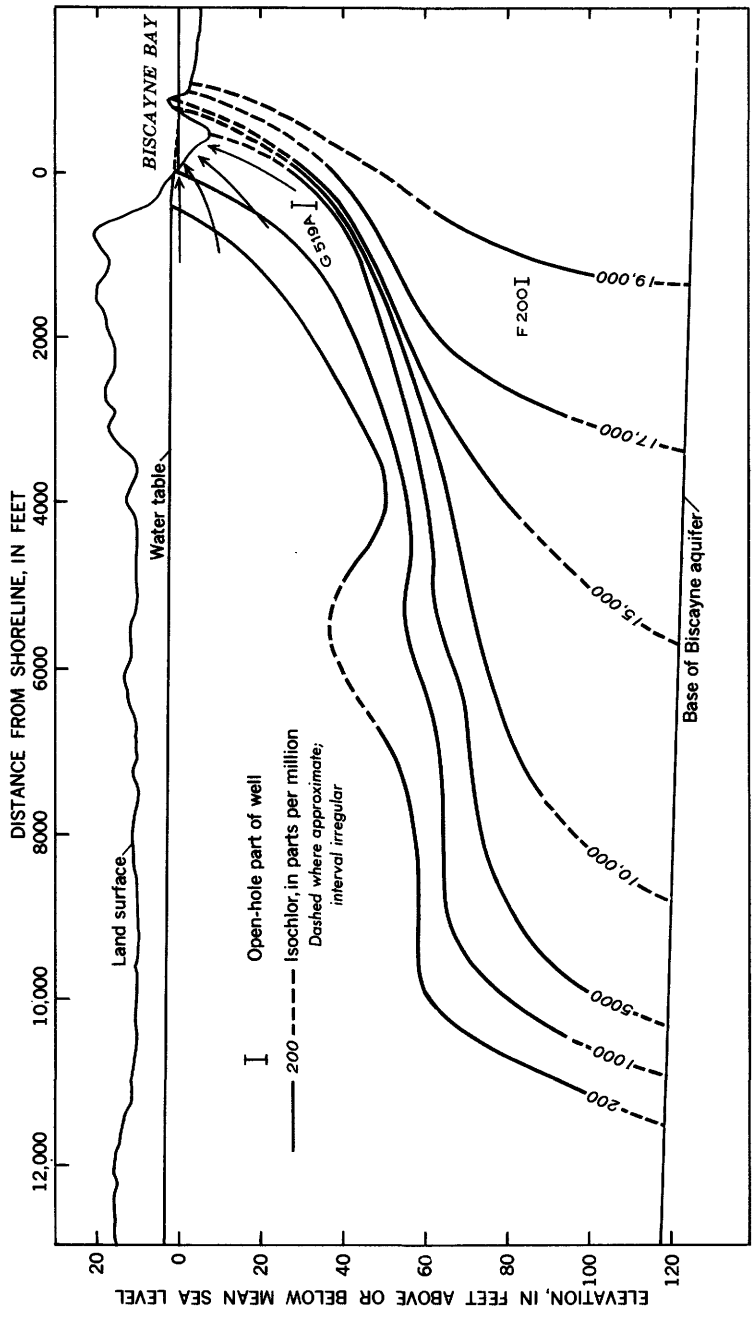

FIGURE 8.—Cross section through the Silver Bluff area, near Miami, Fla., showing the zone of diffusion, November 2, 1954.

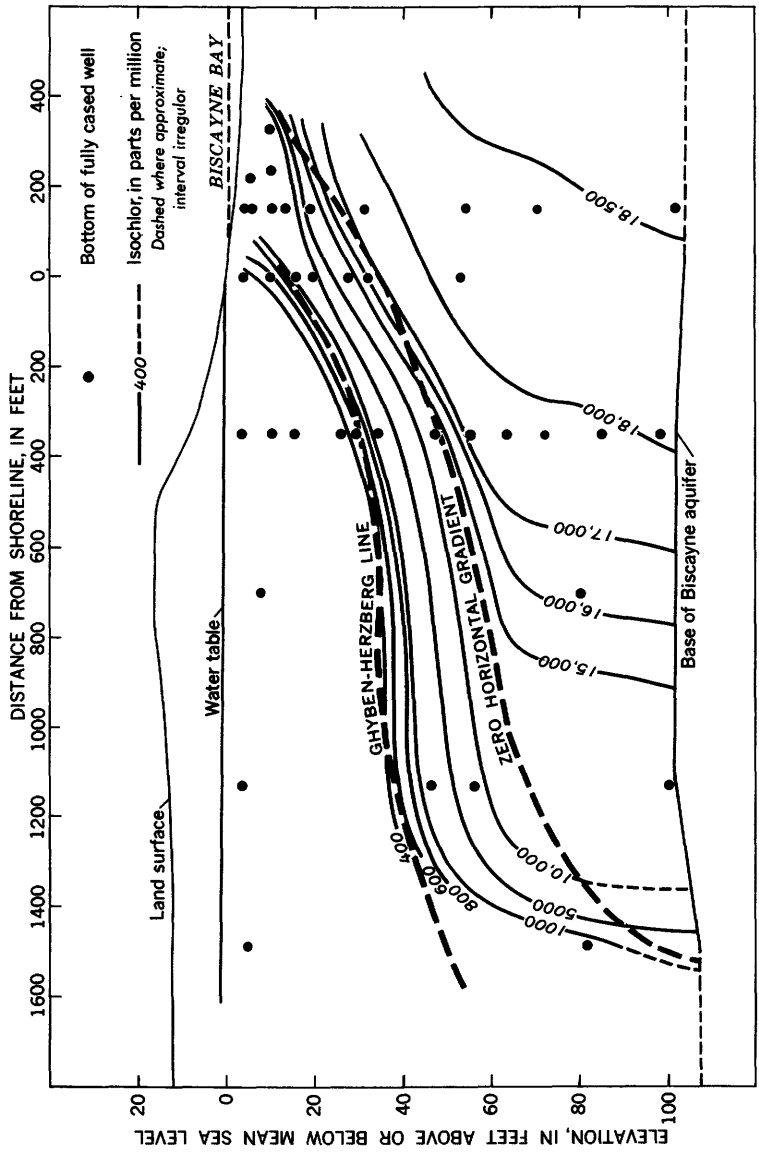

FIGURE 9.—Cross section through the Cutler area, near Miami, Fla., showing the position of the line of zero horizontal gradient (traced from fig. 17) within the zone of diffusion, September 18, 1958.

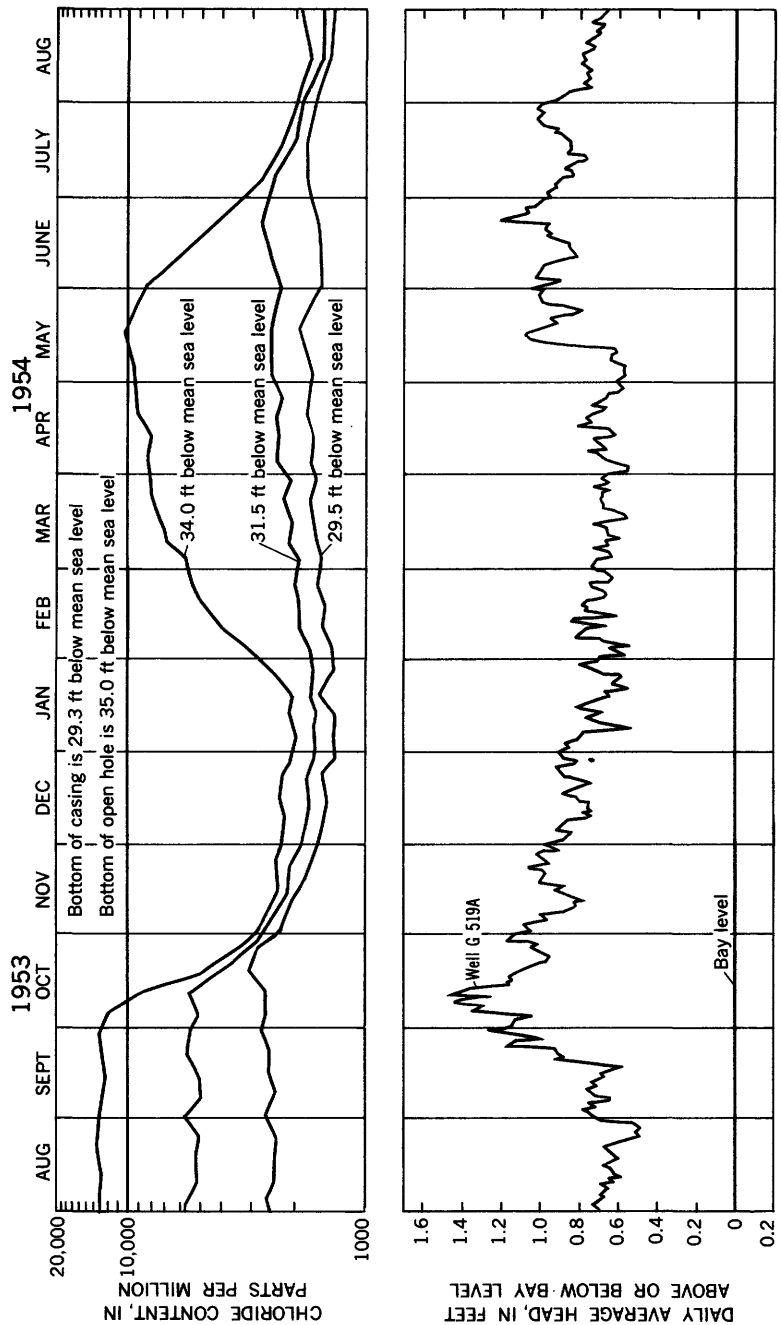

FIGURE 10.—Graph showing fluctuations of chloride content and water level in well G 519A in the Silver Bluff area, near Miami, Fla.

salt water was rapidly expelled from the aquifer, and the zone in which the concentration gradient is steep (immediately below well G 519A in fig. 8) was depressed downward and seaward.

A ground-water velocity test using fluorescein dye as a tracer was performed at the site of well G 519A on January 4, 1954. The results of the test indicated that water containing 1,500 to 2,000 ppm chloride (in the open-hole part of well G 519A, fig. 8) was flowing seaward at a rate of more than 70 fpd (feet per day). This is significant in that it demonstrates a large discharge of salt from the zone of diffusion.

A rough calculation of the quantity of salt being discharged at the shoreline is pertinent. If the base of the zone in which water flows seaward in the Silver Bluff area is assumed to be at the 5,000 ppm isochlor (fig. 8), the thickness of this zone at well G 519A is about 35 feet. If the average velocity through this thickness is 70 fpd and the effective porosity of the limestone is 0.2, then the seaward discharge of water in a vertical strip 1-foot wide is 490 cubic fpd.

From figure 8, the average chloride content of the water discharging at the shoreline is about 1,900 ppm. Ten units of water having a chloride content of 1,900 ppm contains about the same quantity of salt as one unit of sea water, which has a chloride content of about 19,000 ppm. Therefore, in the 1-foot strip, roughly 49 cubic fpd of ocean water must become incorporated into the seaward flow. This calculation indicates that as much as 10 percent of the total seaward flow may be sea water.

DISPERSION

As observations show that the diffused zone remains essentially unchanged while large quantities of salt are flushed back to the sea, a mechanism much stronger than molecular diffusion is acting to recreate the zone of diffusion.

In recent years, extensive studies have been made of the process of dispersion. This process consists of two separate mechanisms: convection, the mechanical transfer of one fluid into the region of another, and molecular diffusion (Bosworth, 1949, p. 465). During the to-and-fro movement of the salt-water front that results from ocean tides, variations of fluid velocity in the pores of a permeable medium cause an intermingling of fluids of different concentration, after which the blending is completed by molecular diffusion. As shown in figure 11, tidal fluctuations decrease landward. (See fig. 9 for the location of the bottoms of wells.) Consequently, the rate of dispersion created by the tide also decreases landward.

As shown by Cooper (see p. C1–C12), the coefficient of dispersion due to tides can be as much as 100 times greater than molecular diffusion in an aquifer of homogeneous sand and even greater in an

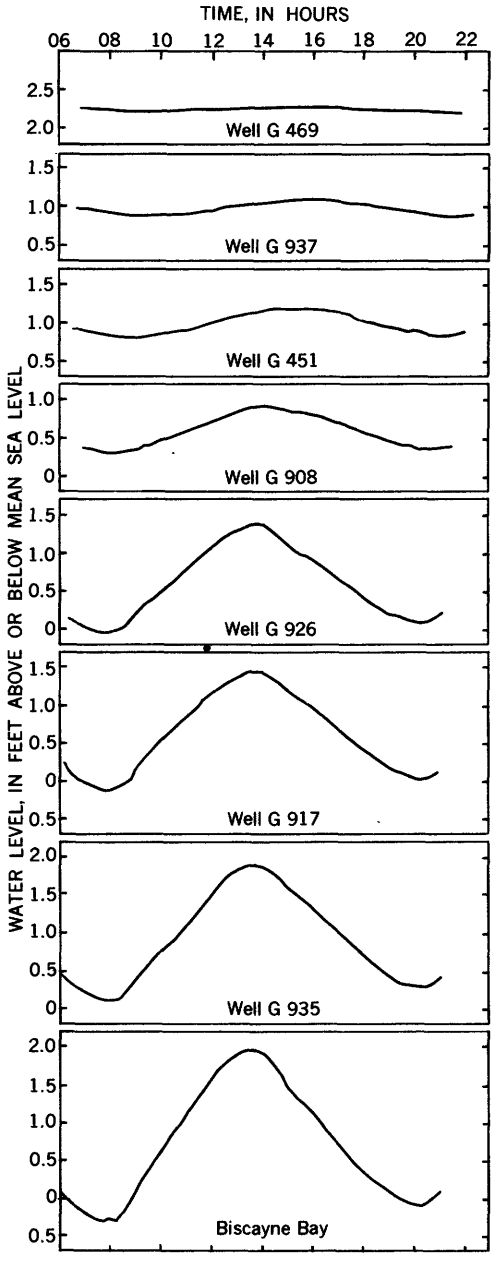

FIGURE 11.—Hydrographs showing the landward decrease in tidal fluctuation in the Cutler area, near Miami, Fla., September 18, 1958.

aquifer of nonuniform permeability. In the suggested mechanism, elements of salt water under tidal stimulus move greater horizontal distances in permeable beds than in adjacent less permeable beds, and the salt-water projections thus formed will be integrated by the upward cross-bed flow of fresh water.

Movement of ground water caused by the tide has both horizontal and vertical components. Clearly, a mechanism that permits very rapid transportation and dispersion of salt is available.

HYDRAULIC GRADIENT IN THE SALT-WATER ZONE

SILVER BLUFF AREA

Evidently the dispersion must occur at a rate great enough to maintain the zone of diffusion while a large quantity of salt water discharges seaward. To maintain this equilibrium, some means of transporting the salts from the floor of the sea through the aquifer and into the zone of diffusion must be available. However, in the regions below and seaward of the zone of diffusion (figs. 8, 9) the concentration gradient is too small to make possible the transportation of a large quantity of salt by dispersion. Therefore, the transportation of salts must be by a flow of water and be accompanied by a loss of head.

In figure 12, the daily-average water level and head in well F 200 is compared with the daily-average water level and head in Biscayne Bay. The chloride content of water in the well ranged from 18,300 to 18,800 ppm during the period shown. The water level in the well, which closely represents the head of ocean water in the aquifer, is higher than the surface of the bay during periods of heavy rainfall, as shown by the unblackened intervals in figure 12*A*, and lower than the bay during dry periods, as shown by the blackened intervals. In figure 12*B*, the daily-average head of the water in the bay has been algebraically subtracted from the daily-average head in well F 200, so that the head in the well each day is referred to that in the bay for that day. When the head in figure 12*B* is positive, salt water flows seaward; and when it is negative, salt water flows inland. Clearly, the negative heads reflect the head losses due to the inland flow of sea water through the aquifer.

The head in well G 519A (fig. 10), computed in the same manner as that for well F 200, is never negative. This indicates that the movement of water is always seaward at that point in the aquifer. Therefore, during the intrusion part of the salt-water flow cycle, there must be a line somewhere between the bottoms of these two wells (within the zone of diffusion shown in fig. 8) where the water has the same head as the ocean and where the water is flowing neither inland nor seaward. The water along this line cannot be stagnant,

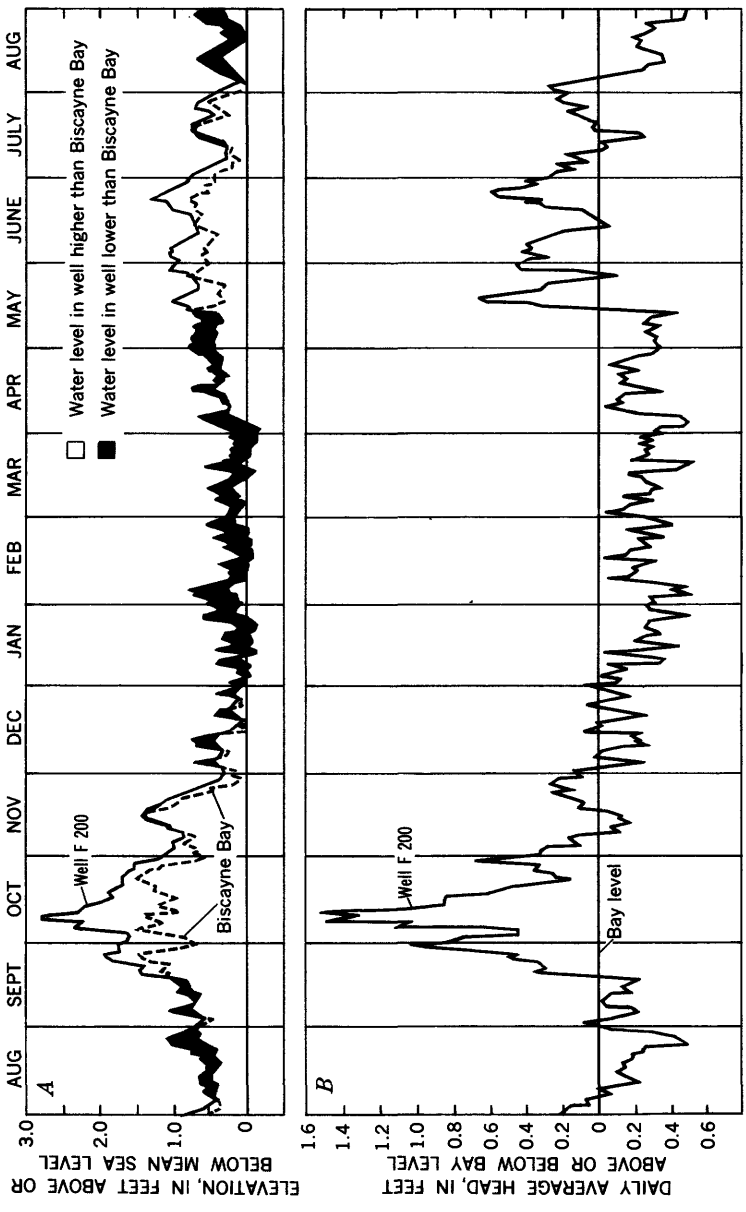

FIGURE 12.—Hydrographs of daily-average water level and head in well F 200 and in Biscayne Bay. *A*, Daily-average water level in well and in bay; *B*, daily-average head in well compared to bay level.

however, because continuity requirements would then be violated; so salt water along this line must be flowing vertically upward. Thus, a cyclic flow of salt water—inland from the floor of the sea to the zone of diffusion and then seaward through the fresh-water flow section—has been demonstrated.

CUTLER AREA

Wells in the Cutler area were drilled as part of the investigation of factors relating to the cyclic flow. These wells were fully cased to make possible the collection of water samples and the measurement of pressure heads at isolated depths. The bottoms of the wells are indicated as dots in the cross sections of the Cutler area (figs. 9, 14–19).

In figure 13, the daily-average fresh-water heads in the salt-water region are referred to the daily-average heads of Biscayne Bay.

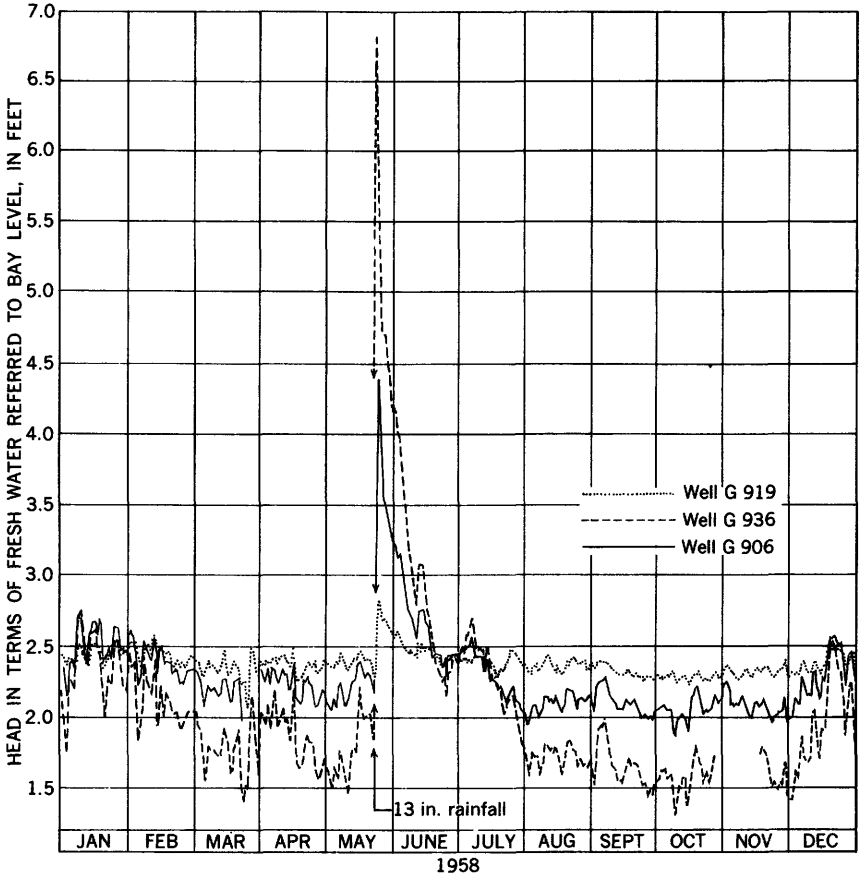

FIGURE 13.—Hydrographs of wells G 906, G 919, and G 936 in terms of equivalent fresh-water head.

Where the density varies from point to point, measurements of head do not indicate the direction of movement directly. For this reason the observed salt-water heads in the wells have been converted to fresh-water heads by computation. Also, the hydrographs of wells G 906 and G 919 have been adjusted for the density of the columns of salt water between the bottoms of the wells (which are 97.9 and 101.5 ft below mean sea level, respectively) and the horizontal plane at 100 ft below sea level in the aquifer. Well G 936 required no adjustment because it terminated at the plane. The heads of the wells as related to the location of the wells (see fig. 9) shows how the gradient—in terms of water of constant density along the plane 100 ft below mean sea level—fluctuated during 1958.

A 13-inch rain in May 1958 produced a large seaward gradient. As the head declined after this rain, the hydrographs crossed at about 2.4 ft; this indicates reversal to a landward gradient. The fresh-water head in static sea water at a depth of 100 ft below mean sea level is 2.5 ft; thus, the gradient in the salt-water region of the aquifer reverses direction at a fresh-water head that compares closely with the theoretical head. The landward gradients show that salt is transported inland from the floor of the sea to the zone of diffusion by a flow of water.

Along the bottom of the aquifer, the salt disperses continuously landward in the direction of decreasing concentration. A seaward flow of water opposes the dispersion, and a landward flow supports it.

POTENTIAL IN THE FRESH-WATER AND SALT-WATER ENVIRONMENTS

Ground water of uniform density moves in the direction of decreasing head, but where the density varies from point to point the distribution of head does not indicate the direction of movement directly. This is illustrated in figure 14, where the figures at the bottoms of the well casings are daily-average water levels referred to the daily-average bay level. The concentration of salt water in the casing is the same as that in the aquifer at the bottom of the casing; the head values, as shown, are the original data. Obviously, all flow cannot converge upon the sink surrounded by the −0.2-foot contour, and diagrams constructed from the original data are not usable.

In figures 15 to 17 the lines of equal fresh-water potential are shown for high, low, and average tide on September 18, 1958. For wells containing salty water, the equivalent head of fresh water has been computed, so that all heads are the same as if the casings had been filled with fresh water at the time of measurement.

719-580 O—64——5

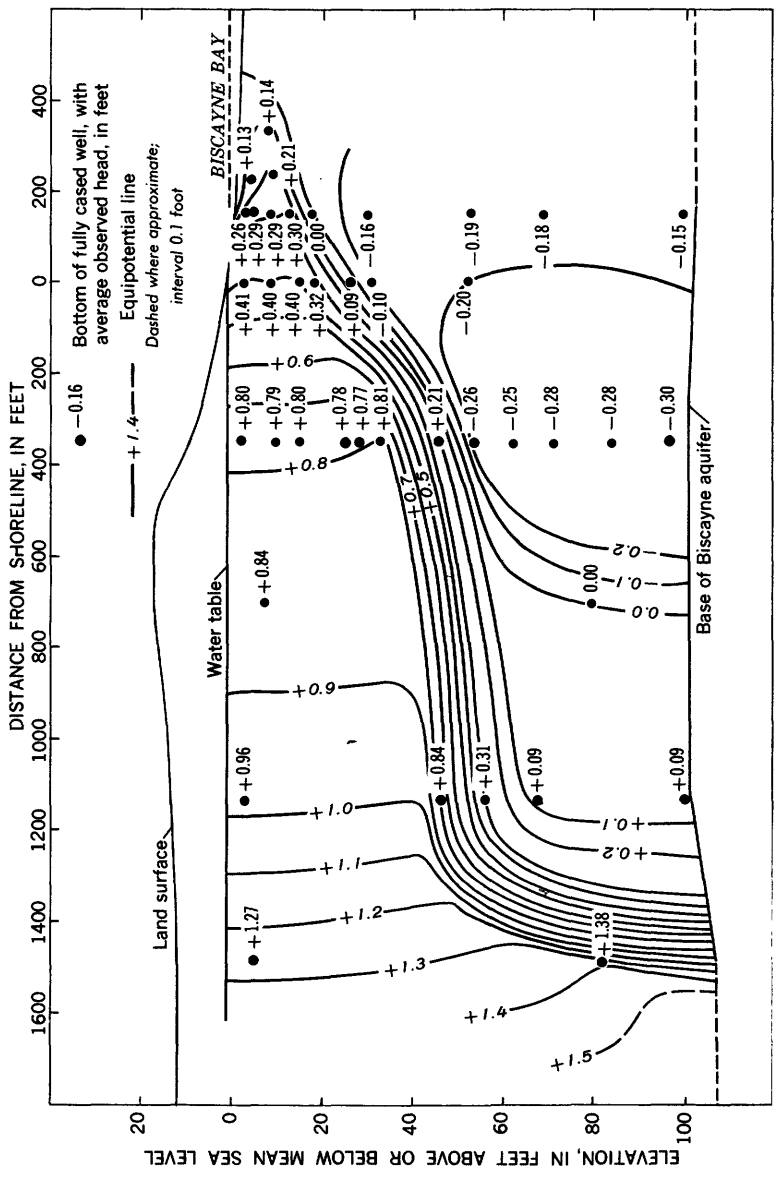

FIGURE 14.—Cross section through the Cutler area, near Miami, Fla., showing lines of equal head in terms of environmental water; average for September 18, 1958.

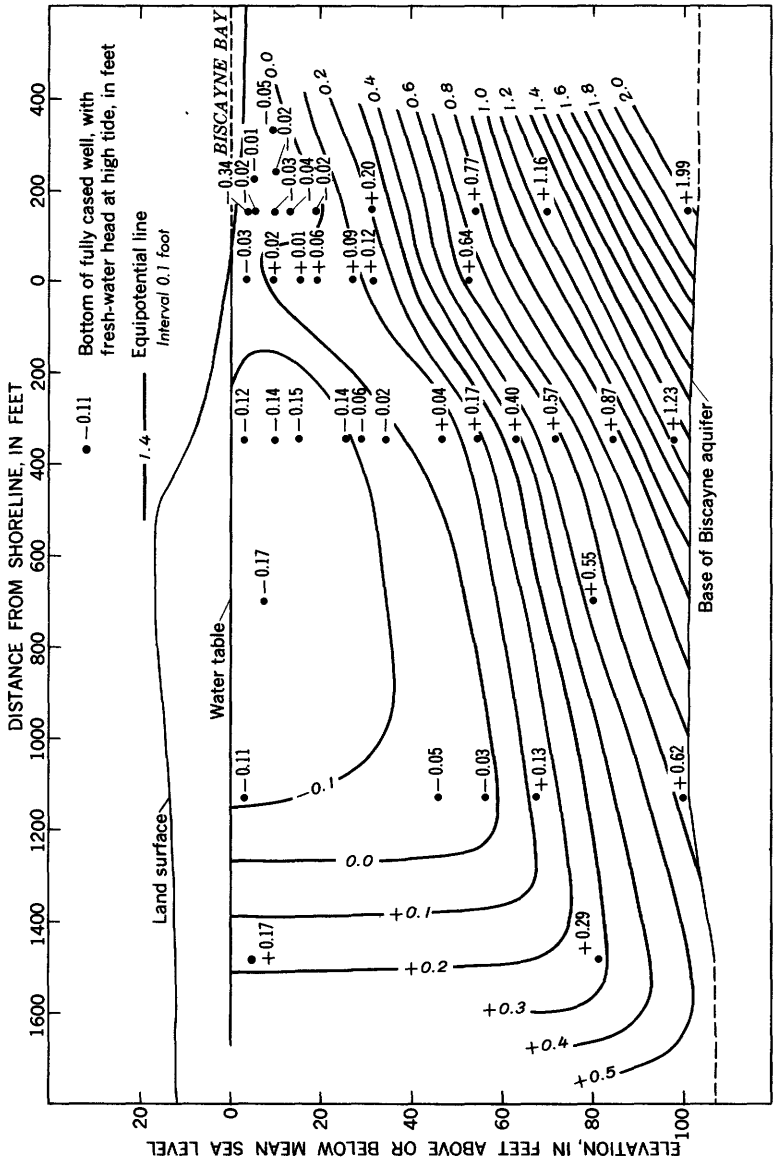

FIGURE 15.—Cross section through the Cutler area near Miami, Fla., showing lines of equal fresh-water potential at 1335 EST (bay high tide), September 18, 1958.

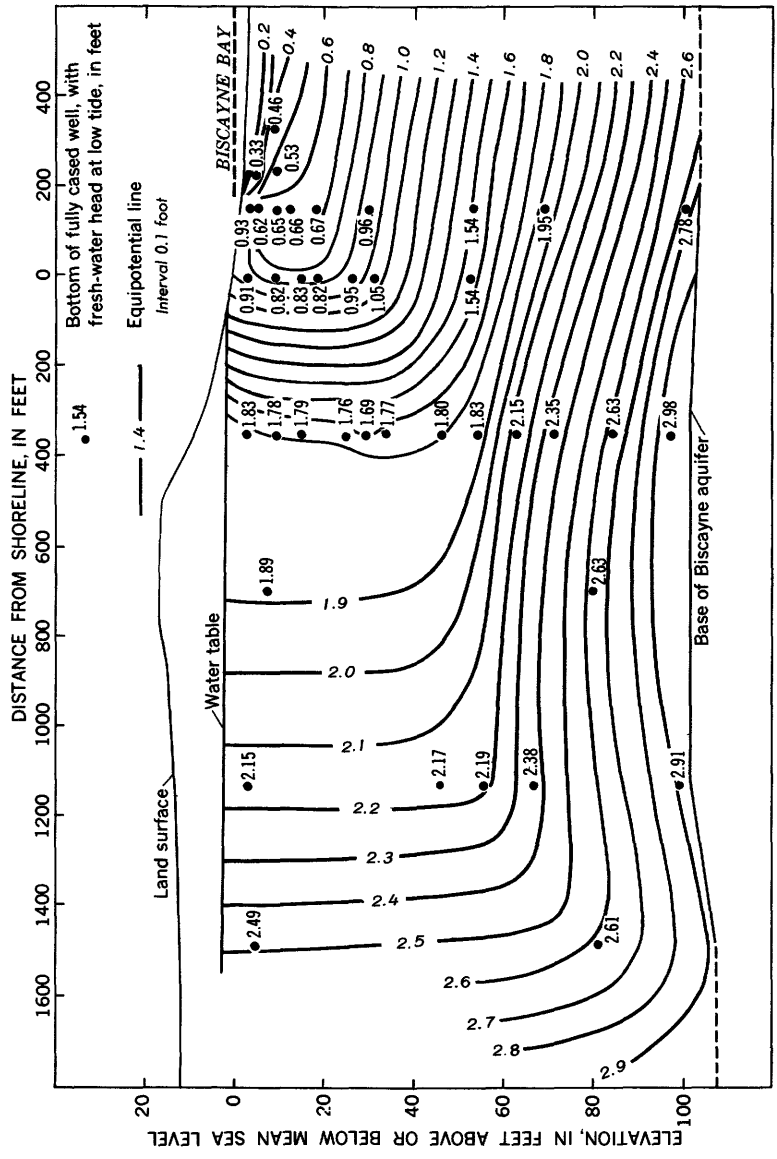

FIGURE 16.—Cross section through the Cutler area, near Miami, Fla., showing lines of equal fresh-water potential at 0750 EST (bay low tide), September 18, 1958.

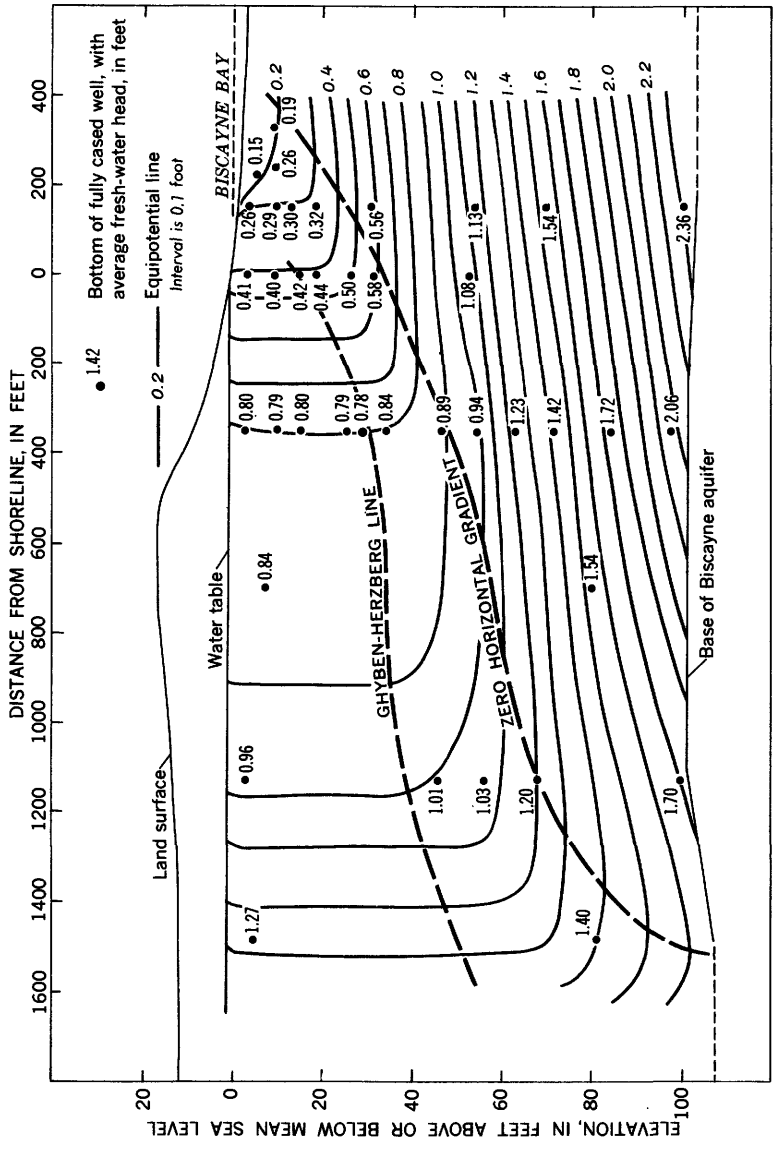

FIGURE 17.—Cross section through the Cutler area, near Miami, Fla., showing lines of equal fresh-water potential for a low-head condition; average for September 18, 1958.

Conversion of observed salt-water head to fresh-water head in a given well is accomplished by application of the equation

$$p=\rho g l$$

where p is the pressure at the bottom of the casing, ρ is the density of the water in the casing, g is the acceleration due to gravity, and l is the measured length of water column above the casing terminus. Equating the right term of the above equation for fresh-water and salt-water columns,

$$\rho_f g l_f=\rho_s g l_s$$

$$l_f=\frac{\rho_s}{\rho_f} l_s,$$

where the subscripts f and s refer to fresh water and salt water, respectively. The density of fresh water is assumed to be 1,000 gm per cm^3.

The following table (which uses observed daily-average data for well G 906, September 18, 1958, fig. 9) gives a typical computation:

Salt-water head, in feet above mean sea level	0.60
Depth to bottom of casing, in feet below mean sea level	97.90
Length of salt-water column (l_s), in feet	98.50
Chloride content of water in casing, in ppm	18,000
Density (ρ_s) of water in casing	1.0240
Length of equivalent fresh-water column (l_f), in feet	100.86
Fresh-water head, in feet above mean sea level (obtained by subtracting depth to bottom of casing from l_f)	2.96
Daily-average level of Biscayne Bay, in feet above mean sea level	.90
Daily-average fresh-water head, in feet above daily-average level of Biscayne Bay	2.06

The equipotential lines in the upper, fresh-water part of the aquifer indicate the potential of fresh water in a fresh-water environment and hence indicate comparative potentials. As flow lines must be nearly perpendicular to these equipotential lines, a seaward movement of fresh water is indicated.

In the lower and seaward part of the aquifer, the equipotential lines indicate the potential of fresh water in a region occupied by salt water. The fresh-water equipotential surfaces in a region occupied by salt water will be horizontal if the salt water is static. As the equipotential lines in the salt water regions of figures 15 to 17 are not horizontal but slope inland in figure 15, seaward in figure 16, and inland in figure 17, the salt water is not static but must be in motion in the direction of the slope. The daily-average equipotential diagram (fig. 17) indicates that the instantaneous movements occurring throughout the day average out in such a way as to produce a net inland movement of salt water on this date. On the other hand, the

seaward slope throughout the aquifer in the daily-average equipotential diagram for May 29, 1958 (fig. 18) indicates that a high head, resulting from heavy recharge (see fig. 13), causes all water in the aquifer to move seaward.

In the low-head equipotential diagram (fig. 17), the pattern of fresh-water equipotential lines serves as a guide for separating the region of seaward-flowing water from that of the inland-flowing water. Such a separation is formed by a line passed through the points of horizontality of the individual equipotential lines. This line is shown in figure 17. Clearly, along this line water is flowing neither inland nor seaward, but as the flow must be continuous between the lower and upper regions, the water at all points along this line must be flowing upward. The position of this line of zero horizontal gradient in the zone of diffusion (see fig. 9) indicates that water containing as much as 16,000 ppm chloride may have a seaward horizontal component of flow. The Ghyben-Herzberg line in figure 9 indicates the position of a sharp interface according to the Ghyben-Herzberg principle.

PATTERNS OF FLOW OF FRESH AND SALT WATER

A flow net for a low-head condition is shown in figure 19. The gradients for the horizontal components of flow were determined from the head distribution along horizontal planes in the fresh-water equipotential diagram of figure 17. These horizontal gradients were plotted at vertical lines spaced at intervals of 100 feet starting from the shoreline. Stream tubes then were constructed by maintaining the product of the vertical thickness of the stream tube and the horizontal gradient constant throughout the flow net.

The permeability of the Biscayne aquifer in the Culter area is not uniform, as indicated by the irregularly spaced lines in the upper part of the equipotential diagrams (figs. 15–18). As construction of the flow net depends on homogeniety, adjustment for the variations in permeability was necessary.

The flow net was constructed to scale and was reduced horizontally in the preparation of figure 19. In the reduction, alternate streamlines were omitted, except for the dashed lines at the midpoints of flow tubes in the landward-flow region; these were retained to show details of the flow pattern there.

The seaward flow of water at the shoreline is represented by 16 flow tubes, of which 14 originate inland and 2 originate at the floor of the sea. Thus, about seven-eighths of the total discharge at the shoreline is fresh water moving seaward from inland parts of the aquifer, and the remaining one-eighth represents a return of sea water that entered the aquifer at the floor of the sea.

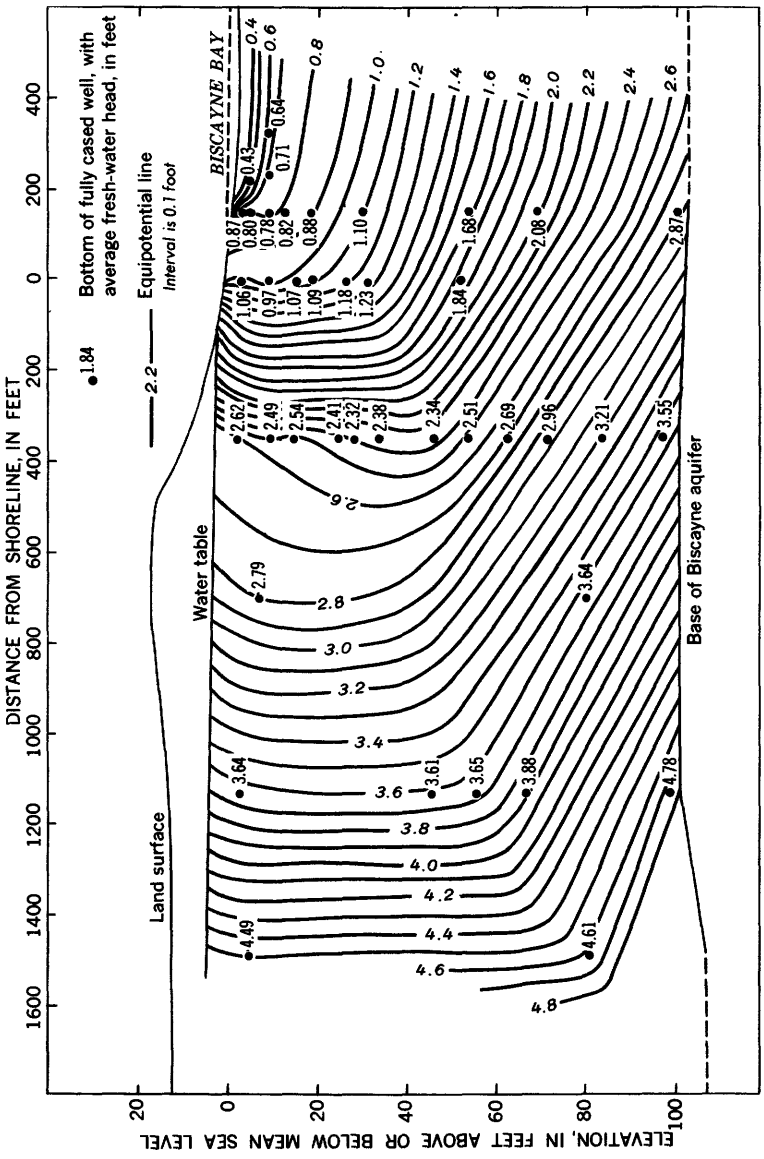

FIGURE 18.—Cross section through the Cutler area, near Miami, Fla., showing lines of equal fresh-water potential for a high-head condition average for May 29, 1958.

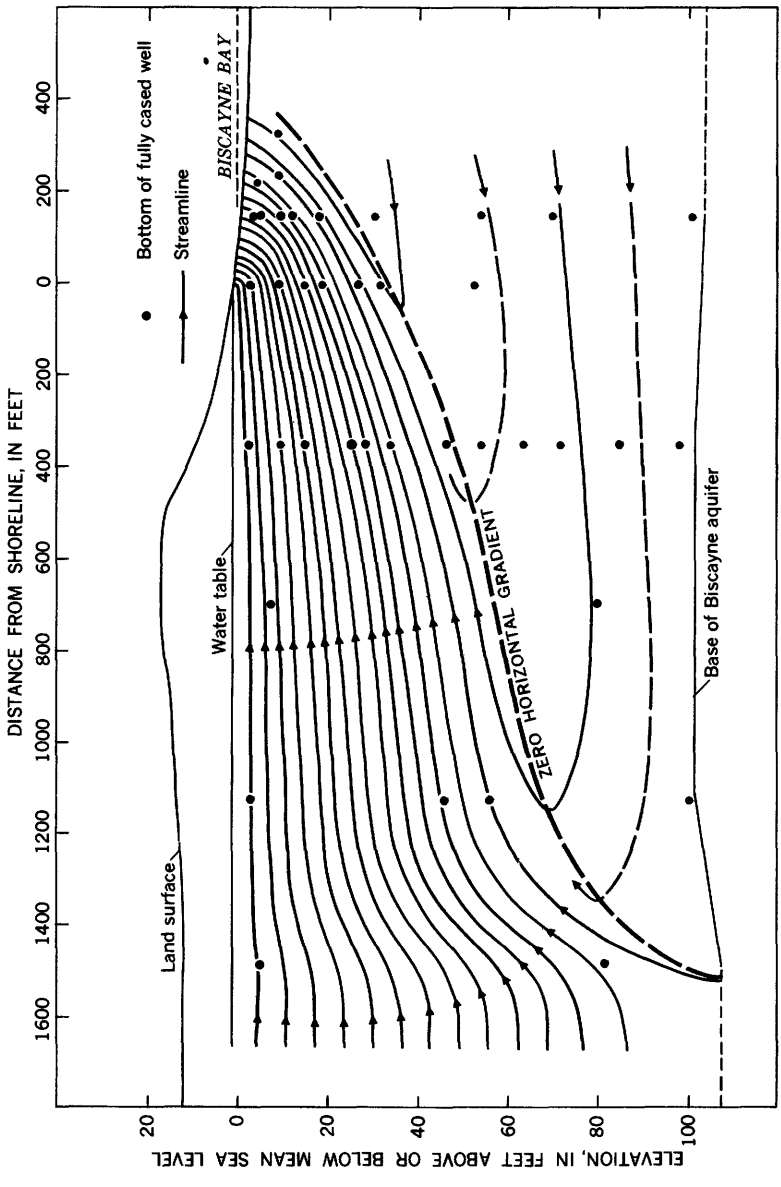

FIGURE 19.—Cross section through the Cutler area, near Miami, Fla., showing the patterns of flow of fresh and salt water for a low-head condition, September 18, 1958.

719-580 O - 64 - 6

Significant features in the flow net are the zero-horizontal-gradient line, which separates the seaward and landward horizontal components of flow, and the streamline that separates the water into two regions according to whether it originated as fresh water or sea water. These two lines intersect at the base of the aquifer.

SUMMARY

Lines of equal fresh-water potential in wells show that the salt water in the Biscayne aquifer of the Miami area, Florida, is not static as explanations of the dynamic balance commonly assume. When the fresh-water head is high after heavy recharge, water in all parts of the aquifer moves seaward, and large volumes of salt water are expelled from the aquifer. As the head declines, a landward gradient forms in the lower part of the aquifer, and salt water flows inland into the zone of diffusion to a line along which there is no horizontal component of flow; the salt water then moves upward and returns to to the sea. The cyclic flow of salt water that takes place during intrusion acts to limit the extent to which salt water occupies the aquifer because part of the inland flow of salt is continuously returned to the sea.

THE PATTERN OF FRESH-WATER FLOW IN A COASTAL AQUIFER

By Robert E. Glover

ABSTRACT

Formulas are developed for the flow pattern followed by the seaward-moving fresh ground water as it nears a beach. Under steady-flow conditions, a sharply defined interface is formed between the fresh and salt water. Along the interface the pressure of the static salt water, owing to its greater density, is counterbalanced by the pressures which drive the fresh water seaward. The fresh water escapes through a gap between this interface and the shoreline, and an increase in the flow of fresh water widens the gap. Tidal action causes a diffusion of salt water across the interface, but this salt is carried back to sea with the fresh-water flow.

INTRODUCTION

Where permeable beds underlie a land area near the sea and extend some distance seaward from the shoreline, the infiltration of rainfall causes a continuous flow of fresh water toward the sea. Under these conditions an extensive body of fresh water, often a valuable source of water supply, commonly is present beneath the land. Because the flow of fresh water toward the sea must balance the supply from rainfall infiltration, a seaward gradient must be present. The water table under the land, therefore, has the form of a mound. The density difference between sea water and fresh water is only about one-

fortieth of the density of fresh water, and for this reason the fresh-water body has a thickness below sea level of about 40 feet for each foot of elevation of the water table above sea level (Badon Ghyben, 1889; Herzberg, 1901). Near the seashore, however, dynamic factors become significant. If static conditions alone were to prevail here, the fresh-water body would taper to a knife edge at the beach and there would be no way for the fresh water to escape. When the dynamic factors are considered, it is found that the fresh water flows through a narrow gap between a fresh water–salt water interface and the water-table outcrop at the beach (Hubbert, 1940). In the analyses that follow, however, the flow through the seepage surface above sea level is assumedly negligible. A short distance back from the beach the static conditions are closely met. Under steady-flow conditions the fresh water-salt water interface would be sharply defined, but tidal action and the rise and fall of the water table maintain a zone of diffusion between the fresh and salt water.

FLOW NET

A close representation of the flow conditions near a beach can be obtained by modifying a solution previously obtained for the flow of ground water under gravity forces (Kozeny, 1953). The flow net for the present conditions can be obtained from the relationship

$$x+iy=\frac{K}{2\gamma Q}(\phi+i\psi)^2 \tag{1}$$

where

x=the distance measured horizontally landward from the shoreline, in feet;
y=the distance measured vertically downward from sea level, in feet;

and

$i=\sqrt{-1}$.

If

Q=the fresh-water flow per unit length of shoreline, in square feet per second;
K=the permeability of the strata carrying the fresh-water flow, in feet per second;

and

γ=the excess of the specific gravity of sea water over that of fresh water (dimensionless),

then

$$\phi=(\gamma Q/K)^{1/2}[x+(x^2+y^2)^{1/2}]^{1/2} \tag{2}$$

and

$$\psi=(\gamma Q/K)^{1/2}[-x+(x^2+y^2)^{1/2}]^{1/2}. \tag{3}$$

The interface between the fresh water and sea water can be plotted from the expression

$$y^2-\frac{2Q}{\gamma K}x-\frac{Q^2}{\gamma^2K^2}=0. \tag{4}$$

The width of the gap through which the fresh water escapes to the sea is

$$x_0 = -\frac{Q}{2\gamma K}. \tag{5}$$

As used here, the potential ϕ, expressed in feet of fresh water, can be identified with the pressure head which drives the fresh water. The flow function ψ also is expressed in feet of fresh water. The product $K\psi$ then has the same dimensions as Q. The stream function has the property that, for a selected value $\psi=\psi_1$, the product $K\psi_1$, substituted in expression 3, yields a streamline. The fresh-water flow above this streamline is nQ.

The potential along the line $y=0$ is

$$\phi_0 = (2\gamma Qx/K)^{1/2}. \tag{6}$$

This is the height of the water table at the distance x back from the shoreline. A plot of this flow net is shown in figure 20.

Some features of this solution deserve comment. If the supply of fresh water to the aquifer decreases so that Q decreases, then the width of the gap through which the fresh water can escape also decreases. The seaward flow of fresh water is proportional to the square of the potential ϕ_0 measured at a selected distance $x=x$ from the shoreline.

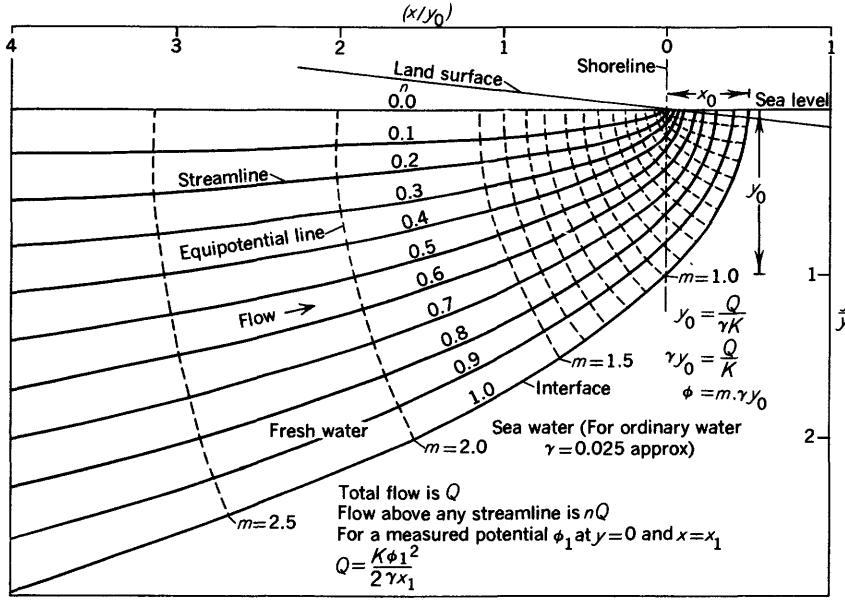

FIGURE 20.—Flow pattern near a beach.

In times of drought, the fresh-water body is conserved because the seaward flow is diminished. Thus, once established, the fresh water does not quickly waste away.

The pattern of flow described in this paper is based on the assumption that the salt water is essentially static. Cooper has hypothesized (see p. C1–C12) that where a zone of diffusion exists between the salt water and the fresh water, the salt water is not static but flows in a cycle from the floor of the sea to the zone of diffusion and back to the sea. Cooper reasoned that this flow is induced by the dispersion of salt produced by a reciprocative motion of the salt-water front. Such a circulation would alter the balance between the two fluids to an extent that depends on the magnitude of the circulation.

INTERFACES BETWEEN SALT WATER AND FRESH WATER IN COASTAL AQUIFERS

By HAROLD R. HENRY

ABSTRACT

In a coastal aquifer, a steady flow of fresh water toward the sea limits the encroachment of the sea water. Under the assumption that the salt water and fresh water do not diffuse into one another so that a sharp interface exists, this action is treated for steady two-dimensional flow.

Exact solutions for the position of the interface and the boundary velocities in artesian aquifers are derived for several sets of boundary conditions. A hodograph plane is used to circumvent the boundary problem that arises because the position of the interface is not known in advance, and a complex potential is related to the hodograph by conformal mapping. Also derived is an equation for the interface in a water-table aquifer receiving uniform vertical recharge. The derivation involves physical approximations to avoid an additional boundary problem due to the unknown position of the water table.

Interfaces are computed for artesian aquifers of finite thickness and semi-infinite length that have vertical and horizontal seepage faces and for a range of fresh-water discharges in several geometries of artesian aquifers of finite thickness and length. Only when the salt water extends very short distances into the aquifer do the interfaces in finite artesian aquifers differ significantly from those in semi-infinite artesian aquifers with the same discharge. Where the salt-water wedge extends inland from the shore a distance many times the thickness of the aquifer, the position of the interface, except near the shore, can be obtained approximately by using a Dupuit-type assumption. Comparisons with field data indicate that the computed interface corresponds approximately with the position of the zone of diffusion.

The position of the interface in a water-table aquifer receiving uniform vertical recharge is found by employing the relaxation technique in a modified hodograph plane. Interfaces are computed for an extremely large rate of recharge and, more realistically, for a smaller rate. For the large rate of recharge the position of the interface is much deeper and farther seaward than that obtained by use of the Dupuit assumption, but for the smaller rate the difference between the interfaces obtained by the two methods is negligible.

INTRODUCTION

The location of the interface between the fresh water and sea water in a coastal aquifer is obviously significant in the practical use of ground water. The seaward flow of fresh water in the aquifer is necessary to keep salt water from encroaching farther into the aquifer. Exact solutions for the location of the interface have been obtained for several boundary conditions under the assumptions that the flow is steady, that the salt and fresh water do not diffuse into one another, and that there is no interfacial tension. The effects of diffusion are considered on pages C70–C84.

The first analyses (Badon Ghyben, 1889; Herzberg, 1901) treated the salt-encroachment phenomenon as a simple buoyancy problem in which static fresh water floated on the heavier sea water. In this method, hydrostatic conditions are assumed to apply vertically below a point of observation of piezometric level in the fresh water. This determines the elevation of a point on the interface where the pressure is balanced by the hydrostatic conditions prevailing in the salt water. If the assumption that constant piezometric head exists on a vertical line is used together with a one-dimensional application of Darcy's law, the position of the interface can be estimated as a function of steady fresh-water discharge (Kitagawa, 1939; Todd, 1953) by the method used by Dupuit (1863) for gravity seepage in a two-dimensional aquifer.

In nature the interface is not sharp; instead, the salt and fresh water merge gradually through the process of mechanical dispersion aided by chemical diffusion. As discussed by Cooper on pages C8–C11, the width of the zone of dispersion depends on the pore characteristics of the aquifer and on the relative magnitude of the fluctuations due to recharge and tidal activity. If this zone is narrow as it is under some field conditions (Brown, 1925), the assumption of a sharp interface might be used to obtain a first approximation of the fresh water flow pattern and the location of the dispersion zone.

ACKNOWLEDGMENTS

The writer thanks Prof. Richard Skalak of Columbia University and the U.S. Geological Survey for his advice throughout the preparation of this paper. The study was suggested by H. H. Cooper, Jr., of the Geological Survey. Thanks are also due E. M. Laursen of Michigan State University for helpful discussions.

This paper is based in part on the writer's Ph. D. dissertation at Columbia University.[1]

[1] Henry, H. R., 1960, Salt intrusion into coastal aquifers: New York, Columbia Univ. Ph. D. dissertation.

ARTESIAN AQUIFERS

The type of aquifer to be considered here is one that is overlain in the coastal area by an impervious bed that confines the water under pressure and locally prevents recharge from rain. In nature, water would enter such an aquifer in an inland area of recharge and would flow into the coastal segment approximately horizontally. The idealized configurations analyzed are shown in figures 21 and 22. In each of these it is supposed that water enters horizontally along the line *EF* and flows out along the seepage face *AB*. In figure 21 the seepage face is vertical; in figure 22 it is horizontal. In each case, general expressions are derived for a finite aquifer as shown. Then the equations are modified for aquifers that extend to infinity in a landward direction. Another limiting case which is treated is that of an aquifer that not only extends to infinity in the landward direction but also is of infinite thickness.

The general expressions are used to compute the location of the interfaces for the semi-infinite aquifers with horizontal and vertical seepage faces and for several finite values of the aquifer-aspect ratio $\xi=l/d$ and of the discharge parameter $a=Q/(k_1 d)$. Here Q is the fresh-water discharge per foot of shoreline and k_1 is the product of the permeability $\bar{k}$ of the aquifer and the buoyancy ratio $\frac{\rho_s-\rho_0}{\rho_0}$, where ρ_s and ρ_0 represent, respectively, the densities of the salt and fresh water.

The inflow surface *EF*, assumed to be vertical for analytical convenience, apparently differs widely from the nearly horizontal outcrop areas found in most field conditions. However, if the recharge were to occur a great distance inland from the toe of the salt-water wedge, the streamlines of fresh-water flow would be almost straight and parallel immediately upstream from the nose of the wedge. Under this condition the flow in the aquifer would correspond closely to that in the present schematization. If other factors remain constant, one would expect the position of the interface to remain almost constant as l varies, since there would probably be little consequent change in the fresh-water flow pattern at D, the toe of the wedge. This expectation is borne out by the computations.

Although this analysis is for artesian aquifers, the computed interfaces may apply approximately under certain conditions to a water-table aquifer. If the water table is a streamline—that is, if the quantity of recharge in the vicinity of the salt wedge is small compared with the total recharge—and if the water table is very flat in comparison to the interface, the present computations should provide an estimate of the interface position.

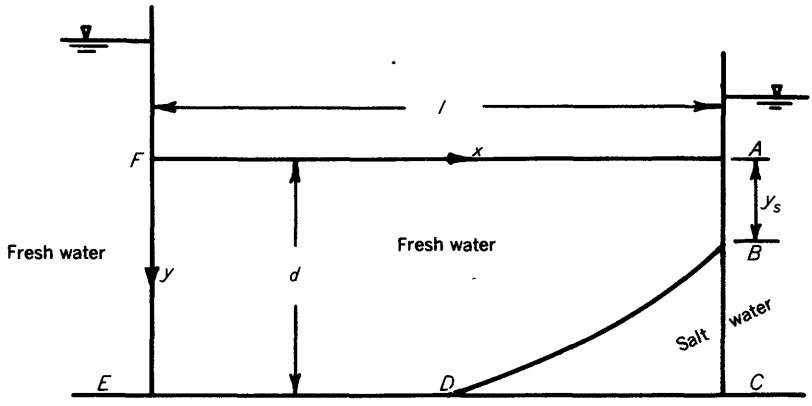

A Schematic sketch of Case 1 (z plane)

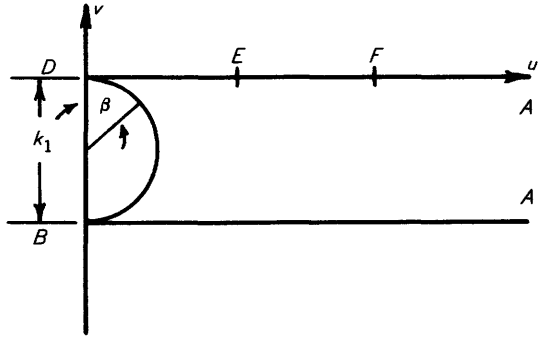

B Hodograph ($\bar{q}$ plane)

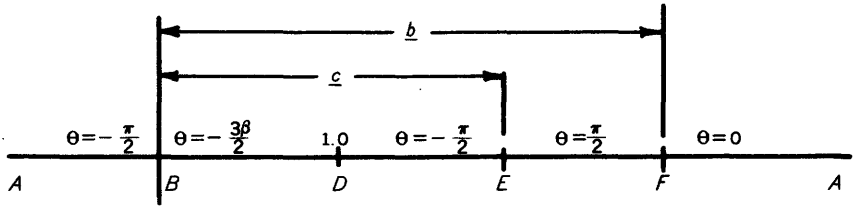

FIGURE 21.—Schematic sketch and complex planes for artesian aquifer with vertical outflow face.

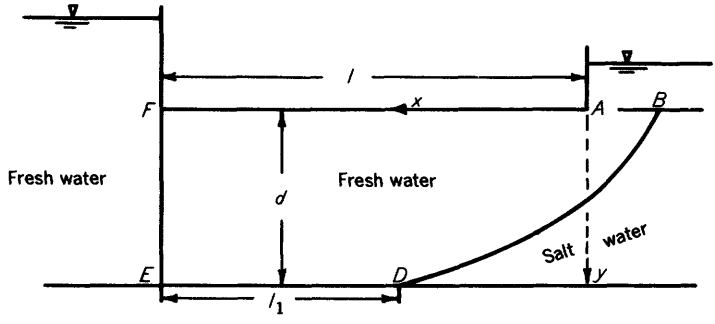

A Schematic sketch of Case 2 (z plane)

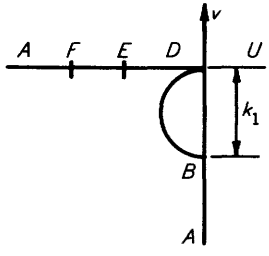

B Hodograph (q plane)

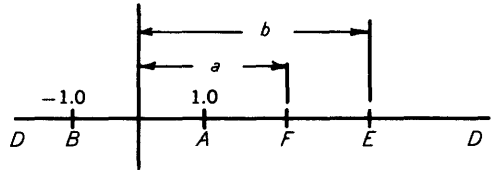

C t plane, $t=\cosh\left(-\frac{\pi k_1}{q}\right)$

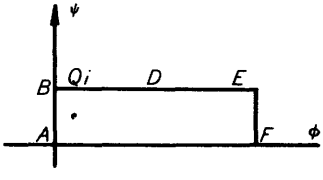

D f plane, $f=\phi+i\psi$

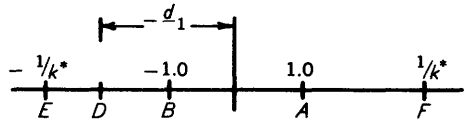

E w_1 plane, $w_1=\mathrm{sn}\left[\left(\frac{2if}{Q}+1\right)K\right]$

FIGURE 22.—Schematic sketch and complex planes for artesian aquifer with horizontal outflow face.

NOTATION

The symbols used most frequently herein are defined below:

$a = Q/k_1 d$, dimensionless.
A, B, C, D, E, F = points on the boundary of the aquifer.
$\underline{a}, \underline{b}, \underline{c}, \underline{d}, \underline{e}$ = coordinates of points in the complex plane.
d = depth of aquifer, ft.
$f(z)$ = complex velocity potential $= \phi + i\psi$, ft² per sec.
$f'(z)$ = first derivative of f with respect to z, ft per sec.
$f''(z)$ = second derivative of f with respect to z, sec^{-1}.
h = piezometric head, in feet of fresh water.
$i = \sqrt{-1}$.
J = the elliptic modular function.
k = permeability of sand, ft².
$\overline{k}$ = transmission coefficient $= k\rho_0 g/\mu$, ft per sec.
k_1 = transmission coefficient times the density difference ratio $= \overline{k}\,\frac{\rho_s - \rho_0}{\rho_0}$ ft per sec.
K = complete elliptic integral of first kind.
K' = complete elliptic integral of first kind with complementary modulus.
k^* = modulus of elliptic integral.
$k' = \sqrt{1 - k^{*2}}$
Q = net fresh-water discharge per unit length of beach, ft² per sec.
l = length of aquifer, ft, for artesian aquifer.
= half width of island, ft, for water-table aquifer.
p = pressure, lbs per ft².
$\underline{q}$ = complex velocity $= u + iv$, ft per sec.
q = conjugate complex velocity $= u - iv$, ft per sec.
$\vec{q}$ = vector velocity, ft per sec.
t, w, λ = complex variables.
u = horizontal velocity, ft per sec.
v = vertical velocity, ft per sec.
x, y = coordinates, ft (when used as subscripts, these denote differentiation).
z = complex variable.
α = the integral, $-\frac{3}{2\pi}\int_0^1 \frac{\beta(t)}{t-\lambda}\,dt$
β = central angle in hodograph plane.
ρ = density of solution, slugs per ft³.
ρ_0 = density of fresh water, slugs per ft³.
ρ_s = density of sea water, slugs per ft³.
ϕ = velocity potential $= \overline{k}h$, ft² per sec.
ψ = stream function, ft² per sec.
$\tau + i\theta$ = the auxiliary variable, $-\ln[-f''(z)]$.
ξ = aspect ratio $= l/d$, dimensionless.

GOVERNING EQUATIONS AND BOUNDARY CONDITIONS

It is assumed that there is no dispersion of salts, so that a sharp interface separates the salt water from the fresh water. Darcy's law for a homogeneous fluid then applies to the flow of the fresh water, and under steady conditions the salt water in the aquifer below the interface will be static. In the mathematical statement of the

problem, the interface is treated as a free boundary which must be located so that the pressure on its fresh-water side is equal to the static pressure on its salt-water side.

The use of Darcy's law (Darcy, 1856) for the velocity components u and v,

$$u=-\frac{\partial\phi}{\partial x},\ v=-\frac{\partial\phi}{\partial y} \tag{1}$$

in the continuity equation

$$\frac{\partial u}{\partial x}+\frac{\partial v}{\partial y}=0 \tag{2}$$

yields Laplace's equation on ϕ

$$\nabla^2\phi=0, \tag{3}$$

where ϕ is the usual velocity potential for laminar groundwater flow:

$$\phi=\bar{k}\left(\frac{p}{\rho_0 g}-y\right),$$

where y is measured downward.

In terms of the fresh-water potential ϕ, the boundary condition to be satisfied on the unknown interface BD (see figs. 21, 22) and on the seepage face AB is: $p=\left(\frac{\phi}{\bar{K}}+y\right)\rho_0 g=\rho_s g y+B$, where B is a constant, or

$$\phi=\phi_0+k_1 y, \tag{4}$$

where $k_1=\bar{k}\,\frac{\rho_s-\rho_0}{\rho_0}$ and ϕ_0 is a constant. Equation 4 may be written in dimensionless form using $\phi'=\frac{\phi}{Q}$ and $y'=yxd$:

$$\phi'=\phi_0'+\left(\frac{k_1 d}{Q}\right)y'. \tag{4a}$$

The dimensionless parameter $\frac{Q}{k_1 d}\equiv a$, which occurs here, is designated the discharge parameter. For a given discharge parameter, all flows with similar aquifer geometry will be similar. This can be easily demonstrated by dimensionless analysis also.

A stream function ψ can be defined as usual by $\psi=-\int u dy+\int v dx$, so that ψ and ϕ satisfy the Cauchy-Rieman equations and a complex velocity potential $f(z)$ exists where

$$f(z)=\phi+i\psi. \tag{5}$$

The derivative of $f(z)$ yields the conjugate of the complex velocity $q=u+iv$:

$$-f'(z)=u-iv\equiv\bar{q}. \tag{6}$$

The method of solution used is a conformal mapping technique which begins with a conformal mapping of the boundaries of the fresh-water flow system onto a hodograph or q plane. For this procedure, the values of u and v or a relationship between u and v is required for every point on the boundary. In this problem there are boundaries of four different types—namely, boundaries of constant head, boundaries which are fixed streamlines, the interface, and the seepage surface. Referring to figures 21 and 22, EF is of the first type, on which ϕ is constant; and FA and ED are of the second type, on which ψ is constant. On the interface DB and on the seepage surface AB the values of ϕ are controlled by the hydrostatic pressure in the salt water as expressed in equation 4. On the interface ψ is constant, but on the seepage surface the distribution of ψ is unknown.

For a straight boundary on which the head or potential is constant in the original plane of the flow, the velocity vector is everywhere perpendicular to the boundary, and the corresponding boundary in the hodograph plane is of the form $u=$(constant) v. For a straight boundary in the original plane of the flow which is also a streamline, the hodograph line is parallel to the original boundary and also of the form $u=$(constant) v.

The equation of the boundary in the hodograph plane corresponding to the seepage face AB can be obtained as follows. The velocity u_r along the face is

$$u_r=u\cos\alpha+v\sin\alpha=-\frac{\partial\phi}{\partial r}, \tag{7}$$

where r is the distance measured along the surface of seepage and α is the angle between the seepage surface and the horizontal. The value of α is $\frac{\pi}{2}$ for figure 21A and zero for figure 22A. From equation 4 $\frac{\partial\phi}{\partial r}=-k_1\frac{\partial y}{\partial r}=k_1\sin\alpha$. Substitution of this into equation 7 yields the desired relation:

$$k_1\sin\alpha+u\cos\alpha+v\sin\alpha=0. \tag{8}$$

The hodograph equation for the interface is also obtained by use of equation 4. Differentiation of equation 4 with respect to the distance s along the interface BD yields:

$$\frac{\partial\phi}{\partial s}=-k_1\frac{\partial y}{\partial s}. \tag{9}$$

Since the interface is a streamline, $\frac{\partial\phi}{\partial s}$ is the total velocity $(u^2+v^2)^{1/2}$. Multiplying equation 9 by $\frac{\partial\phi}{\partial s}$ gives:

$$u^2+v^2+k_1v=0. \tag{10}$$

Thus, in the hodograph plane the interface is represented by a semicircle of diameter k_1. The hodographs for figures 21*A* and 22*B* are shown in figures 21*B* and 22*B*.

CASE 1, VERTICAL OUTFLOW FACE

The hodograph for case 1, which is shown in figure 21*B*, may be transformed into the upper half of the λ plane shown in figure 21*C* by use of the auxiliary functions q_1 and q_2 as defined below and by use of the elliptic modular function as defined by Nehari (1952) and by Jahnke and Emde (1945). Using

$$q_1=\frac{i}{k_1}\bar{q}+1 \tag{11}$$

$$q_2=1-\frac{1}{q_1}, \tag{12}$$

the required transformation function $\lambda=\lambda(q_1)$ is given by

$$\lambda(q_1)=J(q_2), \tag{13a}$$

where $J(q_2)$ is the elliptic modular function of q_2. The values of λ corresponding to the flow boundaries can be computed by using the inverse of the elliptic modular function. Thus,

$$1-\frac{1}{q_1}=\frac{iK'(\lambda)}{K(\lambda)}\equiv i\frac{K'}{K}(\lambda), \tag{13b}$$

where K is the complete elliptic integral of the first kind and K' is the complete elliptic integral of the first kind with complementary modulus. Values of K'/K for λ real and between zero and unity are given by Hayashi (1930). Within this range, arbitrary values of λ may be substituted into equation 13b and corresponding values of q computed. For other ranges, the use of certain identities which follow from the properties of elliptic modular functions is required to permit use of the tabular values. For $-\infty<\lambda\leqq 0$, one may use

$$\frac{1}{1-\lambda}=J(q_1) \tag{14a}$$

$$q_1=i\frac{K'}{K}\left(\frac{1}{1-\lambda}\right) \tag{14b}$$

and for $1\leqq\lambda<\infty$ one may use

$$\frac{1}{\lambda}=J(q_1-1) \tag{15a}$$

$$q_1-1=i\frac{K'}{K}\left(\frac{1}{\lambda}\right). \tag{15b}$$

Equations 13, 14, and 15 may be considered alternate forms of the same transformation between q_1 and λ.

To complete the solution of the problem, it is necessary to express the complex potential f, or some function of f, in terms of $\bar{q}$ so that equation 6 or some similar equation can be integrated. Because the distribution of ψ on AB in figure 21*A* is unknown, it is not possible to relate the boundaries of the flow in the f plane directly to those in the λ plane. An indirect method developed by Hamel (1934) is utilized instead. Use is made of the function $\tau+i\theta$ defined by

$$\tau+i\theta=-ln[-f''(z)]. \tag{16}$$

It follows that $-\theta$ is the argument of $-f''(z)$. The second derivative $-f''(z)$ may be written

$$-f''(z)=\frac{du-idv}{dx+idy}. \tag{17}$$

From equation 17 and an inspection of the hodograph, it is found that

$$\theta_{AB}=-\frac{\pi}{2};\ \theta_{BD}=-\frac{3\beta}{2};\ \theta_{DE}=-\pi;\ \theta_{EF}=-\frac{\pi}{2};\ \theta_{FA}=0. \tag{18}$$

The angle β in the second of equations 18 is the angle indicated in the hodograph in figure 21*B*.

Figure 21*C* shows that the values of θ are known at all points of the real axis of the λ plane. Values of θ can then be obtained for all points of the upper half plane by a Fourier integral. Subsequently, values of τ are obtained by integrating the Cauchy-Rieman equations for τ and θ. Muskat (1937) gave details of this procedure, which yields

$$\tau+i\theta=\tau_0+\frac{1}{\pi}\int_{-\infty}^{\infty}\frac{\theta(t)(\lambda t+1)}{(t-\lambda)(1+t^2)}dt, \tag{19}$$

where τ_0 is an arbitrary constant and the integral is taken along the real axis.

Evaluating the integral in 19 and substituting in 16 yields

$$-f''=\frac{-\sqrt{\lambda(\underline{c}-\lambda)(\underline{b}-\lambda}}{1-\lambda}\exp\left(-\tau_0+\frac{3}{2\pi}\int_0^1\frac{\beta(t)}{t-\lambda}dt\right), \tag{20}$$

where $\underline{b}$ and $\underline{c}$ are the coordinates of points F and E, respectively, in the λ plane. Substituting the derivative of equation 6 into equation 20 and solving for z yields

$$\frac{z}{\eta}=\int e^{\tau+i\theta}d\bar{q}+\text{constant}, \tag{21}$$

where η, a constant of integration, serves as a reference length that may vary with changes in $\underline{b}$ and $\underline{c}$, and where

$$e^{\tau}=\frac{1-\lambda}{\sqrt{\lambda(\underline{c}-\lambda)(\underline{b}-\lambda)}}e^{\alpha} \tag{22}$$

and

$$e^{\alpha}=\exp\left(-\frac{3}{2\pi}\int_0^1\frac{\beta(t)}{(t-\lambda)}dt\right). \tag{23}$$

Hamel and Gunther (1935) and Muskat (1935) gave tabulated and graphical values of e^{α} as a function of λ. Thus, the velocities at the boundaries of the flow and the location of the interface can be computed by substituting arbitrary real values of λ into the proper one of equations 13, 14, and 15 and, subsequently, graphically or numerically integrating equation 21. Assigning numerical values to $\underline{b}$ and $\underline{c}$ in equation 22 corresponds to assigning values to the parameters $l/d=\xi$, the aspect ratio of the aquifer, and $\frac{Q}{k_1 d}=a$, the discharge parameter.

If the relative positions of the levels of the fresh water and the salt water in figure 21*A* are such that point *D* coincides with *E*, that is, if the interface reaches to the upstream reservoir, then $\phi_E=\phi_D$ and

$$e^{\tau}=\sqrt{\frac{1-\lambda}{\lambda(\underline{b}-\lambda)}}e^{\alpha}. \tag{24}$$

This case is mathematically identical with that of seepage through a rectangular dam with no tailwater, in which the permeability $\bar{k}$ has been replaced by k_1. Muskat (1935) gave numerical solutions for the discharge *Q* and the height of seepage surfaces *AB* for four such situations. Muskat plotted computed boundary velocities for two cases and also drew in the free surface without calculation by following the general features computed by Hamel and Gunther (1935) for a dam with a tailwater. Muskat's curves have been inverted and relabeled to fit the present application in figures 23 and 24.

When the aquifer extends an infinite distance to the left in figure 21*A*, the point *E* in the hodograph coincides with point *F*, and e^{τ} becomes

$$e^{\tau}=\frac{1-\lambda}{(\underline{c}-\lambda)\sqrt{\lambda}}e^{\alpha}. \tag{25}$$

Moreover, if the aquifer also extends an infinite distance downward, the hodograph points *D*, *E*, and *F* coincide, and e^{τ} becomes

$$e^{\tau}=\frac{1}{\sqrt{\lambda}}e^{\alpha}. \tag{26}$$

The numerical solution for this case is given in a later section.

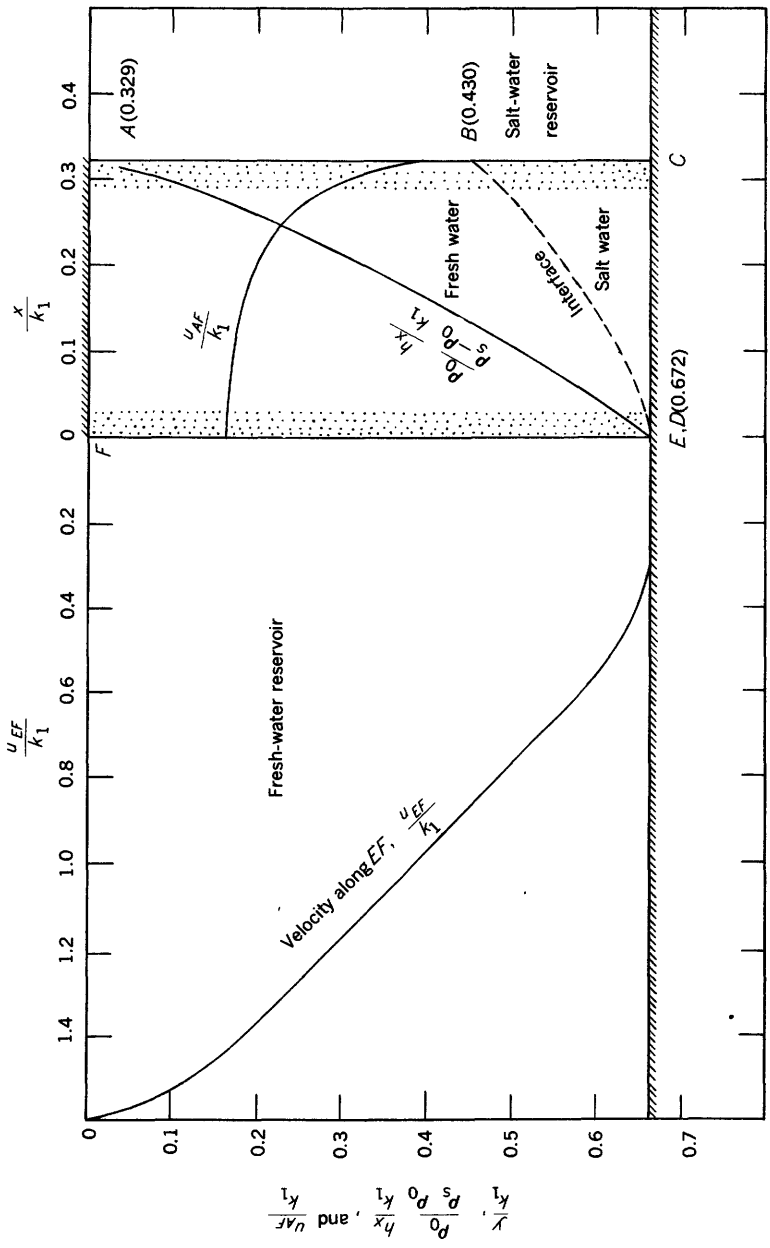

FIGURE 23.—Numerical solution for a short sand formation (an inversion of Muskat's case 3).

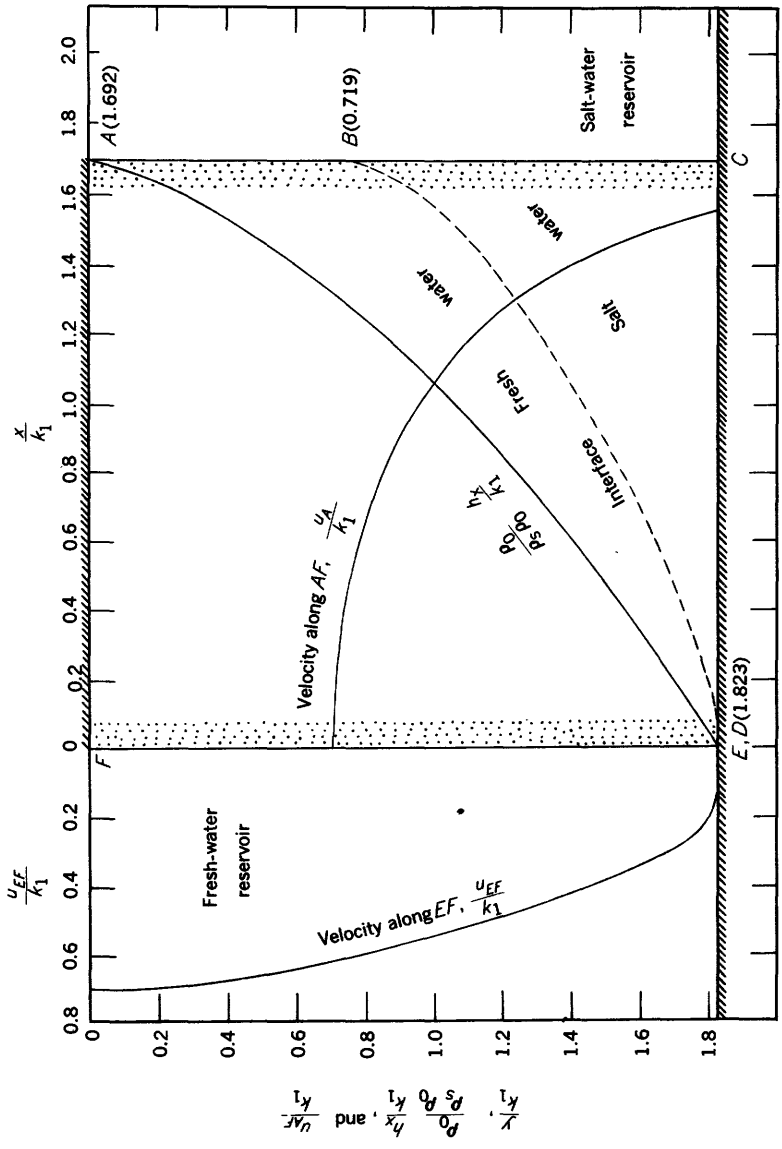

FIGURE 24.—Numerical solution for a short sand formation (an inversion of Muskat's case 4).

CASE 2, HORIZONTAL OUTFLOW FACE

Figure 22*A* represents a flow in which the seepage face *AB* is horizontal. The hodograph or q plane for this case is shown in figure 22*B*. The hodograph can be transformed to the upper half of the τ plane of figure 22*C* by

$$t=\cosh\frac{\pi k_1}{\bar{q}} \tag{27a}$$

or, inversely, by

$$\bar{q}=\frac{-\pi k_1}{\cosh^{-1}t}. \tag{27b}$$

In the complex-potential plane $f=\phi+i\psi$, the boundaries of the flow form the rectangle shown in figure 22*D*, where the potential along the seepage face *AB* is assumed to be zero. The rectangle in the f plane is now mapped into the upper half of the t plane. This is accomplished by first mapping f into the upper half of the w_1 plane of figure 22*E* using the Schwarz-Christoffel theorem

$$w_1=sn\left[\left(if\frac{2}{Q}+1\right)K\right] \tag{28a}$$

or, inversely,

$$\frac{f}{Q}=\frac{1}{2i}\left(\frac{sn^{-1}w_1}{K}-1\right), \tag{28b}$$

where

$$sn^{-1}w_1=\int_0^{w_1}\frac{dW}{\sqrt{(1-W^2)(1-K^*W^2)}} \tag{28c}$$

and

$$K=sn^{-1}(1,\ k^*), \tag{28d}$$

where k^* is the modulus of the elliptic integral.

The w_1 plane can be mapped into the t plane of figure 22*C* by the linear transformation

$$w_1=\frac{td_1-1}{d_1-t}, \tag{29}$$

where $-d_1$ is the coordinate of point *D* in the w_1 plane. The relation between the coordinates a and b of the t plane and the values of d_1 and k^* of the w_1 plane are found by substituting the respective values of w_1 and t into equation 29:

$$a=\frac{d_1+k^*}{k^*d_1+1} \tag{30}$$

$$b=\frac{k^*-d_1}{k^*d_1-1}. \tag{31}$$

Thus the problem is in principle solved, since $\overline{q}$ is expressed parametrically in terms of f through equations 27b, 28b, and 29, and, in principle, equation 6 can be integrated to give

$$\frac{zk_1}{Q}=-\int\frac{k_1 df}{\overline{q}Q}+\text{constant}. \tag{32}$$

The numerical solution of a particular problem requires given values of either $\underline{a}$ and $\underline{b}$ or $\underline{d}_1$ and k^*. Assuming either pair of values corresponds in effect to assigning values to the two dimensionless quantities $Q/(k_1 d)$ and ξ.

For the horizontal strip of aquifer semi-infinite in length in figure 22*A*, the points E and F are at an infinite distance to the left, the two corresponding points in the hodograph are coincident, and, in the t plane, $\underline{a}=\underline{b}$. Also, in figure 22*D*, E and F would be at infinity to the right. In the w_1 plane this requires $k^*=0$ and the points E and F at infinity. Equation 28b, transforming the w_1 plane into the f plane, degenerates into

$$f=\frac{Q}{\pi}\cosh^{-1} w_1. \tag{33}$$

The relation between the w_1 and t plane is still expressed by equation 29, and equations 30 and 31 degenerate into $\underline{a}=\underline{b}=\underline{d}_1$.

Finally, if in figure 22*A*, in addition to l becoming infinite, the vertical thickness d becomes infinite also, the points D, E, and F will coincide in the hodograph. Then the mapping of the q plane into the f plane is obtained by

$$\frac{f}{Q}=\frac{-k_1}{\overline{q}}. \tag{34}$$

In this instance, equation 32 can be integrated to yield

$$\frac{zk_1}{Q}=\frac{1}{2}\left(\frac{f}{Q}\right)^2. \tag{35}$$

This is mathematically identical to a seepage problem solved by Kozeny (1953) for a free-surface flow in a semi-infinite aquifer draining downward through a horizontal outflow face when k_1 is substituted for $\overline{k}$. This correspondence between the Kozeny solution and the salt-intrusion problem for the semi-infinite aquifer was noted and utilized by R. E. Glover on pages C32–C35.

COMPUTATIONS FOR SEMI-INFINITE AQUIFERS, CASES 1 AND 2

For case 1, equations 18 and 26 are substituted into equation 21 and values of $\overline{q}$ are computed from the appropriate one of equations 13, 14, 15. Then equation 21 is integrated numerically. Along

AB, λ varies from $-\infty$ to 0 and the corresponding values of $\bar{q}$ are computed from equation 14b, which in this case is

$$\frac{u}{k_1}=\frac{K'}{K}\left(\frac{1}{1-\lambda}\right). \tag{36}$$

Values of $\frac{K'}{K}$ can be found in Hayashi's tables (1930). Values of e^{α} are taken from Hamel and Gunther (1935). The integration indicated by equation 21 was performed by the trapezoidal rule. The computed depth y_s of the seepage surface AB expressed in dimensionless form is $y_s k_1/Q=0.741$, as shown in figure 25.

For the interface BD, equation 10 yields

$$\frac{\bar{q}}{k_1}=\frac{-i}{2}(e^{i\beta}-1), \tag{37}$$

and use of equations 18 and 26 yields

$$\int\frac{e^{\tau+i\theta}}{k_1}d\bar{q}=\int\frac{e^{\alpha-i\beta/2}}{2\sqrt{\lambda}}d\beta. \tag{38}$$

Solving for the x and y coordinates from equation 21 gives, in dimensionless form,

$$\frac{x-x_B}{\eta}=\frac{1}{2}\int_{\pi}^{\beta}\frac{e^{\alpha}\cos\frac{\beta}{2}}{\sqrt{\lambda}}d\beta \tag{39a}$$

$$\frac{y-y_B}{\eta}=\frac{1}{2}\int_{\pi}^{\beta}\frac{e^{\alpha}\sin\frac{\beta}{2}}{\sqrt{\lambda}}d\beta. \tag{39b}$$

Values of β corresponding to given values of λ were computed using equation 13b, which in view of equations 11 and 37 may be rewritten

$$\tan\frac{\beta}{2}=\frac{K'}{K}(\lambda). \tag{40}$$

The discharge is obtained by integrating $u\,dy$ over the seepage surface AB or, in terms of the present parameters,

$$\frac{Q}{k_1\eta}=-\int_{\infty}^{0}e^{\tau}\left(\frac{u}{k_1}\right)\frac{du}{k_1}. \tag{41}$$

Equations 39a and 39b are divided by equation 41 to obtain the dimensionless coordinates in the form $\frac{xk_1}{Q}$ and $\frac{yk_1}{Q}$, as shown in figure 25. The integrals of equations 39a, 39b, and 41 were computed by the trapezoidal rule to give the coordinates of the interface.

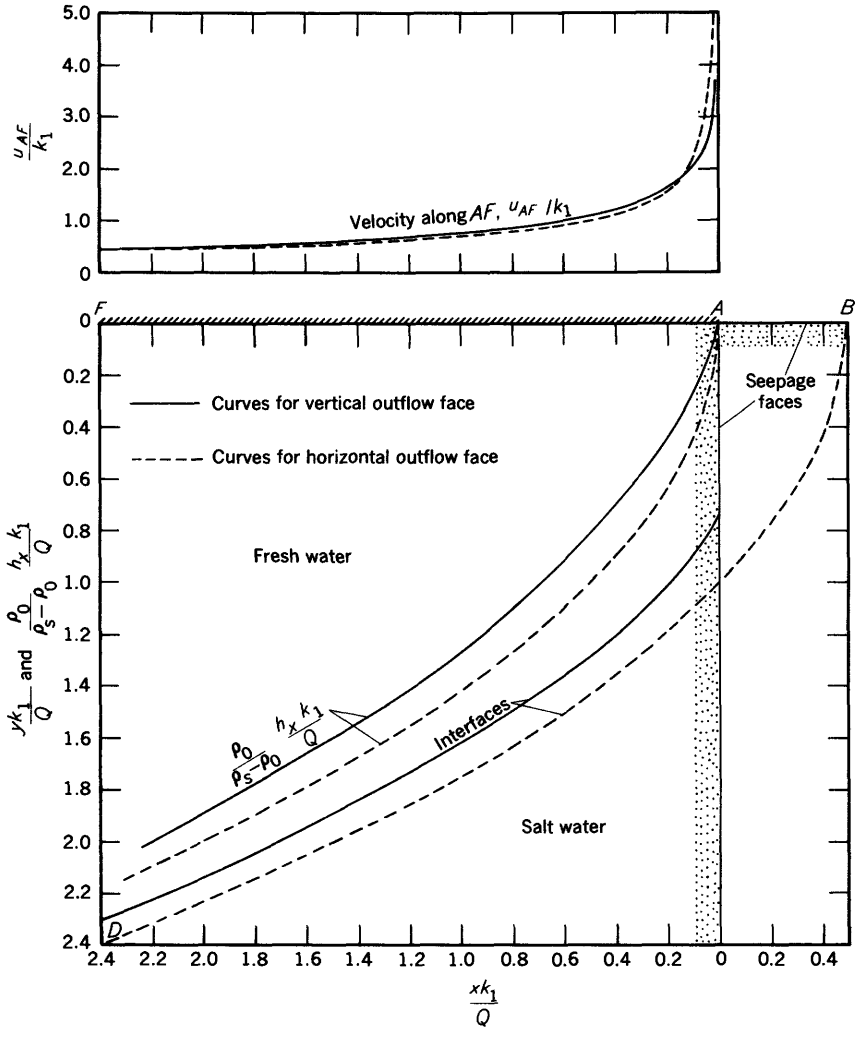

FIGURE 25.—Numerical solution for semi-infinite artesian aquifers with vertical and horizontal outflow faces.

The piezometric head h_x on the boundary AF is indicated by the line labeled $\frac{\rho_0 h_x k_1}{(\rho_s-\rho_0)Q}$ in figure 25. This line indicates what the position of the interface would be if hydrostatic conditions prevailed along vertical sections in the fresh-water body. This computation requires first the computation of u versus x as shown by the solid curve in the upper graph. This is determined by a graphical integration of equa-

tion 21 by using equation 15 for the relation between λ and q_1. The head is subsequently computed by

$$h_x - h_A = y_0 \left(\frac{\rho_s - \rho_0}{\rho_0}\right) = \int_0^x \frac{u}{k}\, dx \tag{42a}$$

or, in dimensionless form,

$$\frac{y_0 k_1}{Q} = \int_0^{\frac{xk_1}{Q}} \frac{u}{k_1}\, d\left(\frac{xk_1}{Q}\right) = \int_0^{u/k_1} \frac{u}{k_1}\, e^{\tau}\, \frac{du}{k_1}, \tag{42b}$$

in which h_x represents the head on AF at any abscissa and h_A represents the head at A, in feet of fresh water. Equation 42b was integrated graphically to derive the curve shown in figure 25.

Computations for the semi-infinite aquifer of case 2, in which the outflow face is horizontal, were performed as follows. The width of the seepage surface AB was first obtained by substituting $y=0$, $x=x_s$, $\psi=Q$, $\phi=0$ into equation 35. The result, in dimensionless form, is $\frac{x_s k_1}{Q} = -\frac{1}{2}$, as shown in figure 25. The interface was computed by substituting $\psi=Q$ and $\phi=k_1 y$ into equation 35, giving

$$\left(\frac{yk_1}{Q}\right)^2 - 2\left(\frac{xk_1}{Q}\right) - 1 = 0, \tag{43}$$

which is plotted as the dashed curve labeled "interface" in figure 25.

The piezometric head on AF in the form $y_0 k_1/Q$ is obtained by substituting $\psi=0$, $y=0$ into equation 35, which yields

$$y_0 k_1/Q = \sqrt{2xk_1/Q}. \tag{44}$$

The velocity along AF is given by differentiating ϕ as obtained from equation 35:

$$\frac{u}{k_1} = \frac{-1}{k_1}\frac{\partial \phi}{\partial x} = -\sqrt{Q/2xk_1}. \tag{45}$$

COMPUTATIONS FOR FINITE AQUIFERS, CASE 1

The range of λ, values of θ, the relation between $\overline{q}$ (or u, v) and λ, and the specific form of equation 21 for each part of the boundary are given below in the most useful form for computations of finite aquifers with vertical outflow faces. For the outflow face AB (see fig. 21*A*),

$$-\infty < \lambda \leqq 0;\ \theta = -\frac{\pi}{2};\ \frac{u}{k_1} = \frac{K^1}{K}\left(\frac{1}{1-\lambda}\right);\ v = -k;\ \frac{y}{\eta} = -\int_{\infty}^{u} e^{\tau}\, \frac{du}{k_1}. \tag{46}$$

For the interface *BD;*

$$0 \leqq \lambda \leqq 1;\ \theta = -\frac{3\beta}{2};\ \frac{u}{v+k_1} = \tan\frac{\beta}{2} = \frac{K^1}{K}(\lambda);\ u^2 + v^2 + k_1 v = 0;\ \overline{q} = \frac{-ik_1}{2}(e^{i\beta} - 1);$$

$$\frac{x - x_B}{\eta} = \frac{1}{2}\int_{\pi}^{\beta} e^{\tau} \cos\frac{\beta}{2}\, d\beta;\ \frac{y - y_B}{\eta} = \frac{1}{2}\int_{\pi}^{\beta} e^{\tau} \sin\frac{\beta}{2}\, d\beta. \tag{47}$$

For the boundary segment *DE;*

$$1 \leqq \lambda \leqq c;\ \theta = -\pi;\ \frac{u}{k_1} = \frac{K^1}{K}\left(\frac{1}{\lambda}\right);\ \frac{x - x_D}{\eta} = -\int_0^u e^{\tau}\,\frac{du}{k_1}. \tag{48}$$

Equations 46, 47, and 48 are sufficient to define the relative magnitudes of the length and depth and, therefore, the aspect ratio ξ and also the location of the interface. Similar equations on *EF* and *FA* could be applied as a check on the overall dimensions. Computation of the discharge parameter $a = Q/k_1 d$ requires the use of equation 41, which applies equally to finite and semi-infinite aquifers. The specific values of the constants b and c (see equation 22 and fig. 21*C*) used in the computations and the corresponding values of a and ξ are given in table 1. The integrations indicated were performed by the trapezoidal rule using a choice of increments and scales intended to maintain three-place accuracy. The results shown graphically in figure 26 are referred to the same discharge by dividing the dimensionless coordinates given by equations 46, 47, and 48 by the dimensionless discharge given by equation 41.

TABLE 1.—*Parameters for computations plotted in figure 26*

b	c	$a = Q/k_1 d$	$\xi = l/d$
10	1	1. 021	0. 49
5	1	. 896	. 56
2	1	. 709	. 70
1. 2	1	. 663	. 93
1. 00235	1	. 309	1. 64
1. 00200	1. 00100	. 340	2. 14

The first four series of parameters in table 1, which correspond to the dashed curves in figure 26, are values from Muskat's (1935) cases 3, 4, 5, and 6 for gravity seepage of water through a rectangular dam having an impermeable base and no tailwater. His cases 3, 4, 5, and 6 are mathematically identical to the present problem when the interface reaches to the recharge reservoir, but he computed only the dimensions of the aquifer, the width of the outflow face, and the discharge; so the shape of the interfaces for these four cases are estimated.

The interface for the semi-infinite aquifer is shown also in figure 26. Only for a very short aquifer or a very short encroachment distance does the interface for the limited aquifer differ significantly from the corresponding part of the interface for the semi-infinite aquifer.

COMPUTATIONS FOR FINITE AQUIFERS, CASE 2

For the horizontal outflow face (fig. 22), equations 27 through 32 are applicable. The specific forms of the equations for the various

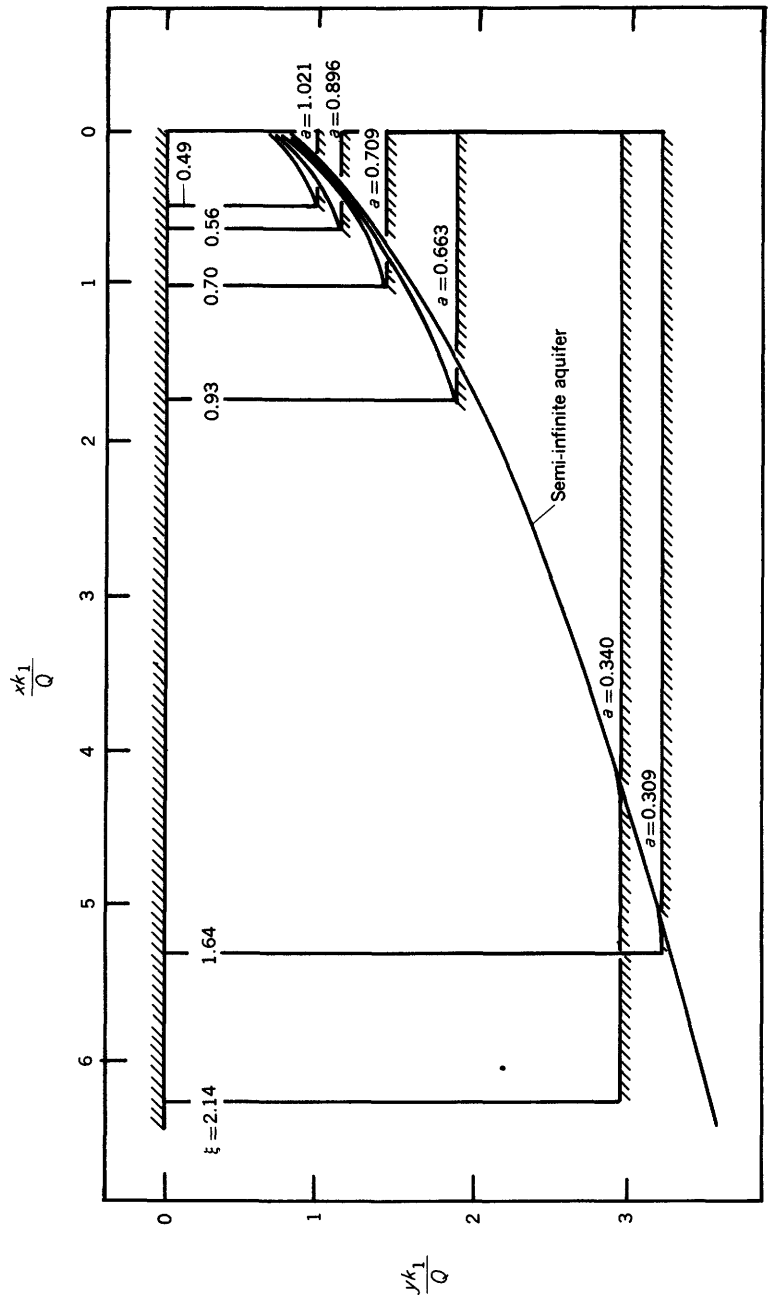

FIGURE 26.—Interfaces for vertical outflow face. Dashed curves are from Muskat's cases 3, 4, 5, and 6.

segments of the boundary and of the interface are as follows. The reference by Byrd and Friedman (1954) was helpful in determining the most convenient forms for the elliptic integrals. For the outflow face *AB:*

$$1 \geqq w_1 \geqq -1;\ -\infty < v \leqq -k_1;\ t = \cos\frac{\pi k_1}{v};\ \frac{x_s k_1}{Q} = -\int_0^Q \frac{k_1}{v}\frac{d\psi}{Q};\ \frac{\psi}{Q} = \frac{1}{2}\left(1 - \frac{sn^{-1}w_1}{K}\right). \tag{49}$$

For the interface *BD:*

$$-1 \geqq w_1 \geqq -d_1;\ 0 \leqq \frac{u}{v} < \infty;\ t = -\cosh\frac{\pi u}{v};\ \frac{xk_1}{Q} = \int_0^{yk_1} \frac{u}{v}\frac{d\phi}{Q};\ \frac{yk_1}{Q} = \frac{\phi}{Q} = \frac{-sn^{-1}(A, k')}{2K}, \tag{50}$$

where

$$k' = \sqrt{1-k^{*2}} \text{ and } A = \frac{\sqrt{w_1^2 - 1}}{k' - w_1}.$$

For the upper boundary *AF:*

$$1 \leqq w_1 \leqq 1/k^*;\ -\infty \leqq u \leqq u_F;\ t = \cosh\frac{\pi k_1}{u};\ \frac{lk_1}{Q} = \int_0^{\phi_F} \frac{k_1}{u}\frac{d\phi}{Q};\ \frac{\phi}{Q} = \frac{sn^{-1}(A, k')}{2K} \tag{51}$$

where u_F and ϕ_F are values of velocity and potential for which $w_1 = 1/k^*$. The segment *DE* of length l is given by

$$-d_1 \geqq w_1 \geqq 1/k^*;\ 0 \geqq u \geqq u_E;\ t = -\cosh\frac{\pi k_1}{u};\ \frac{l_1 k_1}{Q} = \int_{d_1 k_1}^{\phi_E} \frac{k_1}{u}\frac{d\phi}{Q};\ \frac{\phi}{Q} = \frac{-sn^{-1}(A, k')}{2K}, \tag{52}$$

where u_E and ϕ_E are values of velocity and potential that yield $w_1 = 1/k^*$. The two shortest interfaces in figure 27 were computed by use of the foregoing theory and the values of the parameters in table 2.

TABLE 2.—*Parameters for the two shortest interfaces in figure 27*

d_1	k^*	a	ξ
2	1/2	1. 56	0. 13
1/sin 89°	sin 89°	. 578	. 89

The integrals were evaluated by using the trapezoidal rule. The difficulty presented by the infinite value of u/v at the nose of the interface was circumvented by locating point D by computing l_1 along *ED* after obtaining l along *AF*.

For ξ approximately equal to or greater than unity, formulas 49 through 52 lead to elliptic integrals with moduli between sin 89° and sin 90°. To use the tabulated values of the elliptic integrals more

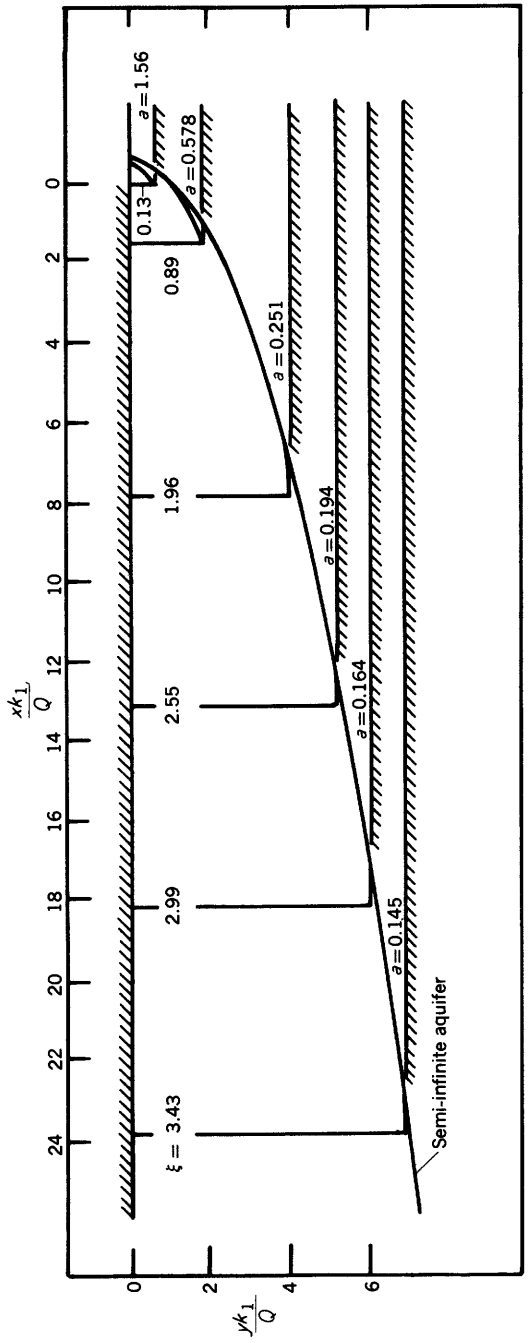

FIGURE 27.—Interfaces reaching to recharge reservoir, horizontal outflow face.

efficiently, the following alternative parametric relations between f and t were used

$$\frac{f}{Q}=\frac{K}{K'}\left[1-\frac{sn^{-1}w_1}{K}\right];\ t=\frac{w_2(k^*+1-2\underline{d}_2k^*)-2+\underline{d}_2+k\underline{d}_2}{w_2(1-k^*)+\underline{d}_2(k^*-1)} \tag{53a}$$

$$\frac{f}{Q}=\frac{K}{K'}\left[1+\frac{sn^{-1}w_3}{K}\right];\ t=\frac{-w_3(1+k^*+2\underline{d}_3k^*)-(2+\underline{d}_3+\underline{d}_3k^*)}{(1+k^*)w_3-\underline{d}_3(1-k^*)}, \tag{53b}$$

where $\underline{d}_2$ and $\underline{d}_3$ are the coordinates of the point D in the w_2 and w_3 planes, respectively, as shown in figure 28, and $\underline{d}_3=\dfrac{-1}{k^*\underline{d}_2}$.

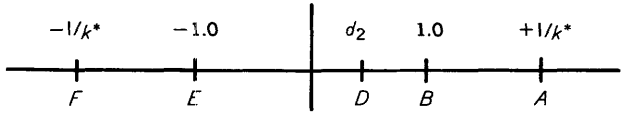

$A\ w_2$ plane, $f/Q=K/K^1[1-\frac{sn^{-1}w}{K}]+1$

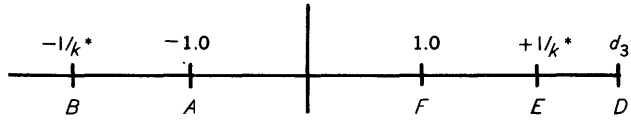

$B\ w_3$ plane $f/Q=K/K^1[\frac{sn^{-1}w_3}{K}+1]$

FIGURE 28.—Alternative transformations of f for horizontal outflow face.

Equation 53a is suited for computation of the outflow face AB, the interface BD, and the segment DE. The special form of f in equation 53a used for computation along AB is:

$$1\leqq w_2\leqq 1/k^*;\ \frac{\psi}{Q}=\frac{1-sn^{-1}(A,k')}{K'}. \tag{54}$$

The form for the interface:

$$1\geqq w_2\geqq \underline{d}_2;\ \frac{\phi}{Q}=\frac{K}{K'}-\frac{sn^{-1}(w_2,k^*)}{K'}. \tag{55}$$

The form for the segment *DE:*

$$\underline{d_2} \geqq w_2 \geqq -1; \frac{\phi}{Q} = \frac{K}{K'} - \frac{sn^{-1}(w_2, k^*)}{K'} \tag{56}$$

Equation 53b is useful for computation of the total length of the aquifer along face *AF* for which

$$-1 \leqq w_3 \leqq -1; \frac{\phi}{Q} = \frac{K}{K'} + \frac{sn^{-1}(w_3, k^*)}{K'} \tag{57}$$

The assumed values of $\underline{d_2}$ and k^* and resulting computed values of the aspect ratio ξ and discharge parameter a, using these alternative transformations, are given in table 3 for $\underline{d_2} = -1$.

TABLE 3.—*Parameters for the four longest interfaces in figure 27*

$\underline{d_2}$	$\underline{k^*}$	$\underline{a}$	ξ
−1	sin 89°	0. 145	3. 43
−1	sin 88°	. 164	2. 99
−1	sin 86°	. 194	2. 55
−1	sin 80°	. 251	1. 96

The corresponding interfaces reach to the recharge reservoir and are the four longest shown in figure 27.

Four instances in which $\underline{d_2} > -1$ and the interface do not extend to the recharge reservoir were computed and are shown in figure 29; the parameters are given in table 4.

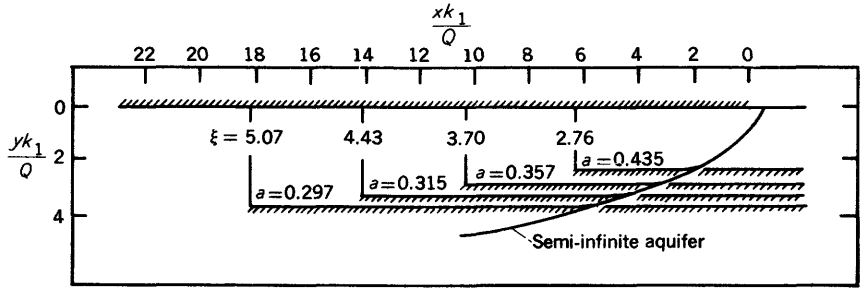

FIGURE 29.—Interfaces intersecting base of aquifer near ocean, horizontal outflow face.

TABLE 4.—*Parameters for the interfaces in figure 29*

$\underline{d_2}$	$\underline{k^*}$	$\underline{a}$	ξ
−sin 11°	sin 89°	0. 297	5. 07
−sin 14°	sin 88°	. 315	4. 43
−sin 21°	sin 86°	. 357	3. 70
−sin 27°	sin 80°	. 435	2. 76

In both figures 27 and 29 the results are presented in dimensionless form, which may be interpreted as holding the discharge constant in all instances. The interface for the semi-infinite aquifer is shown for comparison.

DISCUSSION OF RESULTS

Two significant conclusions are evident from these results. The first is that when the length of the salt-water wedge is greater than the aquifer depth, the interface in a finite aquifer is very nearly the same as that in a semi-infinite aquifer except at the lower end, and the difference between them may be neglected for most engineering purposes. The second conclusion is that changing the value of the aspect ratio of the aquifer has no appreciable effect upon the position of the interface, which is primarily determined by the dimensionless discharge parameter $a=Q/k_1d$.

The results for semi-infinite aquifers may also be compared to the interface derived under assumptions analogous to those used by Dupuit (1863) for gravity seepage in a two-dimensional aquifer. The Ghyben-Herzberg assumption that the pressure is hydrostatic in a vertical section is adopted, and one-dimensional flow according to Darcy's law is assumed in the horizontal direction. After integration, the coordinates of the interface are found to be

$$x=\frac{1}{2}\frac{y^2k_1}{Q}+\text{constant}. \tag{58}$$

The constant of integration cannot be determined for this solution without a field measurement of the coordinates of at least one point on the interface. If the constant is chosen equal to $-Q/2\overline{k}$, equation 58 would be identical with the equation for the interface for the semi-infinite aquifer having a horizontal outflow face. However, a common, though usually tacit, assumption is that the constant is zero (Kitagawa, 1939; Todd, 1953). Equation 58, with the constant set equal to zero, is plotted in figure 30 along with the curves for the semi-infinite aquifers of cases 1 and 2. Except near the ocean, this result is likely to be accurate enough for practical purposes of estimating the position and shape of the interface. The uncertainties in estimating the discharge and the aquifer permeability may be greater than the differences shown in figure 30.

To illustrate the application of equation 58 to a particular field condition, use is made of data obtained by Kohout for the Biscayne aquifer in the Cutler area near Miami, Fla. (See p. C12–C32, this report.) Figure 31 shows Kohout's isochlors, on which the interfaces for high, mean, and low tides are superposed. The interfaces were computed as if the flow were completely steady at each of the three instantaneous stages of the tide. The data necessary to plot the coordinates of the

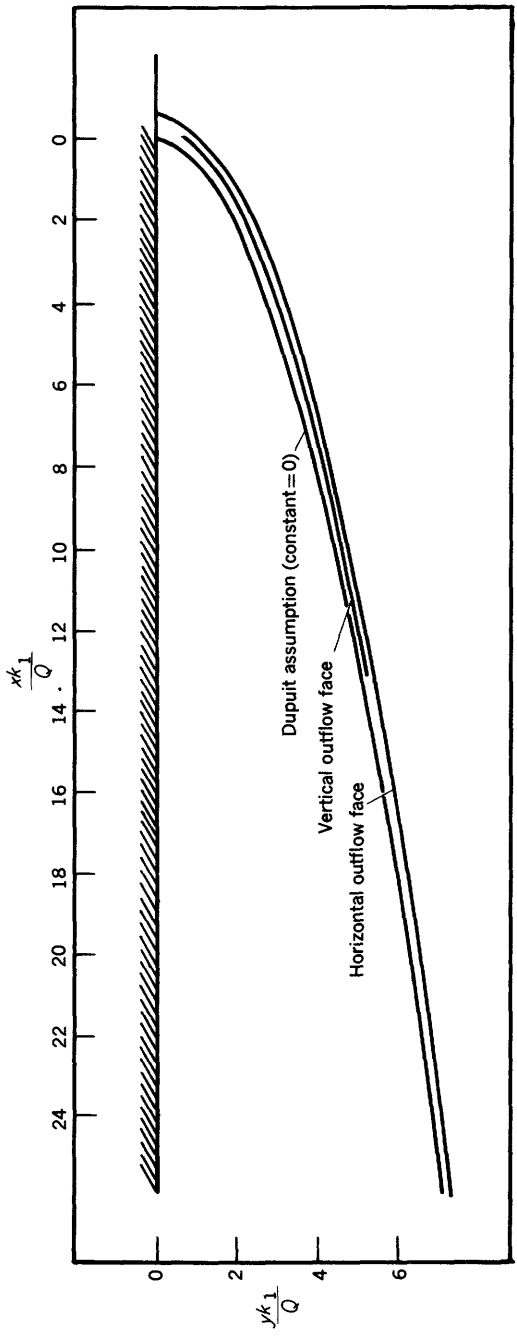

FIGURE 30.—Comparison of interfaces in semi-infinite artesian aquifers.

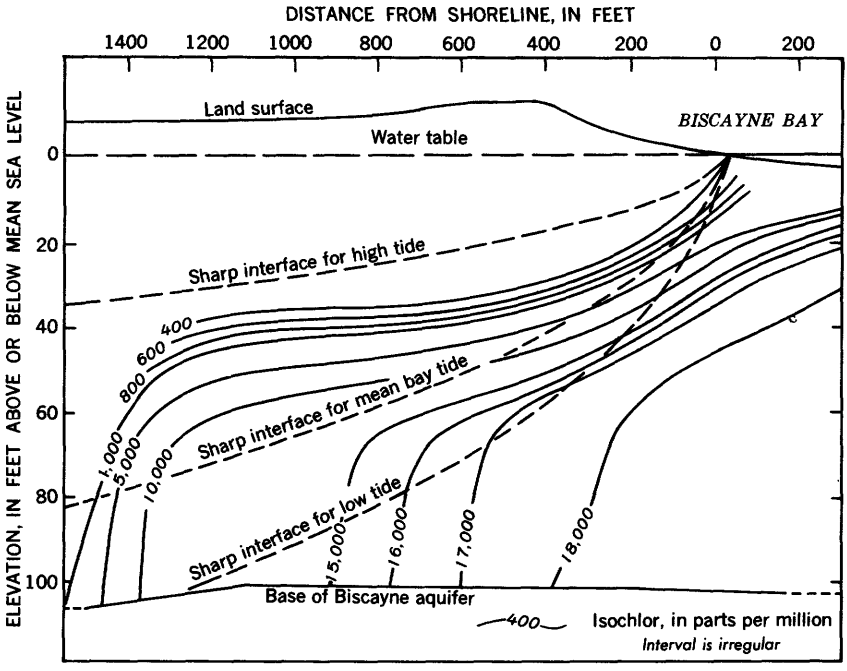

FIGURE 31.—Section through the Cutler area near Miami, Fla., showing isochlors on September 18, 1958, and interfaces computed as if conditions were steady at high, mean, and low tides.

interface are values of Q/k_1 for the three conditions and are estimated from the piezometric slopes shown by Kohout. For an average permeability of 8,000 feet per day as indicated by Kohout, the three interfaces represent steady conditions for Q=76, 440, and 840 foot^2 per day, respectively.

The interface corresponding to the mean bay level indicates the approximate location of the center of the dispersion zone except very near the ocean and at the inland extremity. With the same exceptions, the interfaces for high tide and low tide effectively circumscribe the dispersion zone. The solution for a sharp interface thus seems to give a first approximation of the location of the zone of diffusion. It is necessary, of course, to include the effect of dispersion to reproduce the gradual change from fresh to salt water. The inclusion of the dispersion also results in the change from the sharp toe of the salt-water wedge to the snub nose shape of the isochlors that intersect the bottom of the aquifer in figure 31. The condition including dispersion is discussed on pages C70–C84.

WATER-TABLE AQUIFERS RECEIVING VERTICAL RECHARGE

Where vertical recharge is absent, as assumed in the treatment of artesian aquifers, the vertical components of the velocity are small; so conditions are favorable for use of the Dupuit assumption. However, where vertical recharge exists, the influence of vertical components of the velocities may be appreciable. This is illustrated schematically in figure 32*A*, which shows the approximate position of the streamlines for fresh water seepage into a long oceanic island or peninsula. Here, x is the horizontal distance from the shore, l is the half width of the island, y is the depth below sea level to the interface, and V_0 is the rate of uniform vertical recharge per unit area.

The Dupuit equation for Q, the discharge per unit length of shore line, is

$$Q=-\overline{k}y\frac{dh}{dx}, \tag{59}$$

where $\overline{k}$ is the transmission coefficient, the piezometric head h is assumed to be constant in a vertical section, and y is assumed to include the entire depth of flow. The effect of a uniform recharge is to cause Q to increase with distance toward the shore according to the relation

$$Q=V_0(l-x). \tag{60}$$

Since the Dupuit equation makes no provision for vertical velocities, its application here requires the assumption that the recharge V_0 enters the aquifer through a continuous distribution of recharge wells from which flow occurs uniformly over the depth y. Using this assumption and the equality $h=\frac{\rho_s-\rho_0}{\rho_0}y$, the substitution of equation 60 into equation 59 and subsequent integration yields the following approximate relation between the coordinates of the interface:

$$y/l=\sqrt{\frac{V_0}{k_1}\left[\frac{2x}{l}-\left(\frac{x}{l}\right)^2\right]}, \tag{61}$$

where $k_1=\overline{k}\frac{\rho_s-\rho_0}{\rho_0}$, ρ_s is the density of salt water, and ρ_0 is the density of fresh water.

The object of the present paper is to find the position of the interface more precisely by use of the methods for potential flow in two dimensions.

GOVERNING EQUATIONS AND BOUNDARY CONDITIONS

In figure 32*A*, Laplace's equation applies to the region $ABDF'A$, where AB is the outflow seepage face on the ocean floor, BD is the

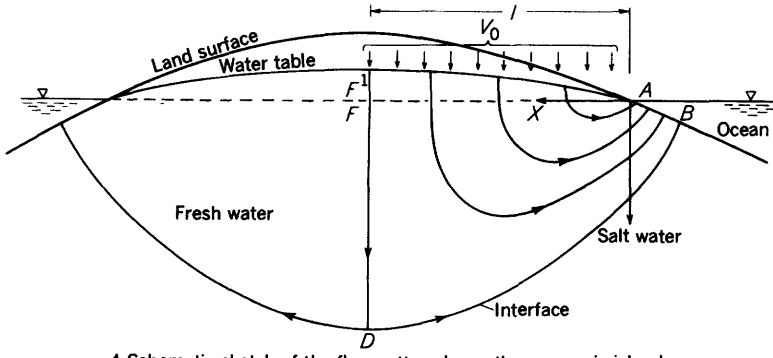

A Schematic sketch of the flow pattern beneath an oceanic island receiving uniform vertical recharge (not to scale)

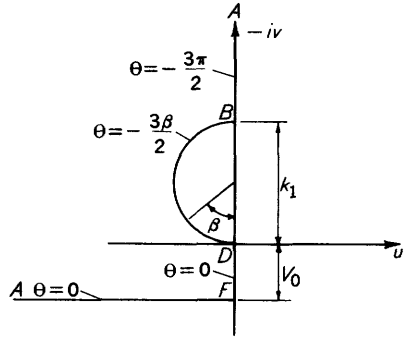

B hodograph ($\bar{q}$ plane) for region *ABDF*

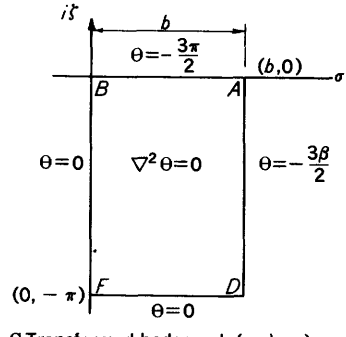

C Transformed hodograph (*w* plane)

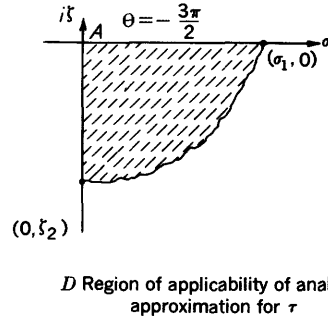

D Region of applicability of analytic approximation for τ

FIGURE 32.—Schematic sketch and complex planes for a water-table aquifer.

interface separating the static salt water from the flowing fresh water, DF' is a line of symmetry, and $F'A$ is the water table at which the uniform recharge V_0 enters the zone of saturation. The seepage face that occurs above sea level at A is small in relation to AB and is neglected in the analysis.

In satisfying the requirements imposed upon ϕ by the physical conditions at the boundaries of the flow system, a difficulty arises from the fact that the positions of both the water table $F'A$ and the interface BD are unknown. The hodograph is used to circumvent the difficulty pertaining to the position of the interface. The condition $\phi=k_1y$ on the interface leads to a semicircular hodographic representation of BD with diameter k_1 as shown in figure 32B and explained previously. The difficulty due to the unknown position of the water table is avoided by taking the x axis as the upper boundary of the flow region and by assuming that the vertical component of the velocity everywhere along the positive x axis is V_0. This is equivalent to ignoring the slight inclination of the streamlines in the saturated region $AFF'A$ above sea level. This approximation probably will not affect the computed position of the interface appreciably because the distance between the water table and the x axis is small in comparison to the total depth of flow. The approximation is similar to an assumption made by Kirkham (1958) in the solution of a drainage problem. Under these assumptions, the horizontal line FA in the hodograph represents the upper boundary of the flow region. The other lines delineating the boundaries of the hodograph are obtained by inspection of the flow boundaries in figure 32A. To yield the vertical line AB on the hodograph, the ocean bed AB is assumed to be horizontal. Thus, each segment of the boundary of the flow pattern has a known location in the hodograph plane.

The velocity potential ϕ which satisfies Laplace's equation in the z plane (the x, y plane in fig. 32A) also satisfies Laplace's equation in the q plane (fig. 32B). Values of ϕ are known only on a part of the boundary—namely, AB, the seepage face on the horizontal ocean floor. However, a method of solution is available by use of the auxiliary variable $\tau+i\theta$ introduced by Hamel (1934) and defined by

$$\tau+i\theta=\ln\left[\frac{d(\bar{q}/k_1)}{d(z/\eta)}\right], \tag{62}$$

where η is a constant of integration which serves as a reference length. The function θ is seen to be the complex argument of $\frac{d\bar{q}}{dz}=\frac{du-idv}{dx+idy}$, values of which can be obtained for each segment of the boundary. The boundary values of θ are indicated in figure 32B.

They are obtained by inspection except on the interface. The details of obtaining the value $\theta=-\frac{3\beta}{2}$ on the interface are similar to those given by Muskat (1935) in the solution for the free surface of seepage through a dam and to those of obtaining equations 18. If

values of τ can also be obtained along the boundaries, then the coordinates of the interface can be obtained by integrating equation 62. Thus,

$$z/\eta = \int e^{-(\tau+i\theta)} \frac{d\bar{q}}{k_1} + \text{constant.} \tag{63}$$

To obtain values of τ along the boundaries, values of θ must first be obtained in the interior of the region, after which the Cauchy-Riemann equations can be integrated for τ along the boundaries.

NUMERICAL SOLUTION

To facilitate the numerical determination of θ and the subsequent integration for τ, the hodograph is transformed into the rectangle in the $w=\sigma+i\zeta$ plane shown in figure 32*C*. The mapping function is

$$w = ln \frac{V_0 - i\bar{q} + k_1 a}{V_0 - i\bar{q} - k_1 a}. \tag{64}$$

This function maps the outflow face AB onto the σ axis in the interval (0, 0) to ($\underline{b}$, 0); the upper boundary of the region FA onto the ζ axis in the interval (0, 0) to (0, $-\pi$); the centerline of the island DF on the line $\zeta=-\pi$ in the interval (0, $-\pi$) to ($\underline{b}$, $-\pi$); and the interface BD on the line $\sigma=\underline{b}$ in the interval ($\underline{b}$, 0) to ($\underline{b}$, $-\pi$). The value of a in equation 64 is given by $a=\frac{1}{2}\sinh \underline{b}$ where $\underline{b}=\cosh^{-1}\left(\frac{2V_0}{k_1}+1\right)$. Since $\tau+i\theta$ is an analytic function of $\bar{q}$ and thus of w, the variation of θ throughout the rectangle in the w plane is described by Laplace's equation, $\frac{\partial^2\theta}{\partial\sigma^2}+\frac{\partial^2\theta}{\partial\zeta^2}=0$. The boundary values of θ in the w plane are the same as those at the corresponding points of the $\bar{q}$ plane. Before a solution for θ throughout the rectangle can be obtained the values of θ must be obtained for corresponding values of ζ on BD. These are found by substituting numerical values of $\beta=-2\theta/3$ into the following equations, obtained by applying the interface conditions to equation 64:

$$\zeta = \tan^{-1}\left[\frac{-2a\sin\beta}{1-\left(2\frac{V_0}{k_1}+1\right)\cos\beta}\right], \tag{65}$$

The solution for θ throughout the rectangle can then be obtained by any suitable numerical procedure. The procedure used herein consists of improving an initial guess by the relaxation technique applied to the finite-difference form of Laplace's equation in an appropriate grid system. After θ is determined, its normal derivatives at the

boundaries are obtained graphically and values of τ are computed by numerical integration of the Cauchy-Reimann equations along the boundaries. The integrals for the four boundary segments are:

on BD:

$$\tau-\tau_D=-\int_{-\pi}^{\zeta}\frac{\partial\theta}{\partial\sigma}\,d\zeta \tag{66a}$$

on DF:

$$\tau-\tau_D=-\int_{b}^{\sigma}\frac{\partial\theta}{\partial\zeta}\,d\sigma \tag{66b}$$

on AB:

$$\tau-\tau_B=-\int_{b}^{\sigma}\frac{\partial\theta}{\partial\zeta}\,d\sigma \tag{66c}$$

on FA:

$$\tau-\tau_F=-\int_{-\pi}^{\zeta}\frac{\partial\theta}{\partial\sigma}\,d\zeta \tag{66d}$$

The variation of τ is from the minimum value τ_D at D to infinity at A. In the application of equation 63, the reference length η absorbs the constant $e^{-\tau_D}$. The infinite value of τ at A necessitates a modification in the computations in the immediate vicinity of A. An analytical approximation for τ is obtained from the solution of the boundary value problem for the infinite quarter plane indicated in figure 32D, in which σ_1 and ζ_2 represent the limits of validity of the approximation. Along AB in the region $\theta\leq\sigma\leq\sigma_1$,

$$\tau-\tau_1\approx-3ln\frac{\sigma}{\sigma_1} \tag{67a}$$

where τ_1 is the value of τ at σ_1. Similarly along FA, in the region $\theta\geq\zeta\geq\zeta_2$

$$\tau-\tau_2\approx-3\ ln\frac{\zeta}{\zeta_2} \tag{67b}$$

The values σ_1 and ζ_2 are chosen within the range of overlap of applicability of equations 66c and 67a, and 66d and 67b.

After the boundary values of τ are determined, equation 63 may be integrated to yield the coordinates of the interface. Thus:

$$\frac{x-x_B}{\eta}=\frac{1}{2}\int_{\pi}^{\beta}e^{-\tau}\cos\beta/2d\beta \tag{68}$$

$$\frac{y-y_B}{\eta}=\frac{1}{2}\int_{\pi}^{\beta}e^{-\tau}\sin\beta/2d\beta. \tag{69}$$

The integration indicated in these equations is performed numerically after τ has been determined by a numerical integration of equation 66a. Equations 68 and 69 apparently determine the shape of the interface but not its coordinates because ν is unknown. The value of y_B is zero because the ocean floor is assumed to coincide with the x axis. The value of x_B, the distance from A to B, is given by the sum of the following two equations:

$$\frac{x_1-x_B}{\eta}=-\int_1^{-v_1/k_1} e^{-\tau}d(-v/k_1) \tag{70}$$

$$\frac{x_A-x_1}{\eta}=e^{-\tau_1}\int_{-v_1/k_1}^{\infty}\left(\frac{\sigma}{\sigma_1}\right)^3 d(-v/k_1). \tag{71}$$

Equations 70 and 71 are developed, respectively, from the two equations 66c and 67a used to determine τ on AB. Equation 70 is integrated numerically for values of the variables corresponding to $\sigma>\sigma_1$ (see fig. 32D). For values of the variables corresponding to $\sigma<\sigma_1$, equation 71 is used. The values v_1 and x_1 correspond to the value $\sigma=\sigma_1$. The values of v/k_1 are determined as a function of σ-by applying the outflow face conditions to equation 64a which yields

$$-v/k_1=a\coth(\sigma/2)-V_0/k_1. \tag{72}$$

The infinite integral 71 is evaluated by first obtaining an analytic approximation to $d(-v/k_1)$ near $\sigma=0$ by a series expansion:

$$d(-v/k_1)=\frac{-ad\sigma}{\cosh\sigma-1}\approx\frac{-2ad\sigma}{\sigma^2}. \tag{73}$$

By letting the range of application of the approximations 73 and 67a be identical, the integral in 71 reduces to

$$\frac{x_A-x_1}{\eta}=\frac{ae^{-\tau_1}}{\sigma_1}. \tag{74}$$

The dimensionless half width of the island l/η is obtained by subtracting the length of the outflow face AB from the total horizontal length $\frac{x_D-x_B}{\eta}$ of the interface. A division of the dimensionless coordinates x/η and y/η by l/η produces the more conventional dimensionless coordinates x/l and y/l. Thus, for any given V_0/k_1, the dimensionless coordinates can be obtained. Where desirable the absolute coordinates can then be obtained by multiplying these by the half width of the island.

The total depth of the fresh-water lens can be computed independently, except for the evaluation of τ, by another method. Applying to equation 63 the conditions on DF yields

$$\frac{y_F - y_D}{\eta} = \int_0^{V_0/k_1} e^{-\tau} d(v/k_1), \tag{75}$$

where τ is determined by equation 66b. The values of v/k_1 are determined by applying the conditions on DF to equation 64, which yields

$$v/k_1 = V_0/k_1 - a \tanh \frac{\sigma}{2}. \tag{76}$$

Equation 75 is integrated numerically. The half width l of the island can also be computed independently, except for the evaluation of τ, by summing the following two equations:

$$\frac{x_F - x_2}{\eta} = \int_0^{-u_2/k_1} e^{-\tau} d(-u/k_1) \tag{77}$$

$$\frac{x_2 - x_A}{\eta} = e^{-\tau_2} \int_{-u_2/k_1}^{\infty} \left(\frac{\zeta}{\zeta_2}\right)^3 d(-u/k_1). \tag{78}$$

Equations 77 and 78 correspond, respectively, to the two equations 66d and 67b used to determine τ on DF. Equation 77 is integrated numerically for values of the variables corresponding to $\zeta < \zeta_2$ (see fig. 32_D). For values of the variables corresponding to $\zeta > \zeta_2$ equation 78 is used. The values u_2 and x_2 correspond to the value $\zeta = \zeta_2$. The values of u/k_1 are determined as a function of ζ by applying the conditions on FA to equation 64. This yields

$$u/k_1 = a \cot (\zeta/2). \tag{79}$$

The infinite integral 78 is evaluated by first obtaining an analytic approximation to $d(u/k_1)$ near $\zeta = 0$ by a series expansion:

$$d(u/k_1) = \frac{-a d\zeta}{1 - \cos \zeta} = \frac{2a d\zeta}{\zeta^2}. \tag{80}$$

If one lets the range of application of the approximations 80 and 67b be identical, the integral in 78 reduces to

$$\frac{x_2 - x_A}{\eta} = \frac{-a e^{-\tau_2}}{\zeta_2}. \tag{81}$$

The depth of the fresh-water lens at D as computed from equation 75 should be the same as the maximum ordinate of the interface as computed from equation 69. Similarly, the half width of the island

as computed by summing equations 77 and 78 should be the same as the maximum abscissa of the interface as given by equation 68 less the distance from A to B as given by the sum of equations 70 and 71.

DISCUSSION OF RESULTS

The procedure outlined above was applied to two values of the recharge parameter V_0/k_1,—namely, 0.755 and 0.0062. The degree of accuracy of the computations is indicated by the fact that the values of l and y_D computed by the two alternative potential-theory methods agreed withir 3 percent.

For an aquifer having a transmission coefficient of $\bar{k}=40$ feet per day and for a density difference ratio of $\frac{\rho_s-\rho_0}{\rho_0}=1/40$, the larger value of V_0/k_1 would correspond to a rate of recharge of 9 inches per day. Such a rate is of course unrealistically high, except possibly for artificial recharge. The purpose of this computation was to investigate how the position and shape of the interface are affected by a high rate of recharge. The effects are shown in figure 33*a*. As one

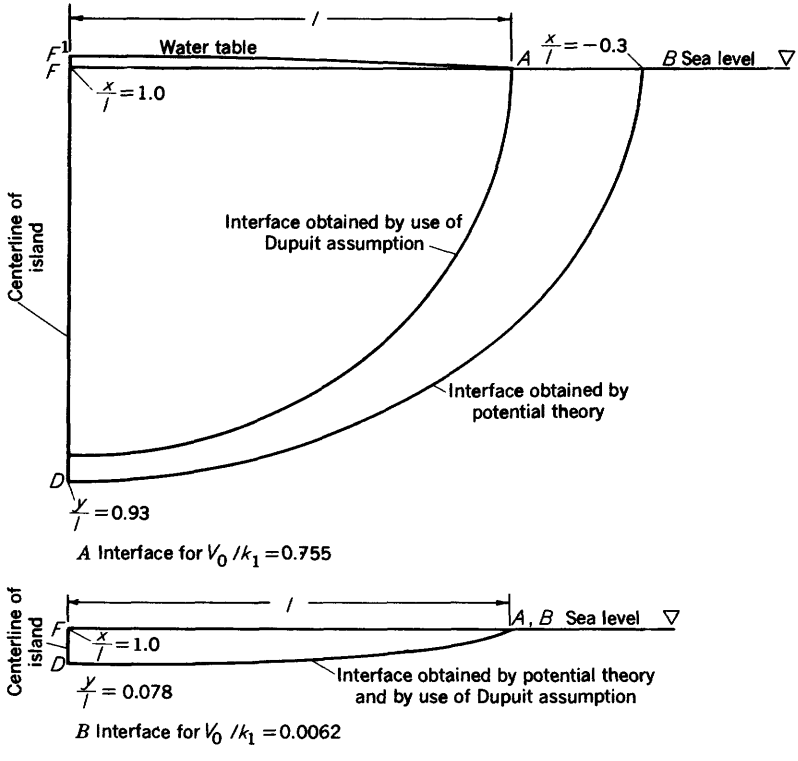

FIGURE 33—Numerical solutions for interfaces in water-table aquifers.

would expect, the maximum depth of the interface DF and the width of the outflow face AB are both large in relation to the half width of the island. However, the significant fact demonstrated is that with very large recharge the interface computed from potential theory is much deeper and more seaward than that computed by use of the Dupuit assumption.

The rate of recharge corresponding to the smaller value of V_0/k_1, with the same values of $\bar{k}$ and $\frac{\rho_s - \rho_0}{\rho_0}$ as used above is 27 inches per year. Although this conforms more nearly to that which could occur naturally, it is still extremely large. Rarely in nature would the recharge parameter V_0/k_1 be as large as 0.0062. Even so, the position of the interface computed by potential theory and by use of the Dupuit assumption are so nearly the same that they are indistinguishable in the plot shown in figure 33*b*. Therefore, the use of the Dupuit assumption appears to give results that are sufficiently accurate for many purposes. Only where l is large and the subject of interest is the position of the interface near the shore would the use of the Dupuit assumption be likely to cause an appreciable error. Other significant features of figure 33*b* are the maximum depth of the interface DF, which is $0.078l$, and the width of the interface AB, which is so small as to be imperceptible on the scale of the figure.

EFFECTS OF DISPERSION ON SALT ENCROACHMENT IN COASTAL AQUIFERS

By HAROLD R. HENRY

ABSTRACT

The problem of salt encroachment, including the effects of dispersion, is treated for an artesian aquifer in which there is a steady seaward flow of fresh water. Darcy's equation with variable density and the continuity equations for water and for salt are the governing equations. In terms of the dimensionless stream function ψ' and the salt concentration c', these equations reduce to

$$\nabla^2\psi' = (k_1 d/Q)\frac{\partial c'}{\partial x}$$

and

$$(D/Q)\nabla^2 c' = \frac{\partial c'}{\partial x}\frac{\partial \psi'}{\partial y} - \frac{\partial \psi'}{\partial x}\frac{\partial c'}{\partial y},$$

where k_1 is the transmission coefficient times the density difference ratio $(\rho_s - \rho_0)/\rho_0$, d is the depth of the aquifer, Q is the net fresh-water discharge, and D is the dispersion coefficient. The effect of tidally induced motion in producing a large effective D is discussed.

The nonlinear-boundary-value problem is reduced to an infinite set of nonlinear algebraic equations by the assumption of Fourier series representations of ψ' and c' and a subsequent application of the Galerkin procedure to yield equations for the Fourier coefficients. A truncated set of these algebraic equations is solved by an iterative scheme, and numerical values of c' and ψ' are presented for a specific problem. The pattern of the concentration c' is compared to the sharp interface that would exist in the limiting case of no diffusion. The pattern of c' for the other extreme, diffusion with no density difference, also is presented for comparison.

The computations show that dispersion induces a landward flow of salt water in the lower part of the aquifer and reduces the extent of salt encroachment.

INTRODUCTION

The extent of encroachment of sea water and the location of the zone of brackish water are significant factors in determining the use of ground water from coastal areas. Using the description of conditions at the interface in terms of the velocity potential of the fresh water, Hubbert (1940) gave the boundary conditions at an interface. These conditions are analogous to those prevailing at the free surface of water seeping by gravity through an aquifer. Glover (see p. C32–C35, this report) utilized an exact solution of this free-surface problem by Kozeny (1953) to represent the solution of the analogous salt-encroachment problem for an artesian aquifer of infinite depth. The writer solved the potential problem for finite aquifers with horizontal and vertical outflow faces. (See p. C35–C70.)

All these analyses treat the interface between the fresh water and salt water as if it were sharp and well defined, whereas in reality the salt water merges with the fresh water in a zone of diffusion. If this zone is a narrow band, as it is in some coastal aquifers (Brown, 1925), the solution for a sharp interface may be used to obtain a first approximation to the fresh water flow pattern. If, on the other hand, the zone of diffusion is extensive, as in the Biscayne aquifer of southeastern Florida (see p. C12–C32, this report), an analysis which takes into account the dispersion process and the entrainment of salt water by the moving fresh water is necessary.

The dispersion of salt water and fresh water in porous media is the result of two phenomena. The first is the mechanical mixing which results because, under a given potential gradient, the fluid in the larger pores will move faster than that in the smaller ones, and also because the fluid near the center of a pore will move faster than that at the periphery. Thus, where a potential gradient exists, filaments of fresh water will extend into the salt water, and vice versa. The second

phenomena is molecular diffusion, which completes the process by diffusing the filaments on a microscopic scale. Although the dispersion process is dominated by mechanical mixing, it may nevertheless be described by a Fickian-type law similar to that used for molecular diffusion (Barrer, 1951)—that is, the dispersive mass transfer is of the form $-D\nabla c$. Whereas the coefficient of molecular diffusion is related to a velocity and a length, both characteristic of the molecular activity, the coefficient of dispersion D depends upon the macroscopic fluid velocity and a length which is characteristic of the aquifer pores.

Several recent studies have increased understanding of the physics of the dispersion in granular media. Wentworth (1948) analyzed the zone of diffusion under the hypothesis of a rinsing action due to tides. Scheidegger (1954, 1958) applied statistical procedures to derive a modification of Darcy's law which includes effects of dispersion. Day (1956) used this approach also in analyzing experimental data of one-dimensional dispersion. Other experiments (Rifai and others, 1956; Ogata; [2] Simpson [3]) indicated that the dispersion coefficient in the direction of the velocity is approximately proportional to the velocity—that is, $D=Mu$—and that the dispersion coefficient in the lateral direction is much smaller. Here, M is a proportionality constant which depends upon the pore characteristics of the aquifer, and u is the velocity that appears in Darcy's law.

The magnitude of the dispersion is determined principally by the movements of water in an aquifer produced by tides and seasonal fluctuations in recharge. However, if inland from the range of tidal effect the fresh water flows seaward at a steady rate and no further recharge near the beach occurs, then one can define "steady-flow" quantities as being the temporal averages of instantaneous quantities averaged over a period of many tidal cycles. In this sense the flow may be considered steady, the sea level constant, and the tides only as a mechanism producing dispersion, as discussed by Cooper (see p. C1–C12). Cooper theorized that the dispersion is sufficient to cause a large amount of salt water to become entrained in the otherwise fresh water flowing seaward and that this induces a motion of salt water from the ocean into the zone of diffusion. This circulating motion of the salt water has been confirmed by the field measurements of Kohout. (See p. C12–C32, this paper.)

The present paper takes into account the effects of dispersion at the salt-water front and derives the flow and concentration patterns. The macroscopic point of view is assumed, and Cooper's ideas concerning the effect of the tides are utilized to determine the approxi-

---

[2] Ogata, Akio, 1958, Dispersion in porous media: Evanston, Ill., Northwestern Univ. Ph. D. dissertation.

[3] Simpson, Eugene, 1960, Transverse dispersion in liquid flow through porous media: New York, Columbia Univ. Ph. D. dissertation.

mate magnitude of the dispersion coefficient under certain field conditions. Experiments indicate that the dispersion is directional and that its magnitude perpendicular to the velocity is much smaller than that in the direction of the velocity. It is assumed here that the flow pattern is approximated by using for D an effective value that is scalar and does not vary with direction or with the magnitude of the velocity but is constant throughout the aquifer. Although these assumptions are broad, they enable analytical demonstrations of certain significant consequences of dispersion which to date have been inferred only on a qualitative basis. These consequences are the circulation of salt water mentioned above and a reduction of the inland extent of salt water.

ACKNOWLEDGMENTS

This paper is based upon the writer's doctoral dissertation at Columbia University.[4] The problem was suggested by H. H. Cooper, Jr., and the research was supported by the U.S. Geological Survey. The writer is grateful to Prof. Richard Skalak for his criticism throughout the preparation of this paper. Mrs. Judy Tasman programmed the computations for the IBM 650 computer.

NOTATION

The symbols used most frequently herein are defined below.

$a = Q/k_1 d$
$b = D/Q$
c = concentration of salt, in mass per unit volume of solution, slugs per ft^3
c_s = concentration of salt in sea water, slugs per ft^3
$c' = c/c_s$
$C = (c' - x/\xi)$
d = thickness of aquifer, ft
D = dispersion coefficient, ft^2 per sec
E = dimensionless coefficient relating the concentration to the density of the solution
$\vec{g}$ = vector acceleration of gravity, ft per sec^2
k = permeability of sand, ft^2
$\bar{k}$ = transmission coefficient of aquifer $= \frac{k\rho_0 g}{\mu}$, ft per sec
k_1 = transmission coefficient times the density-difference ratio $= \bar{k}\,\frac{\rho_s - \rho_0}{\rho_0}$, ft per sec
l = length of aquifer, ft
p = pressure, lbs per ft^2
Q = net fresh-water discharge per unit length of beach, ft^2 per sec
$\vec{q}$ = vector fluid velocity, ft per sec

[4] See footnote 1, p. C36.

u = horizontal velocity, ft per sec
v = vertical velocity, ft per sec
x, y = coordinates, ft (when used as subscripts, x and y denote differentiation)
$x' = x/d$
$y' = y/d$
ρ = density of solution, slugs per ft^3
ρ_0 = density of fresh water, slugs per ft^3
ρ_s = density of sea water, slugs per ft^3
ρ_w = mass of water contained in a unit volume of solution, slugs per ft^3
$\rho' = \frac{\rho - \rho_0}{\rho_s - \rho_0}$
μ = viscosity of water, lb-sec per ft^2
ψ' = dimensionless stream function
$\Psi = (\psi' - y/d) = (\psi' - y')$
$\xi = l/d$ = aspect ratio

FIELD EQUATIONS AND BOUNDARY CONDITIONS

When dispersion is taken into account, the equation of motion, which is Darcy's equation, must be written with density as a variable since the density varies with the salt concentration. The general vector form of Darcy's equation is (Hubbert, 1953; Offeringa and Van der Poel, 1954):

$$\vec{q} = -\frac{k}{\mu}(\nabla p - \vec{\rho g}). \tag{1}$$

In addition to equation 1, equations of continuity must be satisfied for the water and the salt. The conservation of mass of water in steady flow is expressed by

$$\nabla \cdot \rho_w \vec{q} = 0, \tag{2}$$

where ρ_w is the mass of pure water per unit volume of the solution. The conservation of the mass of salt in solution in steady flow is expressed by a similar equation, $\nabla \cdot c\vec{q}_e = 0$, where c is the mass per unit volume of the salt and $\vec{q}_e$ is the effective vector velocity of the motion of the salt. This velocity is the sum of the average fluid velocity q and that due to dispersion, $-D\nabla c$. Thus, the equation of continuity for the salt becomes

$$\nabla \cdot c\vec{q} - \nabla \cdot D\nabla c = 0. \tag{3}$$

It is assumed here that the unsteady effects of the tides and recharge can be averaged and superposed on the steady seaward flow by using a suitable dispersion coefficient D.

In the treatment of equations 1, 2, and 3 it is convenient to introduce the dimensionless quantities

$$u' = \frac{ud}{Q},\ v' = \frac{vd}{Q},\ x' = \frac{x}{d},\ y' = \frac{y}{d},\ c' = \frac{c}{c_s},\ \text{and}\ \rho' = \frac{\rho - \rho_0}{\rho_s - \rho_0}. \tag{4}$$

Equation 2 can be simplified by using the empirical relation between the density ρ of the mixture and ρ_w of the pure water (Baxter and Wallace, 1916) as indicated by

$$\rho=\rho_w+c=\rho_0+(1-E)c, \tag{5}$$

where E is a dimensionless constant which has the approximate value 0.3 for concentrations to as much as that of sea water. Inserting equation 5 into equation 2 yields

$$\nabla\cdot q-\frac{Ec_s}{\rho_0}(\nabla\cdot c'q)=0. \tag{6}$$

The quantity c' has an order of magnitude of unity, so that $\nabla\cdot c'q$ is of the same order of magnitude as $\nabla\cdot q$. For sea water, $\frac{Ec_s}{\rho_0}$ is about 0.008, and hence the order of magnitude of the second term in equation 6 is smaller than that of the first. When the second term is dropped, $\nabla\cdot q=0$, which implies the existence of a stream function that will be defined as a dimensionless quantity by

$$u'=\frac{\partial\psi'}{\partial y'},\ v'=-\frac{\partial\psi'}{\partial x'}. \tag{7}$$

Pressure can be eliminated from equation 1 by writing the scalar forms of equation 1 and differentiating u with respect to y, v with respect to x, and subtracting. A substitution of the derivations of equation 7 then eliminates u and v in favor of ψ', and the use of $\rho'=c'$ obtained from equation 5 yields

$$\nabla^2\psi'=\frac{k_1d}{Q}\frac{\partial c'}{\partial x'}. \tag{8}$$

In equation 3 the dispersion coefficient D is a function of the velocity (Rifai, Kaufman, and Todd, 1956; Simpson[5]) and, therefore, cannot in principle be determined before the problem is solved. Also, in applying equations 1, 2, and 3 to the salt intrusion problem, which is unsteady due to tidal activity, the burden of absorbing all the unsteady terms, which would appear in a more detailed analysis, is put upon D. However, it is assumed for purposes of the analysis that a representative average value of D is given and that its use as a constant scalar throughout the field of flow will not destroy the essential features of the problem. Assuming D constant and sub-

[5] See footnote 3, p. C72.

stituting for u and v in terms of ψ in equation 3 yields the following dimensionless form:

$$\frac{D}{Q}\nabla^2 c' = \frac{\partial \psi'}{\partial y'}\frac{\partial c'}{\partial x'} - \frac{\partial \psi'}{\partial x'}\frac{\partial c'}{\partial y'}. \tag{9}$$

Equations 8 and 9 reveal the two significant parameters of the problem, $k_1 d/Q$ and D/Q.

The model treated in this study is a rectangular confined aquifer in contact with a fresh-water reservoir on one end and the ocean on the other, as shown in figure 34. Along the impermeable boundaries at the top and bottom of the aquifer the normal velocity must be zero, so that ψ is constant. Moreover, along these boundaries the normal diffusive movement of salt must also be zero, so that the derivative $\frac{\partial c'}{\partial y'}$ vanishes. The latter condition requires that the isochlors approach the base of the aquifer vertically. This explains at least in part the prominent blunted shape of the toe of the salt-water wedge observed by Kohout. (See fig. 31.)

Along the vertical boundaries the pressure distributions are hydrostatic, so that $\frac{\partial \psi'}{\partial x'}=0$. Also, along the fresh-water side $c'=0$, and along the ocean side $c'=1$.

The boundary conditions are summarized below. (See fig. 34.)

$$\text{At } y'=0: \psi'=0, \frac{\partial c'}{\partial y'}=0 \qquad \text{At } x'=0: \frac{\partial \psi'}{\partial x'}=0, c'=0$$

$$\text{At } y'=1: \psi'=1, \frac{\partial c'}{\partial y'}=0 \qquad \text{At } x'=1: \frac{\partial \psi'}{\partial x'}=0, c'=1. \tag{10}$$

FOURIER-GALERKIN SOLUTION

A method of solution similar to that used by Poots (1958) in a problem of heat transfer is utilized to solve the nonlinear boundary value problem defined by equations 8, 9, and 10. First, new variables are introduced to simplify the boundary conditions: let

$$\Psi = \psi - y', \; C = c' - \frac{x'}{\xi}. \tag{11}$$

With the primes omitted; with the substitutions $\xi = l/d$, $a = Q/k_1 d$, $b = D/Q$; and with the use of subscripts to denote differentiation, the problem in terms of Ψ and C becomes

$$a\nabla^2\Psi = C_x + \frac{1}{\xi} \tag{12}$$

$$b\nabla^2 C = \Psi_y C_x - \Psi_x C_y + \frac{1}{\xi}\Psi_y + C_x + \frac{1}{\xi} \tag{13}$$

$$\text{At } y=0, 1: \Psi=0, C_y=0 \qquad \text{At } x=0, \xi: \Psi=0, C=0. \tag{14}$$

The functions Ψ and C can be represented by double Fourier series which satisfy the boundary conditions, equation 14, identically:

$$\Psi=\sum_{m=1}^{\infty}\sum_{n=0}^{\infty} A_{m,n}\sin(m\pi y)\cos(n\pi x/\xi) \tag{15}$$

$$C=\sum_{r=0}^{\infty}\sum_{s=1}^{\infty} B_{r,s}\cos(r\pi y)\sin(s\pi x/\xi). \tag{16}$$

If the coefficients $A_{m,n}$ and $B_{r,s}$ are chosen in such a manner that the differential equations 12 and 13 are satisfied, then equations 15 and 16 will constitute the solution. This is accomplished by substituting the Fourier representations for Ψ and C into equations 12 and 13 and applying Galerkin's method (Galerkin, 1915; Duncan, 1938). Galerkin's method in this instance consists of multiplying equation 12 by 4 $\sin(g\pi y)\cos(h\pi x/\xi)$ and equation 13 by 4 $\cos(g\pi y)\sin(h\pi x/\xi)$ after substituting from equations 15 and 16 for C and Ψ, and then integrating each equation over the rectangular domain. This gives an infinite set of algebraic equations for the Fourier coefficients $A_{g,h}$ and $B_{g,h}$, as follows:

$$\epsilon_2 a\pi^2 A_{g,h}\left[g^2+\frac{h^2}{\xi^2}\right]\xi=\sum_{r=0}^{\infty} B_{r,h}\cdot h\cdot N(g,r)+\frac{4}{\pi}W(g,h) \tag{17}$$

$$\epsilon_1 b\pi^2 B_{g,h}\left[g^2+\frac{h^2}{\xi^2}\right]\xi=\frac{\pi}{4}\sum_{m=1}^{\infty}\sum_{n=0}^{\infty}\sum_{r=0}^{\infty}\sum_{s=1}^{\infty} A_{m,n}B_{r,s}(msLR-nrFG)$$
$$+\sum_{n=0}^{\infty} A_{g,n}\cdot g\cdot N(h,n)+\epsilon_1\sum_{s=1}^{\infty} B_{g,s}\cdot s\cdot N(h,s)+\frac{4}{\pi}W(h,g). \tag{18}$$

The notation in equations 17 and 18 is defined below where δ is the Kronecker delta:

$$F=\delta_{(m-r),s}+\delta_{(r-m),s}-\delta_{(m+r),s}$$

$$L=\delta_{(m-r),s}+\delta_{(r-m),s}+\delta_{(m+r),s}$$

$$G=\frac{(-1)^{h+n-s}-1}{h+n-s}+\frac{(-1)^{h-n-s}-1}{h-n-s}-\frac{(-1)^{h+n+s}-1}{h+n+s}-\frac{(-1)^{h-n-s}-1}{h-n-s}$$

$$R=\frac{(-1)^{h+n-s}-1}{h+n-s}+\frac{(-1)^{h-n-s}-1}{h-n-s}+\frac{(-1)^{h+n+s}-1}{h+n+s}+\frac{(-1)^{h-n-s}-1}{h-n-s}$$

$$N(h,n)=\frac{(-1)^{h+n}-1}{h+n}+\frac{(-1)^{h-n}-1}{h-n}$$

$$W(h,g)=\begin{cases}(-1)^h-1/h \text{ if } g=0\\ 0 \text{ if } g\neq 0\end{cases}$$

$$\epsilon_1=\begin{cases}2 \text{ if } g=0\\ 1 \text{ if } g\neq 0\end{cases}$$

$$\epsilon_2=\begin{cases}2 \text{ if } h=0\\ 1 \text{ if } h\neq 0\end{cases}$$

A truncated set of equations 17 and 18 was solved numerically. This gave an approximation to the true solution in a least squares sense for the truncated set of coefficients retained.

NUMERICAL SOLUTION

The selection of the parameters $\xi=\frac{l}{d}$, $a=Q/k_1d$, and $b=D/Q$ for the numerical solutions was governed by two considerations. On one hand it is desirable that the parameters correspond as nearly as possible with field data. For the data presented by Kohout (see p. C12–C32, this report) the field values were approximately $\xi=16$, $a=0.04$, $0.01<b<0.001$. On the other hand, parameters must be chosen that will make the numerical procedures converge. The parameters which will lead to a significantly accurate solution within a manageable truncation of equations 17 and 18 cannot be determined in advance. However, two general observations can be made before making any trials. The first is that values of ξ greater than unity will probably require the values of the index h to be greater than those of g, the difference increasing with ξ. The second is that small values of b should yield a solution approaching that for an interface, which would require terms with large values of g and h to describe accurately the sharp increase in concentration. With these considerations in mind and after some preliminary computations, the values $\xi=2$, $a=0.450$, $b=0.100$ were chosen for initial computations to be performed with the use of a slide rule and a desk calculator. The value $b=0.100$ is about 10 times the average value caused by the tides in the Biscayne aquifer. The value $a=0.450$ yields a corresponding interface which strikes the aquifer bottom approximately at the midpoint of its length for $\xi=2$. An additional case with $\xi=2$, $a=0.263$, $b=0.100$ was chosen to show the effect of varying fresh water discharge. The value of $a=0.263$ yields a corresponding interface which reaches to the upstream reservoir when $\xi=2$ as shown in figure 34*B*.

The computations with slide rule and desk calculator were performed for the following truncation: $A_{1,0}$ through $A_{1,10}$; $A_{2,1}$ through $A_{2,7}$; $B_{0,1}$ through $B_{0,14}$; $B_{1,1}$ through $B_{1,11}$; $B_{2,1}$ through $B_{2,7}$. An iterative procedure was used wherein the nonlinear terms in equation 18 were first assumed to be zero. The resulting linear equations yielded approximations for $A_{g,h}$ and $B_{g,h}$ which were then used to compute numerical values of the quadratic terms. These were substituted in equation 17, and the resulting set of linear equations were solved for new approximations of $A_{g,h}$ and $B_{g,h}$. Three iterative cycles were carried out. The linear systems were rearranged to give a strong main diagonal for the matrix of the coefficients and were then solved by relaxation.

Convergence of the numerical procedure was indicated by the computations with slide rule and desk calculator, and the streamlines and isochlors obtained from three iterative cycles on the Fourier coefficients conformed generally to the pattern measured in the field by Kohout. (See fig. 9.) However, the values of ψ' and c' determined by these computations were not sufficiently accurate at all places in the aquifer, and it appeared that the labor involved in obtaining sufficient accuracy with slide rule and desk calculator would be prohibitive. It was desired that ψ' and c' be determined within two significant figures, and to accomplish this the problem was programmed for the IBM 650 digital computer. The machines at the Watson Computing Laboratories and the Electronic Research Laboratories at Columbia University were used.

Two sets of parameters, $\xi=2$, $a=0.450$, $b=0.100$ and $\xi=2$, $a=0.263$, $b=0.100$ were used in the enlarged truncation: $A_{1,10}$ through $A_{1,15}$; $A_{2,1}$ through $A_{2,10}$; $A_{3,0}$ through $A_{3,5}$; $A_{4,1}$ through $A_{4,3}$; $A_{5,0}$ through $A_{5,2}$; $B_{0,1}$ through $B_{0,20}$; $B_{1,1}$ through $B_{1,10}$; $B_{2,1}$ through $B_{2,5}$; $B_{3,1}$ through $B_{3,3}$; and $B_{4,1}$ through $B_{4,2}$. In the initial machine computations the quadratic terms in equation 18 were assumed to be zero, the resultant linear system consisting of equations 17 and 18 were solved for the $A_{g,h}$ and the $B_{g,h}$, and these were used to compute numerical values for the quadratic terms. Using these terms as constants, the linear system was then solved for new values of the coefficients. After three iterative cycles using the first set of parameters and five using the second set had been run, it was apparent that the numerical procedure was not converging. This was indicated by the fact that the successive computed values for any particular $B_{g,h}$ or $A_{g,h}$ fluctuated, apparently without tending toward any limit. In addition, the computed values of ψ' and c' after successive iterations became progressively more different from what one would expect by comparison with the field data of Kohout. Furthermore, after the fifth iteration for the second set of parameters, the computed values of c' were as high as 1.9, whereas they should not exceed 1.00. The computation of the quadratic terms for each iteration took approximately 14 hours of machine time.

As a result of this experience, a modified procedure employing the digital computer was applied to the set of parameters $\xi=2.0$, $a=0.263$, $b=0.100$. In this procedure, the quadratic terms were first computed from values of the $A_{g,h}$ and $B_{g,h}$ obtained from an assumed distribution of ψ' and c'. An iterative solution of equation 18 was used in which the $B_{0,h}$ were held constant and new values of the $B_{g,h}$ ($g>0$) were computed by several subiterations and vice versa. The subiterative cycle consisted of recomputing the values of the quadratic terms using the revised values of $B_{g,h}$ ($g>0$) while continuing to hold the $B_{0,h}$

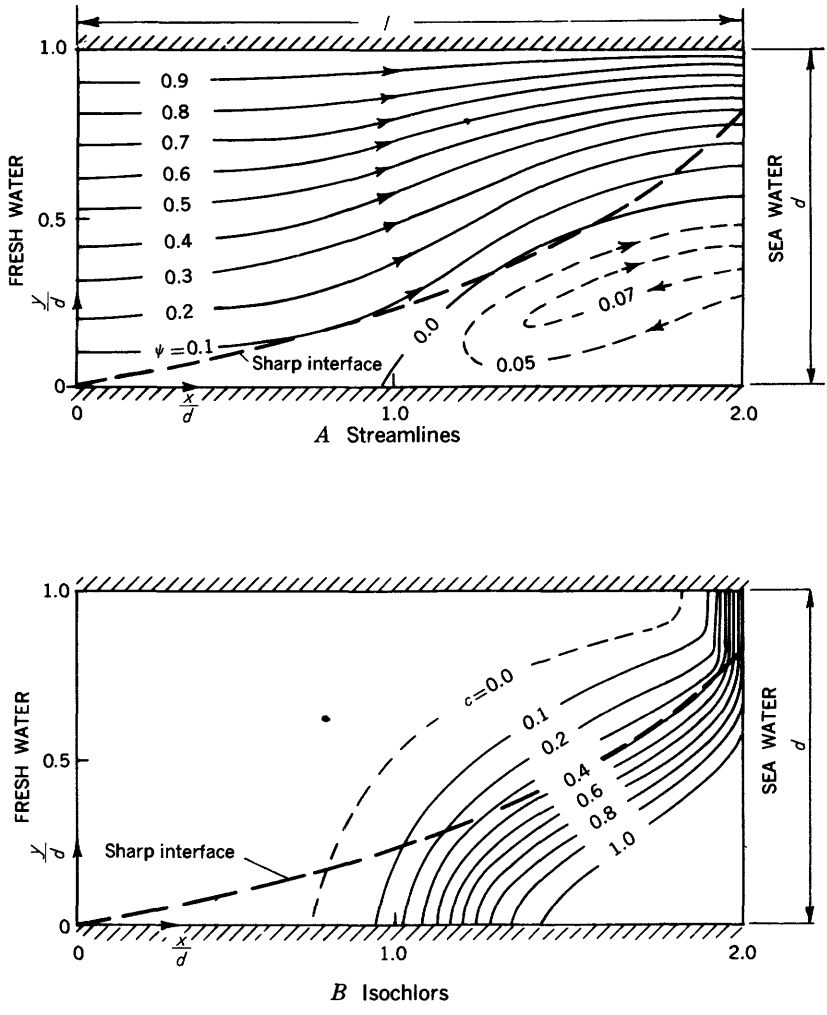

FIGURE 34.—Flow and salt concentration patterns in an idealized mathematical model.

constant and then using these values to recompute the $B_{g,h}$ ($g>0$). During an iteration for the $B_{0,h}$, the roles of $B_{0,h}$ and $B_{g,h}$ ($g>0$) were reversed. Two to four subiterative cycles were used each time the new values of the $B_{0,h}$ or $B_{g,h}$ ($g>0$) were computed.

The procedure was carried out for several iterative cycles. Convergence was obtained in the subiterations as indicated by the fact that the sum of the changes in absolute magnitude of the coefficients $B_{g,h}$ decreased for each subcycle. This same sum also decreased for each overall iterative cycle. The validity of the numerical procedure was also indicated by the fact that the computed values of the mean

concentration on a vertical section (fig. 35) remained zero within ± 0.005 for the last three iterations in the range $0 \gg x/d \gg 0.8$ and began to show an appreciable rise starting at $x/d=0.9$. The value $x/d=0.9$ corresponds to the inland limit of the landward flow along the base of the aquifer (fig. 34). Furthermore, the computed positions of the streamline $\psi'=0$ from the last three iterations fell within a band which departed from a mean position by only ± 5 percent of the length of the salt-water wedge.

The computations appear to have bracketed the solution sufficiently accurately so that several significant conclusions can be drawn as given below.

DISCUSSION OF RESULTS

Figures 34*A* and 34*B* show the streamlines and isochlors for the set of parameters $\xi=2.0$, $a=0.263$, $b-0.100$. These are interpolated from the computed values of ψ' and c' and are drawn to eliminate local variations that appear due to truncation of the Fourier series. Superposed on the streamline and isochlor patterns in figure 34*B* is the corresponding sharp interface for $\xi=2.0$, $a=0.263$, obtained from the solution given on pages C35–C70 of this report. Figure 35 shows for the problem under discussion three curves representing the mean salt concentration in vertical sections. Curve *a* is for dispersion with no density difference as computed from the diffusion equation, the solution of which is $c'=(e^{x'/b}-1)/(e^{\xi/b}-1)$. Curve *b* is for a density difference with no dispersion and is identical to the interface shown in figures 34*A* and 34*B*. Curve *c* is for density difference with dispersion. The ordinate of curve *c* at any x/d is the average of c' taken

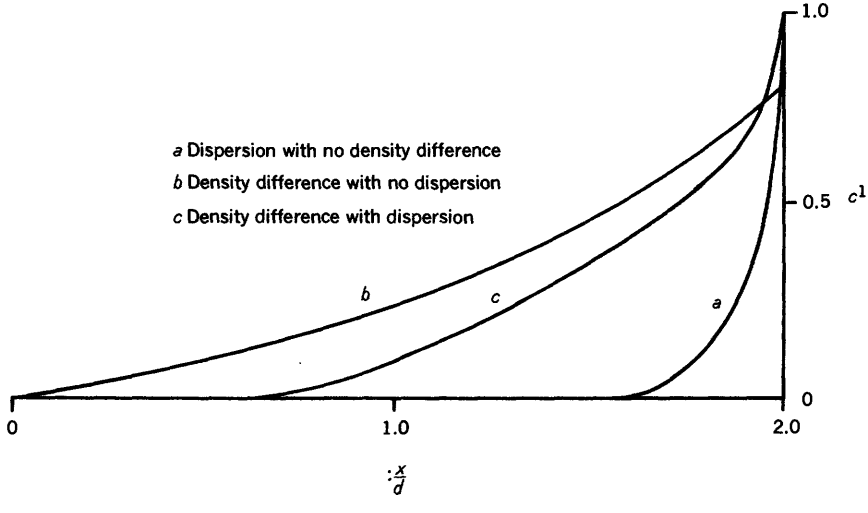

FIGURE 35.—Mean salt concentration in vertical sections.

from figure 34*B* at that x/d. Most of the curve *c* falls between curves *a* and *b*, as expected.

Several features of the numerical solutions are significant. As observed in figure 34*A*, the position of the equivalent sharp interface approximately separates the streamlines of the through flow that originate at the fresh-water end of the aquifer from those of the circulating flow that originate at the ocean end. The isochlors in figure 34*B* approach the base of the aquifer vertically in such a way as to give the toe of the salt-water wedge a blunted shape similar to that observed by Kohout in the Biscayne aquifer. (See p. 14, this report, under the heading "The zone of diffusion.") This shape results from the boundary condition that the concentration gradient normal to the base of the aquifer be zero. Perhaps the two most significant consequences of dispersion that are demonstrated by the solutions are the landward flow of salt water in the lower part of the aquifer and the concomitant reduction of the landward extent of salt water. These two features were predicted by Cooper and were observed in the field by Kohout. (See p. C11–C12.)

REFERENCES

Barrer, R. M., 1951, Diffusion in and through solids: Cambridge Univ. Press, 464 p.

Baxter, G. P., and Wallace, C. C., 1916, Changes in volume upon solution in water of the halogen salts of the alkali metals, IX: Am. Chem. Soc. Jour., v. 38, p. 70–104.

Bear, Jacob, and Todd, David K., 1960, The transition zone between fresh and salt water in coastal aquifers: Berkeley, California Univ., Water Resources Center Contrib. 29, 156 p.

Bosworth, R. C. L., 1949, The mechanisms of diffusional processes: Royal Australian Chem. Inst. Jour. and Proc., p. 460–482.

Brown, J. S., 1925, A study of coastal ground water, with special reference to Connecticut: U.S. Geol. Survey Water-Supply Paper 537, 101 p.

Byrd, P. F., and Friedman, M. D., 1954, Handbook of elliptic integrals for engineers and physicists: Berlin, Springer Verlag, 355 p.

Carrier, G. F., 1958, The mixing of ground water and sea water in permeable subsoils: Jour. Fluid Mechanics, v. 4, p. 479–488.

Cooper, H. H., Jr., 1959, A hypothesis concerning the dynamic balance of fresh water and salt water in a coastal aquifer: Jour. Geophys. Research, v. 64, no. 4, p. 461–467.

Darcy, Henri, 1856, Les Fontaines Publique de la Ville de Dijon [The public fountains of the city of Dijon]: Paris, Victor Dalmont.

Day, P. R., 1956, Dispersion of a moving salt-water boundary advancing through saturated sand: Am. Geophys. Union Trans., v. 37, no. 5, p. 595–601.

Drabbe, J., and Badon Ghyben, W., 1889, Nota in verband met de voorgenomen putboring nabij Amsterdam [Notes on the probable results of the proposed well drilling near Amsterdam]: The Hague, Koninkl. Inst. Ing. Tijdschr., 1888–89, p. 8–22.

Duncan, W. J., 1938, The principles of Galerkin's method: Aeronaut. Research Comm. Rept. and Mem. 1848.

Dupuit, Jules, 1863, Études théoriques et pratiques sur le mouvement des eaux dans les canaux de couvert et á travers les terrains perméables. [Theoretical and practical studies on the movement of water in closed channels and through permeable ground]: 2d ed., Paris, Dunod, 304 p.

Eriksson, Erik, 1958, A note on the dispersion of a salt-water boundary moving through saturated sand: Am. Geophys. Union Trans., v. 39, no. 5, p. 937–938.

Ferris, J. G., 1951, Cyclic fluctuations of water level as a basis for determining aquifer transmissibility: Union géod. géophys. Internat., Assoc. internat. d'hydrologie Sci. Assembleé gén. Bruxelles, v. 2, p. 148–155 [Internat. Union Geodesy and Geophysics, Internat. Assoc. Sci. Hydrology, Brussels, v. 2, p. 148–155].

Galerkin, B. G., 1915, Series solutions of some problems of elastic equilibrium of rods and plates: Moscow, Vestnik Inzhenerov, v. 1, p. 879–908 [in Russian].

Glover, R. E., 1959, The pattern of fresh-water flow in a coastal aquifer: Jour. Geophys. Research, v. 64, no. 4, p. 457–459.

Hamel, G., 1934, Über Grundwasserströmung [On groundwater flow]: Zeitschr. angew. Math. u. Mech., v. 14, p. 130–157.

Hamel, G., and Günther, E., 1935, Numerische Durchrechnung zu der Abhandlung über Grundwasserströmung [Numerical computations in connection with the paper on groundwater flow]: Zeitschr. angew. Math. u. Mech., v. 15, p. 255–265.

Hayashi, K., 1930, Tafeln der Besselschen, Theta, Kugel, und anderer Funktionen [Tables of Bessel, Theta, Spherical, and other functions]: Berlin, Springer Verlag, 150 p.

Henry, H. R., 1959, Salt intrusion into fresh-water aquifers: Jour. Geophys. Research, v. 64, no. 11, p. 1911-1919.

——— 1960, Salt intrusion into coastal aquifers: Internat. Assoc. Sci. Hydrol., Comm. Subter. Waters Pub. 52, p. 478–487.

Herzberg, Alexander, 1901, Die Wasserversorgung einiger Nordseebäder [The water supply on parts of the North Sea coast]: Munich, Jour. Gasbeleucht. u. Wasserversorg., v. 44, p. 815–819, 842–844.

Hodgeman, C. D., 1945, Handbook of chemistry and physics: Cleveland, Chemical Rubber Publishing Co., 2640 p.

Hubbert, M. K., 1940, The theory of ground-water motion: Jour. Geology v. 48, no. 8, pt. 1, 785–944.

——— 1953, Entrapment of petroleum under hydrodynamic conditions: Am. Assoc. Petroleum Geologists Bull., v. 37, no. 8, p. 1954–2026.

Jacob, C. E., 1950, Flow of ground water, chap. 5 *in* Rouse, Hunter (ed.), Engineering hydraulics: New York, John Wiley and Sons, p. 321–385.

Jahnke, Eugene, and Emde, Fritz, 1945, Tables of functions: New York, Dover Pub., 304 p.

Kirkham, Don, 1958, Seepage of steady rainfall through soil into drains: Am. Geophys. Union Trans., v. 39, p. 892–908.

Kitagawa, K., 1939, Un aspect du developement des études des eaux souterraines au Japon [An aspect of the development of the studies on underground waters in Japan]: Japanese Jour. Astronomy and Geophysics, v. 17, p. 141–155.

Kohout, F. A., 1960a, Cyclic flow of salt water in the Biscayne aquifer of southeastern Florida: Jour. Geophys. Research, v. 65, no. 7, p. 2133–2141.

———1960b, Flow pattern of fresh water and salt water in the Biscayne aquifer of the Miami area, Florida: Internat. Assoc. Sci. Hydrol., Comm. Subter. Waters Pub. 52, p. 440–448.

Kozeny, Josef, 1953, Hydraulik: Vienna, Springer Verlag, 588 p.
Muskat, Morris, 1935, The seepage of water through dams with vertical faces: Physics, v. 6, p. 402–415.
———1937, The flow of homogeneous fluids through porous media: New York, McGraw-Hill Book Co., 763 p.
Nehari, Zeev, 1952, Conformal mapping: New York, McGraw-Hill, 396 p.
Nomitsu, T., Toyohara, Y., and Kamimoto, R., 1927, On the contact surface of fresh and salt water near a sandy sea shore: Kyoto Imp. Univ., Mem. Coll. Sci., ser. A., v. 10, no. 7, p. 279–302.
Offeringa, Jan, and Vander Poel, G., 1954, Displacement of oil from porous media by miscible liquids: Am. Inst. Mining Engineers Trans., v. 201, p. 310–316.
Orlob, G. T., and Radhakrishna, G. N., 1958, The effects of entrapped gases on the hydraulic characteristics of porous media: Am. Geophys. Union Trans., v. 39, no. 4, p. 648–659.
Palmer, H. S., 1927, The geology of the Honolulu artesian system: Honolulu Sewer and Water Comm. Rept.
Parker, G. G., 1951, Geologic and hydrologic factors in the perennial yield of the Biscayne aquifer: Am. Water Works Assoc. Jour., v. 43, no. 10, p. 817–835.
Parker, G. G., Ferguson, G. E., and Love, S. K., 1944, Investigations of water resources of southeastern Florida: Fla. Geol. Survey Rept. of Inv. 4, 39 p.
——— 1955, Water resources of southeastern Florida: U.S. Geol. Survey Water-Supply Paper 1255, 965 p.
Poots, G., 1958, Heat transfer by laminar free convection in enclosed plane gas layers: Quart. Jour. Mech. and Appl. Math., v. 11, pt. 3, p. 257–273.
Rifai, M. N. E., Kaufman, W. J., and Todd, D. K., 1956, Dispersion phenomena in laminar flow through porous media: Berkeley, California Univ., Canal Seepage Research Prog. Rept. 2, 157 p.
Scheidegger, A. E., 1958, The random-walk model with auto-correlation of flow through porous media: Canadian Jour. Physics, v. 36, p. 649–653.
Senio, K., 1951, On the ground water near the seashore: Union géod. géophys. Internat., Assoc. Internat. d'Hydrologie Sci. Assembleé gén. Bruxelles, v. 2, p. 175–177. [Internat. Union Geodesy and Geophysics, Internat. Assoc. Sci. Hydrology, Brussels, v. 2, p. 175–177.]
Taylor, G. I., 1953, Dispersion of soluble matter in solvent flowing slowing through a tube: Royal Soc. London Proc., Ser. A, v. 219, p. 186–203.
Todd, D. K., 1953, Sea water intrusion in coastal aquifers: Am. Geophys. Union Trans., v. 34, no. 5, p. 749–754.
———1960, Salt intrusion of coastal aquifers in the United States: Internat. Assoc. Sci. Hydrol., Subter. Waters Comm. Pub. 52, p. 452–461.
Wentworth, C. K., 1948, Growth of the Ghyben-Herzberg transition zone under a rinsing hypothesis: Am. Geophys. Union Trans., v. 29, no. 1, p. 97–98.

U. S. GOVERNMENT PRINTING OFFICE : 1964 O - 719-580